MONTHLY NOTICES

OF THE

ROYAL ASTRONOMICAL SOCIETY

Volume 119 No. 3 1959

Published and Sold by the

ROYAL ASTRONOMICAL SOCIETY
BURLINGTON HOUSE
LONDON, W.1

Price £1 0s. 0d.; *in U.S.A.* $3

Annual Subscription for volume of six numbers: £5 5s. 0d. ; *in U.S.A.* $16

The Geophysical Journal

OF THE

ROYAL ASTRONOMICAL SOCIETY

Editors

A. H. Cook
M.A., Ph.D., F.R.A.S., F.G.S.
National Physical Laboratory
Teddington

T. F. Gaskell
M.A., Ph.D., F.R.A.S.
British Petroleum Company
London

Price £1 per number; in U.S.A. $3. Annual Subscription £3; in U.S.A. $9

Volume 2 No. 3 September 1959

CONTENTS

J. H. Piddington, The transmission of geomagnetic disturbances through the atmosphere and interplanetary space.

B. A. Bolt, Travel times of *PKP* up to 145°

A. H. Cook, The external gravity field of a rotating spheroid to the order of e^3.

H. Charnock, Tidal friction from currents near the sea bed.

Reports on Progress in Geophysics

A. H. Cook, Developments in dynamical geodesy.
H. I. S. Thirlaway, Notes on geophysics in Pakistan.

Reports on Geophysical Discussions of the Royal Astronomical Society

Turbidity currents: high-speed underwater flow of sediment suspensions (1958 November 28).
The automatic reduction of geophysical data (1959 January 23).
Discussion of papers received in the session 1958–59 (1959 March 20).

Orders should be addressed to:

The Assistant Secretary

Royal Astronomical Society, Burlington House, London, W.1

MONTHLY NOTICES

OF THE

ROYAL ASTRONOMICAL SOCIETY

Vol. 119 No. 3

MOTIONS IN THE SUN AT THE PHOTOSPHERIC LEVEL VIII. SOLAR ROTATION AND PHOTOSPHERIC CIRCULATION

H. H. Plaskett

(Received 1959 March 4)

Summary

From spectra exposed 1953 April 21–23, sight-line velocities have been measured at 332 points over the visible surface of the Sun. For any point the sight-line velocity can be expressed as a linear function of velocity components directed to the west and the north. Least-squares solutions of such observation equations for various latitudes reveal an asymmetry of rotational velocities in the equatorial zone and the presence of meridional currents. These motions suggest the existence of a circulation in the photosphere similar to that shown in the upper atmosphere of the Earth. This hypothesis is examined in the light of an investigation by M. J. Lighthill, and an observational test is proposed.

Introduction.—The rate of solar rotation is normally determined as an average in time and over the surface of the Sun. This is necessarily so when successive meridian passages of sunspots are timed, but is equally true in the differential spectroscopic observations introduced by Adams (**3**) where the rate of rotation for a given latitude is found from half the difference of velocity between the northern and southern hemispheres. Provided photospheric motions are random their effect is minimized by such averages and the true rate of rotation is obtained.

It is not, however, certain that photospheric motions are random. Thus, when the systematic errors in Adams' differential method are removed, a time variation in rotation is found (**16**) which may be due to long-lived local velocity fields, the existence of which has been established by A. B. Hart in Papers IV (**8**) and VI (**9**) of this series. These variations in velocity are not, as has been suggested, observational effects originating from the blending of sky and solar spectra. The suggestion arises from a misunderstanding of the origin and nature of scattered light, and is disproved by the simple experiment described in Paper IV.

This paper describes an investigation of systematic photospheric motions. From observations made in 1953 April sight-line velocities, corrected for the observer's motion, are found for 332 points on the solar surface, and are resolved at each point into east–west and south–north components. The latter component is independent of rotation, and its amount makes possible an estimate of the contribution made to the observed angular velocity by the east–west photospheric motion. The observations and measurements are described in the first section of the paper which also contains a sample of the 332 sight-line velocities as functions of the heliographic coordinates. These velocities are broken down into their components in the second section, and the paper concludes with a discussion of the 'equatorial acceleration'.

The Geophysical Journal

OF THE

ROYAL ASTRONOMICAL SOCIETY

Editors

A. H. Cook
M.A., Ph.D., F.R.A.S., F.G.S.
National Physical Laboratory
Teddington

T. F. Gaskell
M.A., Ph.D., F.R.A.S.
British Petroleum Company
London

Price £1 per number; in U.S.A. $3. Annual Subscription £3; in U.S.A. $9

Volume 2 No. 3 September 1959

CONTENTS

J. H. Piddington, The transmission of geomagnetic disturbances through the atmosphere and interplanetary space.

B. A. Bolt, Travel times of *PKP* up to 145°

A. H. Cook, The external gravity field of a rotating spheroid to the order of e^3.

H. Charnock, Tidal friction from currents near the sea bed.

Reports on Progress in Geophysics

A. H. Cook, Developments in dynamical geodesy.
H. I. S. Thirlaway, Notes on geophysics in Pakistan.

Reports on Geophysical Discussions of the Royal Astronomical Society

Turbidity currents: high-speed underwater flow of sediment suspensions (1958 November 28).
The automatic reduction of geophysical data (1959 January 23).
Discussion of papers received in the session 1958–59 (1959 March 20).

Orders should be addressed to:

The Assistant Secretary

Royal Astronomical Society, Burlington House, London, W.1

MONTHLY NOTICES

OF THE

ROYAL ASTRONOMICAL SOCIETY

Vol. 119 No. 3

MOTIONS IN THE SUN AT THE PHOTOSPHERIC LEVEL VIII. SOLAR ROTATION AND PHOTOSPHERIC CIRCULATION

H. H. Plaskett

(Received 1959 March 4)

Summary

From spectra exposed 1953 April 21–23, sight-line velocities have been measured at 332 points over the visible surface of the Sun. For any point the sight-line velocity can be expressed as a linear function of velocity components directed to the west and the north. Least-squares solutions of such observation equations for various latitudes reveal an asymmetry of rotational velocities in the equatorial zone and the presence of meridional currents. These motions suggest the existence of a circulation in the photosphere similar to that shown in the upper atmosphere of the Earth. This hypothesis is examined in the light of an investigation by M. J. Lighthill, and an observational test is proposed.

Introduction.—The rate of solar rotation is normally determined as an average in time and over the surface of the Sun. This is necessarily so when successive meridian passages of sunspots are timed, but is equally true in the differential spectroscopic observations introduced by Adams (**3**) where the rate of rotation for a given latitude is found from half the difference of velocity between the northern and southern hemispheres. Provided photospheric motions are random their effect is minimized by such averages and the true rate of rotation is obtained.

It is not, however, certain that photospheric motions are random. Thus, when the systematic errors in Adams' differential method are removed, a time variation in rotation is found (**16**) which may be due to long-lived local velocity fields, the existence of which has been established by A. B. Hart in Papers IV (**8**) and VI (**9**) of this series. These variations in velocity are not, as has been suggested, observational effects originating from the blending of sky and solar spectra. The suggestion arises from a misunderstanding of the origin and nature of scattered light, and is disproved by the simple experiment described in Paper IV.

This paper describes an investigation of systematic photospheric motions. From observations made in 1953 April sight-line velocities, corrected for the observer's motion, are found for 332 points on the solar surface, and are resolved at each point into east–west and south–north components. The latter component is independent of rotation, and its amount makes possible an estimate of the contribution made to the observed angular velocity by the east–west photospheric motion. The observations and measurements are described in the first section of the paper which also contains a sample of the 332 sight-line velocities as functions of the heliographic coordinates. These velocities are broken down into their components in the second section, and the paper concludes with a discussion of the 'equatorial acceleration'.

1. *Measured sight-line velocities*

In order to get as nearly simultaneous a survey as possible of motions over the whole visible surface a small image of the Sun is formed on the slit of the spectroscope. The slit, oriented east and west, cuts the image in a chord. In Fig. 1 let the x-axis be the slit with origin at O, marked by a wire crossing it, and let the y-axis be directed to the north. Then the equation to the limb of the solar image, centre $C(x_0, y_0)$ and radius ρ_0, is given by

$$(x-x_0)^2+(y-y_0)^2=\rho_0^2.$$

The limb cuts the slit at $A(x_w, 0)$ and $B(x_e, 0)$ so that

$$x_0=\tfrac{1}{2}(x_w+x_e), \qquad \rho_0^2-y_0^2=\tfrac{1}{4}(x_w-x_e)^2.$$

If now the south limb is tangent to a line parallel to the slit and distant a from it, then

$$y_0=\rho_0-a=\tfrac{1}{2}[(x_w-x_e)^2/4a-a]$$
$$\rho_0=\tfrac{1}{2}[(x_w-x_e)^2/4a+a].$$

The coordinates x_w, x_e can be found from the distances measured along a spectrum line (corrected for curvature if necessary) from the shadow of the wire to the

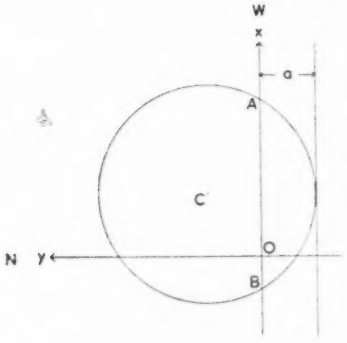

FIG. 1.

bottom and top respectively of the spectrum, the distances being multiplied by a factor for magnification of the spectroscope. We can therefore find the polar coordinates ρ and ϕ (origin C, and ϕ measured counter-clockwise from the west) of any height on the spectrum, and consequently, as set out in Paper I (**19**), its heliographic and equatorial coordinates.

In practice the distance a of the limb from the slit is not known. However two or more spectra, where the limb is displaced by known amounts from an arbitrary fixed origin, may be used to find ρ_0 and the y-coordinate of this arbitrary origin. We can then proceed as above to find the polar coordinates of any height in any spectrum. The advantages of the small image are thus not only that it permits a quick survey of motions over the Sun, but equally important that the data required for finding the heliographic coordinates of any height in a spectrum are given by the spectrum itself. The only quantities to be accurately determined when exposing the spectra are the U.T. of mid-exposure, and the displacement of the limb from a fixed but otherwise arbitrary zero.

1.1. *Observations.*—The prismatic spectroscope (**18**) of the 19·8 m tower was used in the investigation. In order to have the strong telluric water-vapour lines as wavelength standards minimum deviation was set at 5900A, the dispersion being approximately 1·5A mm^{-1}. The slit was covered with a diaphragm 20 mm high crossed by three fine wires perpendicular to the direction of the slit. The central wire, where it crossed the slit (the x-axis), formed the origin O, and the two outer wires were used to find the magnification of the spectroscope. The slit was opened to 0·036 mm. Ilford Thin-Film Half-Tone (R.50) plates were used because of their high photographic resolution.

A specially corrected Wray objective of 5 cm aperture and minimum focal length at 5900A of 148 cm formed a 13·7 mm diameter solar image on the spectroscope slit. The objective, mounted on an optical bench in the axis of the spectroscope, was fed with parallel light from the Sun by the coelostat, secondary flat and Coudé mirrors of the 19·8 m telescope (**17**), the Cassegrain and the main mirrors of the telescope proper having been removed. The objective was squared on and diaphragmed to 2·5 cm aperture to give a focal ratio comparable to that of the spectroscope. An Ilford filter, No. 202 in optical flats, before the objective admitted light on the long wavelength side of 5700A, while a mask before the filter and objective screened off unwanted solar light.

The Guiding Plate, described in Paper I (**19**), was mounted in front of the spectroscope slit. The rocking plate was fixed normal to the incident beam from the objective, and setting was effected solely by the controls on the coelostat and secondary flat. A filar micrometer in the focal plane of the objective and eyepiece permitted measurement of distances and position angles. The coelostat and secondary flat were adjusted so as to make the east–west line in the sky parallel to the direction of the spectroscope slit, and a subsequent careful determination showed that this had been achieved within 0°·1. Correction for this and for a 0°·3 lack of parallelism of the movable wire of the filar micrometer to the east–west line was made in the calculation of the polar coordinates of heights in the spectra.

TABLE I

Exposures

Series	No. Spectra	U.T. 1953	Exp. time sec	Remarks
I	14	April 21.541—21.621	8–9	No spots
II	14	April 22.378—22.461	7·5–11	Small spot on east limb on 22nd and 23rd. Three cloudless days after dispersal of morning fog.
III	14	April 22.576—22.624	9·5	
IV	14	April 23.564—23.624	8·5	

With these arrangements four series of spectra, each series complete in itself, were taken as set out in Table I. As already noted each of the 14 spectra in any one series was a chordal section of the solar image. They were exposed in the following order: diametral section, 2 mm S of diameter, 2 mm N, 4 mm N, 4 mm S, 6 mm S, 6 mm N, diametral section, 1 mm N, 1 mm S, 3 mm S, 3 mm N, 5 mm N, and 5 mm S. The whole image was thus covered in any one series by chords one mm apart. The displacement of the image on the slit by an exactly measured amount was secured by setting the south or north limb of the image

tangent to the movable wire, pre-set by the screw of the Guiding-Plate filar micrometer.

After A. B. Hart's investigation, described in Paper VI (**9**), the spectroscope adjustments and temperature remaining unchanged, the main and Cassegrain mirrors of the 19·8 m telescope were restored. Spectra of the centre of the 18·2 cm diameter image, de-focussed, were obtained and one of these with an exposure of 22 seconds on an Ilford R.50 plate at U.T. 1953 May 24.50905 was subsequently measured for a standard.

1.2. *Measurement of spectra.*—The spectra are measured on a Hilger photo-measuring micrometer with a mm pitch screw of 150 mm length. Settings can be read directly to one micron. The moving stage of the micrometer is provided with a subsidiary stage driven by a Moore & Wright micrometer (read directly to two microns) at right angles to the motion of the main stage. By measurement of a glass scale conversion factors are found and applied to reduce 'mm' measured with this micrometer, and also with the micrometer of the Guiding Plate, to mm of the long screw of the Hilger Micrometer. In the focal plane of the microscope of the Micrometer is placed a mask limiting the height of spectrum to be measured to 0·1 mm; the opening in this mask is crossed by a single fine measuring wire.

1.21. *Standard spectrum.*—The wavelengths of the lines to be measured on all spectra are listed in Table II. For the water-vapour lines these are the wavelengths recommended by the I.A.U. (Transactions **3**, 93, 1928; **4**, 61, 1932). For the solar lines they are I.A.U.—0·003A, as found from M. G. Adam's interferometric investigation (**2**) at 6100A and as partially confirmed by the measures at 5900A quoted in Paper V (**20**).

TABLE II

Wavelengths

Telluric water vapour		Solar lines			
Wavelength I.A.U.	R. No.	Wavelength M.G.A.	Rowl. No.	El.	Velocity Factor km sec^{-1} mm^{-1}
5885·977	5				
5891·661	4	5892·880	4d?	Ni	73·99
5901·468	6	5905·677	4	Fe	74·62
5919·054	5	5916·254	3	Fe	75·13
5919·644	7	5927·794	2	Fe	75·69
5924·272	4	5929·679	2	Fe	75·79
5932·092	5	5930·188	6	Fe	75·81

The settings for these lines on the standard spectrum of 1953 May 24 are measured direct and reverse on the Hilger Micrometer. The measures are made at 12 heights within 1 mm of and symmetrically about the centre of the spectrum, corresponding to approximately the same distances east and west of the centre of the 18·2 cm diameter solar image. The setting for each line referred to an arbitrary origin, the same for all heights, and averaged for the 12 heights is then the standard setting to which measures of the small-image spectra are referred. From these standard settings and the wavelengths of Table II the sight-line velocity V_0 of the standard spectrum is $+0{\cdot}38$ km sec^{-1}. If I.A.U. wavelengths had been adopted for the solar as well as the water-vapour lines this velocity would have been $+0{\cdot}23$ km sec^{-1}.

1.22. *Height measurement of small-image spectra.*—Each of the four series of small-image spectra listed in Table I was measured at pre-computed heights in each spectrum and completely reduced before starting on a new series. The pre-computed heights corresponded to one or more of the heliographic latitudes 0°, ±7°·5, ±15°·0, ..., ±60°·0, ±67°·5, and were found in the following way. Each spectrum of the series was ruled in a dividing engine across an unused spectrum line with scratches separated at nominal 1 mm intervals from the shadow of the central wire (the origin O). These scratches were numbered and their distances, from the origin, and those of the top and bottom of the spectrum, were measured in mm of the long screw of the Hilger Micrometer. For this purpose a low-power objective was used in the microscope and an unmasked single measuring line in the focal plane. No correction for the curvature of the spectrum line was necessary. After multiplication by a factor for spectroscope magnification these distances gave the x-coordinates on the slit of the scratches and of the east and west limbs of the solar image. In accordance with the procedure outlined in the opening paragraphs of this section the polar coordinates and the corresponding heliographic latitudes of these scratches were found; from these the heights in the spectrum (relative to the scratches) of the required heliographic latitudes were obtained by graphical interpolation.

1.23. *Line measurement of small-image spectra.*—With the Hilger Micrometer arranged as described in Section 1.2 to measure line positions over a spectrum height of a tenth of a mm, each spectrum of the series is measured direct and reverse at each of the pre-computed heights. For any one height the spectrum dispersion is reduced to that of the standard spectrum (Section 1.21) by means of the settings of the water vapour lines. The 'curve' of errors is assumed linear and found by least squares. The difference between the reduced settings of the six solar lines and their settings in the standard spectrum, converted by the velocity factors of Table II to km sec^{-1} and averaged, gives us $V_1 - V_0$, the sight-line velocity of the particular latitude relative to that of the standard spectrum. For positions on the solar image where $\sin\theta = \rho/\rho_0 \geq 0{\cdot}775$ the solar wavelengths of Table II must be increased by limb effect. From the interferometric determination of limb wavelengths by M. G. Adam (**2**) the smoothed corrections of Table III, expressed in km sec^{-1}, are derived and applied to the relative velocities $V_1 - V_0$ of such positions on the image.

TABLE III

Correction to $V_1 - V_0$ for limb effect

ρ/ρ_0	Δ_1 km sec^{-1}	ρ/ρ_0	Δ_1 km sec^{-1}
0·000	0·000	0·875	−0·031
0·775	0·000	0·900	−0·057
0·800	−0·002	0·925	−0·102
0·825	−0·007	0·950	−0·182
0·850	−0·016	0·975	−0·322

The standard error s in the velocity of a single line is found as usual from the sum of the squares of the residuals (line velocity − mean velocity for six lines). The mean standard error for the 332 measured spectra is $\bar{s} = 0{\cdot}28(5)$ km sec^{-1}. The individual values of s which contribute to this mean form a sampling distri-

bution which is satisfactorily represented by the theoretical sampling distribution for standard errors. The true standard error σ for a single line is thus given by

$$\bar{s} = \sigma \sqrt{\frac{2}{n-1}} \frac{\Gamma(n/2)}{\Gamma\{(n-1)/2\}},$$

or since our samples each have $n=6$, we find $\sigma = 0{\cdot}30\,\mathrm{km\,sec^{-1}}$. The standard error of the mean of six lines, that is of our relative velocity $V_1 - V_0$, is thus $0{\cdot}30/\sqrt{6} = 0{\cdot}17\,\mathrm{km\,sec^{-1}}$. The greater part of the error due to the measurement of the telluric water-vapour lines is carried forward into the solar lines in the objective adjustment by least squares of the dispersion of the measured spectrum to that of the standard. We therefore accept $0{\cdot}17\,\mathrm{km\,sec^{-1}}$ as the standard error of $V_1 - V_0$, and in view of the narrow spectral height of 0·1 mm available for fixing line positions may regard it as satisfactorily small.

1.24. *Final computations.*—From the actual heights in each spectrum at which $V_1 - V_0$ is measured are computed afresh the polar coordinates of the corresponding points on the image, and their heliographic coordinates B and $L - L_0$. From the polar coordinates of each point are also found the appropriate equatorial coordinates which are required for the correction C_1 for the Earth's orbital and rotational motion. This correction C_1 is found from eqn. (8) of Paper I (**19**) in which we have taken the numerical constant for the orbital correction to be 1730·32, corresponding to a solar parallax of 8″·80, and have correctly found δ_0' from $\tan \delta_0' = Z/\sqrt{X^2 + Y^2}$.

1.3. *Results.*—The sight-line velocity V for an observer motionless with respect to the Sun is given by

$$V = (V_1 - V_0) + 0{\cdot}38 + C_1 + \Delta_1.$$

In this equation $+0{\cdot}38\,\mathrm{km\,sec^{-1}}$ $(= V_0)$ is the measured velocity of the standard spectrum (Section 1.21), C_1 the correction for the observer's motion for the particular point on the Sun to which V refers, and Δ_1 the correction for limb effect (Sec. 1.23).

The total number of values of V so obtained is 332, distributed in latitude as follows:

B	No.	B	No.	B	No.	B	No.
+67·5°	3	+30·0°	18	− 7·5°	28	−45·0°	16
+60·0°	7	+22·5°	20	−15·0°	28	−52·5°	13
+52·5°	11	+15·0°	26	−22·5°	26	−60·0°	11
+45·0°	12	+ 7·5°	25	−30·0°	21	−67·5°	8
+37·5°	17	0·0°	26	−37·5°	16		

This distribution is shown in an orthographic projection in Fig. 2 where open circles show the position of the Series I observations and filled circles the Series II observations. Since the Guiding Plate micrometer was centred with respect to the slit almost identically for Series II, III and IV the filled circles correspond to three determinations of V, the open circles to one. The position angle of the Sun's axis of rotation at the time of observation was approximately $-26°$ (measured from the north) and the slit ran from east to west. The successive positions of the slit on the image can therefore be seen by looking along Fig. 2 from east

south-east to west north-west when the observed points line up in a succession of slightly curved lines.

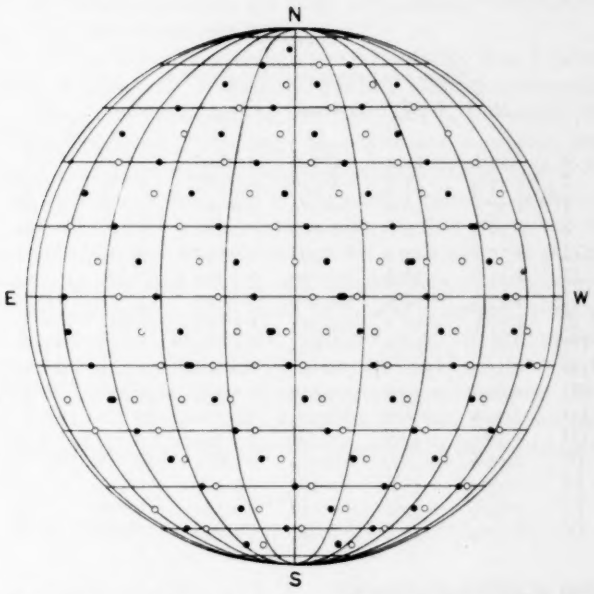

FIG. 2.—*Orthographic projection of the Sun with lines of latitude and longitude spaced at 15° intervals. Open circles indicate the positions where V has been measured in Series I, filled circles in Series II.*

Representative of the complete* table of values of V is Table IV. The values of V are given as a function of the heliographic coordinates; an asterisk attached to V indicates that the correction for limb effect (Table III) is not zero. The roman numeral in the first column shows the series number of the observations from which the velocity has been obtained. The standard error of V is $0{\cdot}17\,\mathrm{km\,sec^{-1}}$ (Section 1.23), and the errors in the equatorial coordinates of the point on the Sun where V has been determined are not likely to exceed

$$\delta B = 1^\circ{\cdot}2: \quad \delta(L-L_0) = 2^\circ{\cdot}2 \sec B.$$

These latter errors have been derived on the assumption that the error in fixing the x-coordinates of the solar limb where it crosses the slit does not exceed 0·2 mm.

The sight-line velocity V at any point on the Sun can be resolved into components u (directed to the west), v (directed along a meridian to the north) and w (directed radially outwards). We thus have

$$u\cos\gamma_1 + v\cos\gamma_2 + w\cos\gamma_3 = V, \tag{1}$$

where the direction cosines of the sight-line with respect to these axés are from Paper I (**19**)

$$\begin{aligned}
\cos\gamma_1 &= \sin(L-L_0)\cos B_0 \sin(\theta+\theta_1)\operatorname{cosec}\theta \\
\cos\gamma_2 &= [\sin B\cos B_0\cos(L-L_0) - \cos B\sin B_0]\sin(\theta+\theta_1)\operatorname{cosec}\theta \\
\cos\gamma_3 &= -\cos(\theta+\theta_1).
\end{aligned} \tag{2}$$

* The complete table will be issued as a supplement to *Communications from the University Observatory, Oxford, No.* 70.

These direction cosines are computed for each point of observation, and are shown for example in the representative Table IV.

TABLE IV

Sight-line velocities V for B = +37°·5

	B	$L-L_0$	$\cos\gamma_1$	$\cos\gamma_2$	$\cos\gamma_3$	V km sec^{-1}
I	+37·1	+19·2	+0·329	+0·640	−0·695	+0·81
I	+37·3	−31·3	−0·519	+0·587	−0·621	−0·59*
I	+37·5	+46·0	+0·719	+0·492	−0·492	+1·23*
I	+37·6	− 3·8	−0·066	+0·677	−0·732	−0·01
II	+37·6	+ 5·3	+0·093	+0·676	−0·731	+0·18
II	+37·6	−56·8	−0·836	+0·402	−0·375	−1·43*
II	+37·3	+28·9	+0·483	+0·599	−0·639	+0·28
II	+37·5	−20·1	−0·343	+0·640	−0·687	−0·53
III	+37·2	+58·6	+0·852	+0·383	−0·357	+1·26*
III	+37·4	+ 6·1	+0·107	+0·672	−0·732	+0·20
III	+37·2	−55·3	−0·820	+0·412	−0·397	−0·86*
III	+37·5	+30·8	+0·511	+0·591	−0·624	+0·65
III	+37·5	−18·7	−0·321	+0·645	−0·693	−0·69
IV	+37·6	+ 8·0	+0·139	+0·671	−0·728	+0·15
IV	+37·5	−51·6	−0·782	+0·445	−0·437	−1·00*
IV	+37·5	+32·2	+0·532	+0·582	−0·616	+0·85*
IV	+37·4	−17·3	−0·297	+0·647	−0·702	−0·06

2. *Analysis of sight-line velocities*

Two points about the analysis of the measured velocities V are to be noted. First it is assumed that all points in the photosphere at any one latitude have a common motion. This is almost certainly not true, but there are not sufficient observations to justify an analysis in longitude as well as latitude. Secondly any radially directed velocity component w, whether due to a general motion or, as originally suggested by St. John and recently revived by Schröter, due to local ascending and descending currents, will show itself as a change of measured solar wavelength from centre to limb. Since our wavelengths have been corrected for this limb effect by Table III, our measured V's will contain no component velocity w, irrespective of whether such motion exists or not. Hence for the analysis of measured velocities eqn. (1) becomes

$$u\cos\gamma_1 + v\cos\gamma_2 = V, \tag{3}$$

and this is the observation equation to be solved for the westerly u and northerly v components of velocity for each latitude.

2.1 *The westerly u-component.*—As a preliminary to finding u and v for each latitude, a least-squares solution is made of eqn. (3) combining north and south hemispheres. This involves reversing the sign of $\cos\gamma_2$ in the southern hemisphere so that the v-component in both hemispheres is directed to the nearer pole. The resulting mean values of v bring out nothing additional to the v's for individual latitudes discussed in Section 2.2, but the mean values of u form a standard of reference and their smoothed values are plotted as a necessarily symmetrical curve in the upper half of Fig. 3. The ordinates in this figure are $u-u_0$, where $u_0 = 1{\cdot}52\cos B$ is the linear velocity which a uniformly rotating Sun would have if its angular velocity were that actually found at $|B| = 67°{\cdot}5$. The curve shows

therefore the equatorial acceleration over and above that existing at $|B| = 67°{\cdot}5$. The smoothed value of u at the equator is $1{\cdot}92\,\mathrm{km\,sec^{-1}}$, while the numerically found value is 1·89. Both are within the range of equatorial velocities which have been found by other observers since 1915.

The interest in the westerly u-component of velocity lies, however, in its values for individual latitudes. A least-squares solution is therefore made of the observation equation (3) at each latitude, north and south, for which $|B| \leqslant 52°{\cdot}5$; individual latitudes poleward of this limit have with one exception less than 11 determinations of V and are unlikely to yield reliable values of u and v. The results are given in Table V where n, in the second column, is the number of observation equations on which the solution is based, and where the values of u and v with their standard errors are in the last four columns. A point of minor interest attaches to the standard error σ_1 of a single observation equation, given in the third column of the table. The mean of σ_1 is $0{\cdot}17\,\mathrm{km\,sec^{-1}}$, the value predicted in Section 1.23 from the internal consistency of the line measurements. This suggests that the local velocity-fields, described by A. B. Hart in Papers IV (**8**) and VI (**9**), and covering a linear distance greater (at least near the centre of the disk) than the 0·1 mm height measured in the 13·7 mm diameter image, have not made any substantial contribution to the dispersion of the observed velocities.

TABLE V

Velocity components as a function of latitude

B	n	σ_1	u	σ_u	v	σ_v
+52°·5	11	0·11	+1·12	0·08	+0·16	0·05
+45·0	12	0·11	+1·15	0·08	+0·26	0·05
+37·5	17	0·22	+1·40	0·10	+0·07	0·09
+30·0	18	0·12	+1·64	0·06	+0·36	0·06
+22·5	20	0·17	+1·82	0·07	+0·21	0·10
+15·0	26	0·15	+1·84	0·05	−0·01	0·11
+ 7·5	25	0·22	+1·75	0·10	+0·17	0·26
0·0	26	0·13	+1·89	0·05	+0·76	0·29
− 7·5	28	0·17	+2·03	0·06	−2·58	0·99
−15·0	28	0·21	+2·00	0·07	−0·96	0·28
−22·5	26	0·17	+1·81	0·06	−0·29	0·14
−30·0	21	0·16	+1·74	0·06	−0·11	0·11
−37·5	16	0·19	+1·40	0·09	−0·07	0·11
−45·0	16	0·19	+1·36	0·09	−0·34	0·09
−52·5	13	0·16	+1·13	0·09	−0·18	0·07

The individual values of u with their standard errors from Table V are plotted as circles in the upper half of Fig. 3. The ordinates are $u - u_0$, that is the excess of equatorial acceleration at the latitude in question over that prevailing at $|B| = 67°{\cdot}5$. The interesting feature of the plot is the asymmetry of u in the equatorial zones; for $|B| < 22°{\cdot}5$ the difference between southern and northern latitudes is approximately twice the standard error of the difference, that is on the 5 per cent level of significance. Least-squares solutions have also been made for the individual latitudes for each of the four series separately, though the number of observation equations is dangerously low. Series I, II, and IV each show the asymmetry of Fig. 3, but Series III shows a reversed asymmetry—presumably the result of chance accumulation of errors in the small number of available observations. Asymmetry about the equator is not a new phenomenon in observations of solar rotation. Hulbrecht (**10**), from observations at Cambridge,

somewhat indirectly inferred that the northern hemisphere gave higher velocities than the southern during the first half of 1911 June.

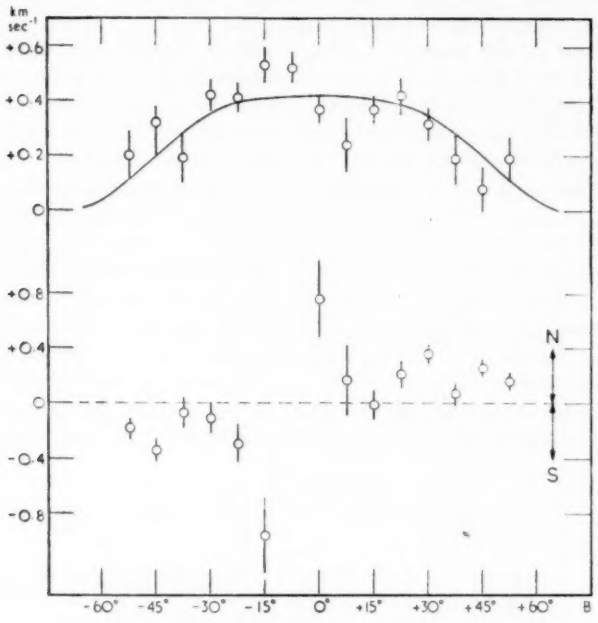

FIG. 3.—*Velocity components u and v as a function of latitude.*

2.2. *The meridional v-component.*—The v-component of velocity is significantly different from zero, and at low latitudes is larger than $u-u_0$, the excess equatorial acceleration. The individual values of v with their standard errors from Table V are plotted as circles in the lower half of Fig. 3, the ordinate scale being half that of $u-u_0$ in the upper half of the figure. The value for $B=-7^\circ\cdot5$ is not shown since for this latitude the mean value of $|\cos\gamma_2|=0\cdot030$ and the derived value for v is probably meaningless. The figure shows well the character of the meridional currents which are directed in each hemisphere towards the nearer pole and which increase towards the equator. By and large these characteristics are repeated in the solutions for each of the four series, though the equatorial strengthening is more marked in Series I and IV than in II and III. Once again these differences between series, each with relatively few observations per latitude, are not to be regarded as significant.

Since for a given latitude the coefficient of v, namely $\cos\gamma_2$, is roughly constant (cf. Table IV), any systematic error δ in V will appear at that latitude as a 'meridional current' of magnitude $\delta\overline{\sec\gamma_2}$. Two examples of this effect are given in Table VI, which is arranged in the same way as Table V. The upper half of Table VI gives the results of solutions of eqn. (3) for $V-0\cdot15$, that is the values of u and v which would have been obtained if the I.A.U. wavelengths of solar lines had been used (Section 1.21). While the values of u are almost identical with those of Table V, as might have been anticipated, the meridional currents are now directed equatorwards.

Comparing Table V and the upper half of Table VI it might be supposed that with an appropriate choice of solar wavelengths the meridional currents would

TABLE VI

B °	n	σ_1	u	σ_u	v	σ_v
+52·5	11	0·11	+1·10	0·08	−0·03	0·05
+45·0	12	0·12	+1·13	0·08	+0·04	0·05
+37·5	17	0·22	+1·41	0·10	−0·18	0·09
+30·0	18	0·12	+1·63	0·06	+0·07	0·06
+22·5	20	0·17	+1·83	0·07	−0·16	0·10
+15·0	26	0·15	+1·83	0·05	−0·50	0·11
+ 7·5	25	0·22	+1·75	0·10	−0·58	0·23
0·0	26	0·13	+1·90	0·05	−0·96	0·30
− 7·5	28	0·15	+1·99	0·06	+0·73	0·86
−15·0	28	0·20	+1·95	0·07	+0·06	0·27
−22·5	26	0·16	+1·81	0·05	+0·32	0·14
−30·0	21	0·17	+1·73	0·07	+0·32	0·11
−37·5	16	0·19	+1·38	0·09	+0·25	0·10
−45·0	16	0·17	+1·31	0·08	−0·08	0·08
−52·5	13	0·18	+1·11	0·10	+0·06	0·08
+52·5	11	0·11	+1·11	0·08	+0·04	0·05
+45·0	12	0·12	+1·14	0·08	**+0·12**	**0·05**
+37·5	17	0·22	+1·40	0·10	−0·10	0·09
+30·0	18	0·12	+1·63	0·06	**+0·17**	**0·06**
+22·5	20	0·17	+1·83	0·07	−0·04	0·10
+15·0	26	0·15	+1·83	0·05	**−0·34**	**0·10**
+ 7·5	25	0·22	+1·75	0·10	−0·33	0·23
0·0	26	0·13	+1·89	0·05	−0·39	0·29
− 7·5	28	0·16	+2·01	0·06	−0·38	0·91
−15·0	28	0·20	+1·96	0·07	−0·28	0·27
−22·5	26	0·16	+1·81	0·05	+0·12	0·14
−30·0	21	0·17	+1·73	0·06	+0·18	0·11
−37·5	16	0·19	+1·39	0·09	+0·14	0·10
−45·0	16	0·18	+1·33	0·08	**−0·17**	**0·09**
−52·5	13	0·17	+1·12	0·09	−0·02	0·08

disappear. To test this hypothesis a 'systematic error' δ was found for each latitude from a least-squares solution of the equation

$$u \cos \gamma_1 + \delta = V.$$

The mean of these 'systematic errors', weighted according to the number of observations per latitude, was $\delta = +0{\cdot}10$ km sec^{-1}. This is the 'systematic error' which will most nearly make the meridional currents disappear. Solving now eqn. (3) for $V - 0{\cdot}10$ we get the values of u and v shown in the lower half of Table VI. It will be seen that though, in accordance with our intention, v is effectively zero everywhere, nevertheless at latitudes $+45°$, $+30°$, $+15°$ and $-45°$ the values of v are approximately twice their standard errors. In short, no matter what we do, meridional currents persist, and it is only the latitude of their place of incidence and their direction which can be changed by applying arbitrary systematic corrections to the observed sight-line velocities V of Table IV.

It would appear, therefore, that there are meridional currents in the photosphere with velocities comparable with those of the excess equatorial acceleration. Adopting the solar wavelengths of M. G. Adam, the system of meridional currents

is that shown in Table V and Fig. 3. That these currents have not been found before is probably the result of confining spectroscopic observations to the limb and the equatorial zone where, from eqns. (2), $\cos\gamma_2$ is small and where, as a consequence, the contribution of meridional currents to the observed sight-line velocities has likewise been small.

3. *The equatorial acceleration*

The existence of motions perpendicular to the direction of rotation suggests the presence of large-scale currents in the photosphere. The fact that these meridional currents have speeds comparable with the excess equatorial acceleration raises the question whether the equatorial acceleration itself is not a manifestation of photospheric circulation. If beneath the photosphere the Sun had a uniform rotation, then the equatorial acceleration and its asymmetry and the meridional currents would bear some resemblance to the general circulation of the Earth's atmosphere. Here in the upper troposphere at all latitudes there is a mean westerly circulation, that is a greater angular velocity than that of the uniformly rotating Earth beneath. In a stimulating paper Lighthill (**12**) has suggested that the mean westerly circulation of the Earth's upper atmosphere is due to a thermal wind, arising from the decrease in ground temperature from equator to poles, and deviated by Coriolis force to blow parallel to the isotherms and isobars. It is tempting to speculate whether a similar mechanism may not be operating in the Sun, and if so what the observational consequences would be.

3.1. *The hydrogen convection zone and polar cooling.*—Assume, as is customary, the existence of Unsöld's hydrogen convection zone in which a not negligible fraction of the heat is transported by convective processes. Assume further that the top of this zone is a level surface rotating with a constant angular velocity ω. Then if overstability is avoided, convection is inhibited by rotation and the critical Rayleigh number for its onset varies according to Chandrasekhar (**5**, **6**, **7**) as the two-thirds power of the Taylor number

$$\left(\frac{2\Omega}{\nu}h^2\right)^2$$

where Ω is the angular velocity at the place, ν is the kinematic viscosity and h the depth of the convection zone. But $\Omega=\omega\sin B$ so that the Taylor number and the critical Rayleigh number steadily increase from the equator to the poles. Correspondingly we may expect an increasing deficiency of heat transfer by convection and therefore a cooling of the top of the hydrogen-convection zone as we proceed polewards. On these grounds we might expect that conditions on the Sun are such as to permit an application of Lighthill's theorem.

3.2. *Application of Lighthill's theorem.*—Following Lighthill (**12**) let us calculate the pressure gradient for an *isothermal* photosphere lying above the top of the hydrogen-convection zone. With our usual axes, x directed to the west, y to the north and z radially outwards, the pressure p at some level $z'=z-z_0$ in the photosphere is

$$p=p_0\exp\left(-\mu gz'/RT_0\right),$$

where p_0 and T_0 are the pressure and temperature at z_0, the top of the hydrogen-convection zone. From Section 3·1, T_0 and possibly p_0 change with increasing y, and the pressure gradient at level z' is

$$\frac{\partial p}{\partial y}=\left(\frac{dp_0}{dy}+\frac{\mu g p_0 z'}{RT_0^2}\frac{dT_0}{dy}\right)\exp\left(-\mu gz'/RT_0\right).$$

This pressure gradient attains a maximum at some height where its value is

$$\left(\frac{\partial p}{\partial y}\right)_{\max} = \frac{p_0}{T_0}\frac{dT_0}{dy}\exp\left\{-\left(1-\frac{T_0 dp_0/dy}{p_0 dT_0/dy}\right)\right\} \simeq 0{\cdot}4\,\frac{p_0}{T_0}\frac{dT_0}{dy}. \qquad (4)$$

On the right hand side we have assumed that the index of the exponential is unity, that is that the temperature T_0 varies with y by a greater fraction of its absolute value than p_0.

According to Jeffreys (**11**) large-scale atmospheric motions fall into two main classes. First there are those in which the pressure and rotational terms in the equations of motion far exceed the inertial and frictional terms so that

$$\left.\begin{aligned} -2\omega v\sin B &= -\frac{1}{\rho}\frac{\partial p}{\partial x} \\ 2\omega u\sin B &= -\frac{1}{\rho}\frac{\partial p}{\partial y} \\ 0 &= -\frac{1}{\rho}\frac{\partial p}{\partial z} - g \end{aligned}\right\}. \qquad (5)$$

These may be called 'heliostrophic' motions in analogy with the meteorological term 'geostrophic', and are such that the pressure gradient is balanced by Coriolis force. Secondly there are those in which the pressure and frictional terms exceed the inertial and rotational terms in which case the equations of motion take the form

$$\left.\begin{aligned} K\frac{\partial^2 u}{\partial z^2} &= \frac{1}{\rho}\frac{\partial p}{\partial x} \\ K\frac{\partial^2 v}{\partial z^2} &= \frac{1}{\rho}\frac{\partial p}{\partial y} \\ 0 &= -\frac{1}{\rho}\frac{\partial p}{\partial z} - g \end{aligned}\right\}. \qquad (6)$$

The motion in this case is down the pressure gradient, viscosity, represented by the terms on the left hand side of the equations, preventing the velocity from increasing steadily. Such motions Jeffreys terms 'antitriptic'.

The equatorial acceleration is thus to be regarded as a heliostrophic motion with $\partial p/\partial x = 0$ and $\partial p/\partial y$ as given by eqn. (4). We thus have from eqns. (5)

$$2\omega u\sin B = -0{\cdot}4\,\frac{p_0}{\rho T_0}\frac{dT_0}{dy} = -0{\cdot}4\,\frac{R}{\mu}\frac{\rho_0}{\rho}\frac{dT_0}{dy},$$

or

$$-\frac{dT_0}{dy} = \left(5\,\frac{\mu}{R}\,\omega u\sin B\right)\frac{\rho}{\rho_0} = \left(2{\cdot}1\times 10^{-9}\right)\frac{\rho}{\rho_0}\ \mathrm{deg\,cm^{-1}}$$

at z_0, the top of the hydrogen-convection zone. The numerical value holds for $\omega = 2{\cdot}18\times 10^{-6}\,\mathrm{sec^{-1}}$ (corresponding to a linear velocity of $0{\cdot}58\,\mathrm{km\,sec^{-1}}$ at $|B| = 67^\circ{\cdot}5$), for $B = 30^\circ$ and for $u = 0{\cdot}38\,\mathrm{km\,sec^{-1}}$ (excess equatorial acceleration at this latitude), and for a mean molecular weight of unity. Since $\rho/\rho_0 < 1$, the numerical value of $2{\cdot}1\times 10^{-9}\,\mathrm{deg\,cm^{-1}}$, or equivalently some three degrees per degree of heliographic latitude, is an upper limit to the temperature gradient at the top of the hydrogen-convection zone which is required to produce the excess equatorial acceleration found at $B = 30^\circ$. It should be noted that the observed

$u \sin B$ is not a constant, as would be the case if the temperature gradient and the density ratio were independent of latitude.

In the equatorial zone where the Coriolis force becomes small we are passing from the heliostrophic regime of eqns. (5) to the antitriptic conditions of eqns. (6). It is therefore not surprising that we have meridional currents down the pressure gradient, that the excess equatorial acceleration changes slowly with latitude and that there are from time to time asymmetries in this acceleration.

The temperature gradient of 3° per degree of latitude can only be regarded as a guide to the order of magnitude. A more exact calculation for a photosphere, not isothermal, but with a temperature gradient corresponding to radiative equilibrium would be justified if the limb-darkening test about to be mentioned were met. In any event such a calculation will demand highly accurate values of the total absorption coefficient for small changes of temperature and pressure, for in this problem we are concerned with the pressure gradient at a constant level, not a constant optical depth.

3·3. *Limb darkening.*—If Lighthill's theorem is to be applicable to the Sun there must be a difference of temperature at the top of the hydrogen-convection zone between the pole and the equator, and correspondingly a difference of limb darkening along a polar and equatorial diameter. To estimate its amount we assume the optical depth to the top of the hydrogen-convection zone always to be large, that is we make a distinction between this zone and the higher-lying zone of photosphere granulation (**21**). Then for total radiation and a photosphere in radiative equilibrium on the Milne-Eddington approximation we have

	Polar diameter	Equatorial diameter
Temperature at z_0	T_0	T_0'
Optical depth at z_0	τ_0	τ_0'
Temp. distribution	$\frac{\sigma}{\pi} T^4 = \frac{3}{4} F_0(\tau + \frac{2}{3})$	$\frac{\sigma}{\pi} T^4 = \frac{3}{4} F_0'(\tau + \frac{2}{3})$
Net flux	$F_0 = \frac{4\sigma}{3\pi} T_0^4/(\tau_0 + \frac{2}{3})$	$F_0' = \frac{4\sigma}{3\pi} T_0'^4/(\tau_0' + \frac{2}{3})$
Surface brightness	$I(0, \theta = B) = \frac{3}{4} F_0(\cos\theta + \frac{2}{3})$	$I'(0, \theta) = \frac{3}{4} F_0'(\cos\theta + \frac{2}{3})$
Hence	$\frac{I(0, \theta = B)}{I'(0, \theta)} = \frac{F_0}{F_0'} = \frac{T_0^4}{T_0'^4} \frac{\tau_0' + \frac{2}{3}}{\tau_0 + \frac{2}{3}}$	

Since the temperature and pressure are higher at θ along an equatorial diameter than at $\theta = B$ along a polar diameter, the equatorial absorption coefficient is higher than the polar coefficient, or $\tau_0' > \tau_0$. That is

$$\frac{I(0, \theta = B)}{I'(0, \theta)} \geqslant \frac{T_0^4}{T_0'^4} \simeq 1 - 4 \frac{T_0' - T_0}{T_0'}.$$

If at the pole we take $T_0' - T_0 = 270°$ (corresponding to 3° per degree of latitude), and $T_0' = 10{,}000°$, then

$$1 > \frac{I(0, \theta = B = \pi/2)}{I'(0, \theta = \pi/2)} \geqslant 0{\cdot}89.$$

Hence, if Lighthill's theorem is applicable to the Sun, there should be a measurable difference of limb darkening between a polar and an equatorial diameter. With one exception the standard limb-darkening determinations have been made along an east–west or an approximately equatorial diameter. The

exception is that of Canavaggia and Chalonge (**4**) which, Professor Chalonge kindly informs me, was made along a diameter between east–west and north–south. This limb darkening is certainly different from that of the east–west determinations of Abbot (**1**), Raudenbusch (**23**) and of Pierce, McMath, Goldberg and Mohler (**15**), but is similar to the east–west determination of Moll, Burger and van der Bilt (**14**). Colour-temperature measurements at the limb are no more helpful. Thus Proisy and Gauzit (**22**) from an accurate visual determination find the pole to be 100° cooler than the equator, while photoelectrically Minnaert (**13**) finds no difference greater than his small error of measurement. Further measures, preferably of surface brightness, are clearly necessary, and on their result must stand or fall the applicability of Lighthill's theorem to the photosphere.

Conclusion.—The observations described in this paper show the presence of meridional currents and asymmetry in equatorial rotation. If, as in Section 3, these motions are regarded as a purely photospheric circulation it follows, since sunspots also show equatorial acceleration, that the visible part of a spot is not anchored to the top of the hydrogen-convection zone, assumed on this interpretation to be in uniform rotation. The motions, however, may be interpreted quite otherwise. For example the spectroscopic abundance of beryllium, deuterium and lithium shows that there is a material connection between the photosphere and the solar interior; it is, therefore, not impossible that the photosphere is revealing in a modified way motions which have their origin in the deep interior. Whatever the interpretation, however, the immediate task is by other and improved methods to confirm or disprove the photospheric motions found in the present investigation.

Work in this and related fields is planned at Oxford. Since the methods will differ from those hitherto employed the present paper will conclude the exploratory series *Motions in the Sun at the Photospheric Level.* For invaluable discussions and in particular for their own contributions to the series I wish to express my thanks to Dr Hart and to Dr Kinman.

University Observatory
Oxford:
1959 *February* 27.

References

(1) C. G. Abbot, *Ann. Smithsonian Inst.*, **4**, 221, 1922.
(2) M. G. Adam, *M.N.*, **108**, 446, 1948: *Comm. Univ. Obs. Oxford*, No. 26.
(3) W. S. Adams, *Papers Mt. Wilson Obs.*, **1**, Part 1, 1911.
(4) R. Canavaggia and D. Chalonge, *Ann. d'Ap.*, **9**, 143, 1946.
(5) S. Chandrasekhar, *Proc. Roy. Soc.* A, **217**, 306, 1953.
(6) S. Chandrasekhar, *Proc. Roy. Soc.* A, **231**, 198, 1955.
(7) S. Chandrasekhar, *Proc. Am. Acad. Sc.*, **86**, 323, 1957.
(8) A. B. Hart, *M.N.*, **114**, 17, 1954: *Comm. Univ. Obs. Oxford*, No. 43.
(9) A. B. Hart, *M.N.*, **116**, 38, 1956: *Comm. Univ. Obs. Oxford*, No. 54.
(10) J. B. Hulbrecht, *Ann. Solar Physics Obs. Cambridge*, **3**, Part 1, 1915.
(11) H. Jeffreys, *Quart. Jour. Met. Soc.*, **48**, 29, 1922.
(12) M. J. Lighthill, *Phil. Mag.* (*Ser.* 7), **45**, 1154, 1954.
(13) M. Minnaert, *Solar Physics, Volta Conf.* (Rome), p. 50, 1953.
(14) W. J. H. Moll, H. C. Burger and J. van der Bilt, *B.A.N.*, **3**, 83, 1925.
(15) A. K. Pierce, R. R. McMath, L. Goldberg, and O. C. Mohler, *Ap.J.*, **112**, 289, 1950.

(16) H. H. Plaskett, *Ap.J.*, **43**, 145, 1916.
(17) H. H. Plaskett, *M.N.*, **99**, 219, 1939; Comm. Univ. Obs. Oxford, No. 19.
(18) H. H. Plaskett, *M.N.*, **112**, 177, 1952; Comm. Univ. Obs. Oxford, No. 33.
(19) H. H. Plaskett, *M.N.*, **112**, 414, 1952; Comm. Univ. Obs. Oxford, No. 34.
(20) H. H. Plaskett, *M.N.*, **114**, 251, 1954; Comm. Univ. Obs. Oxford, No. 44.
(21) H. H. Plaskett, *Vistas in Astronomy I*, 637, 1955.
(22) P. Proisy and J. Gauzit, *C.R.*, **223**, 852, 1946.
(23) H. Raudenbusch, *A.N.*, **266**, 301, 1938.

THE SOLAR EMISSION INTENSITY AT 11 μ

*F. Saiedy and R. M. Goody**

(Received 1959 February 20)

Summary

Observations were made during spring 1958 of the central emission intensity of the Sun at a wave-length of 11·10 μ (901 cm^{-1}), by direct comparison with the emission of a black body at 1300 °K. The solar intensity was reduced to approximately that of the black body by the use of rotating sector disks, and the ratio of intensities was then measured by a calibrated electrical attenuator so that the system was independent of the detector linearity. The only subsidiary measurements needed were the absolute reflectivity of one mirror and the variation of reflectivity with angle of reflection of another.

The slit width of 0·031 μ or 2·5 cm^{-1} was small enough to enter an atmospheric "window" where the terrestrial absorption obeys Lambert's law, thereby allowing extrapolation to extra-terrestrial intensity.

The weighted mean of five measurements of the central intensity was $I_{\odot}(11{\cdot}10\,\mu) = 2{\cdot}408 \pm 0{\cdot}016 \times 10^{10}$ erg cm^{-2} $ster^{-1}$ sec^{-1} (per cm wave-length range). This is equivalent to a central temperature $T_{\odot}(11{\cdot}10\,\mu) = 5036 \pm 30$ °K.

1. *Introduction.*—The astrophysical importance of an accurate determination of the energy–wave-length curve of the Sun is well known (**1**). In recent years attention has been directed towards the longer wave-lengths, ranging from the near infra-red (**2, 3**) to the radio region (**4**).

No measurements of central radiative intensity seem to have been made in the atmospheric window around 10 μ. This is rather surprising, as both solar and terrestrial conditions are here somewhat favourable; there are virtually no Fraunhofer lines, so that a true photospheric continuum may be observed, and the Earth's atmosphere is relatively transparent between the intense bands of H_2O at 6·3 μ and of CO_2 at 15 μ. Optical techniques in this region are now well developed, and—a point of great practical convenience—the energy ratio between the Sun and any possible terrestrial comparison source is very much less than at shorter wave-lengths. For example, Peyturaux (**2**), using a tungsten ribbon lamp at 2900 °K, had to measure an energy ratio of 20 at 2·3 μ; in the present determination the reference source was at 1300 °K and the ratio was 6. At this lower temperature an almost-perfect black-body source may be constructed fairly easily, enabling a direct comparison with the Sun to be made with a very simple optical system.

This paper describes a series of measurements made during spring, 1958, at the Ascot (Berkshire) Field Station of the Department of Meteorology, Imperial College. A grating spectrometer was used, enabling the observations to be made in a small "window" at 11·10 μ (901 cm^{-1}) (**5, 6**). Although there are no known molecular lines in this region, the Earth's atmosphere is by no means transparent, and the study of its opacity forms another aspect of the

* Now at Harvard University.

observations which will be reported elsewhere. It has been studied at lower resolution (7) showing that there is a continuous absorption obeying Lambert's law over most of the region in the spectrum from 8 to 13 μ, so that extrapolation to zero air mass can be made with confidence.

2. *Apparatus.* (*a*) *General layout.*—The equipment is arranged as shown in Fig. 1. The siderostat mirror M was electrically driven and maintained a beam of solar radiation on the paraboloid M_2 (focal length 180 cm). When M was not pointed at the Sun it was fixed so as to reflect a collimated beam of radiation from the black body by M_1 on to M_2. The paraboloid mirror M_2 then forms an image of the Sun or of the black body on the entrance slit of the spectrometer, placed just below the incoming beam. It will be seen that radiation from the Sun and from the black body follow identical paths except that (i) the black-body radiation suffers one additional reflection at the collimating mirror M_1, and (ii) the angles of reflection at the siderostat mirror differ. It therefore becomes necessary to determine the absolute reflectivity of M_1, and the variation of the reflectivity of M with angle of reflection; the methods used are described in Section 3.

The aperture of the system is defined by a metal diaphragm placed at S, the calculated position of the entrance pupil.

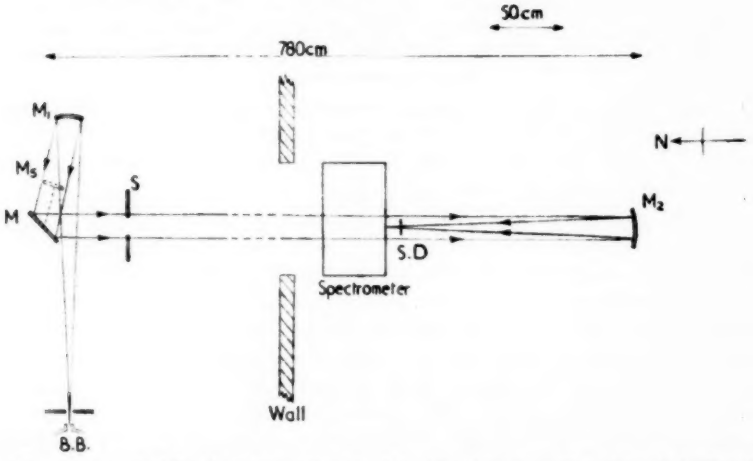

FIG. 1.—*Layout of the observing equipment. The siderostat mirror* M *is shown in position for taking measurements on the black body* B.B. *The sector disks are placed at* S.D *in front of the entrance slit of the spectrometer. The dotted plane mirror* M_5 *(see Section* 3(*b*)*) was placed in this position only when the variation of the reflectivity of* M *was measured.*

(*b*) *The black body.*—The black body is shown in Fig. 2. It consists of a sphere of sillimanite incorporating a heater winding of Kanthal Al wire (m.p. 1520 °K) which can be run directly from a 240 V a.c. line. An additional winding on the exit tube maintains the part adjoining the sphere close to the sphere temperature and so reduces the disturbance caused by the circular exit hole. The inside wall of the sphere opposite the exit tube was roughened to prevent any possibility of specular reflection and the whole of the inside was coated with cobalt oxide (applied as a paste mixed with dextrine and water).

A careful exploration was made of the internal temperature distribution by means of silica-encased platinum, platinum–rhodium thermojunctions passing vertically and horizontally through the sphere, from which it was established that the temperature was uniform within ± 1 °C. The emissivity of cobalt oxide at 10 μ and room temperature is 0·8 (**8**). Assuming this value to be true at 1300 °K, the normal operating temperature, it has been calculated that with the given geometry the departure of the emergent beam from perfect black-body radiation is less than 0·1 per cent. This is about the same error as is introduced in measuring the temperature of the black body.

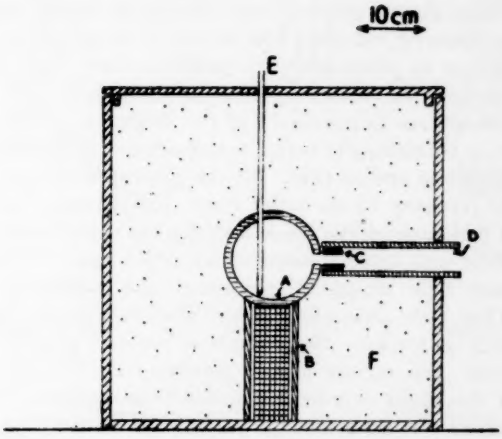

FIG. 2.—*Black body. The heated sphere* (A) *is supported by three refractory bricks* (B). *The small tube* (C) *inside the exit tube* (D) *is separately heated to the same temperature as the sphere. The box is filled with "filter cell" powder* (F). *The thermocouple slides inside the projecting sheath of quartz* (E).

The black body was run continuously from a constant-voltage transformer, a temperature-controlled cut-out being set at a somewhat higher temperature than the normal equilibrium temperature as a safety precaution. The temperature was measured using Pt–Pt 13 per cent Rd thermocouples calibrated by the National Physical Laboratory to an accuracy of ± 2 °C at 1300 °K. The reference thermocouple was placed in a Dewar vessel of water whose temperature was measured with a mercury thermometer, while the other thermocouple was placed inside the heated sphere in a selected position. A Tinsley potentiometer in conjunction with a Cambridge Spot Galvanometer and a Weston Standard Cell was used to measure the e.m.f. The system was capable of detecting 2 μV, while the total e.m.f. produced was 1100 μV. The temperature varied by less than 1 °C during any run.

(*c*) *The spectrometer.*—The infra-red spectrometer was a small double monochromator using two 7 × 5 cm Merton N.P.L. replica gratings having 1000 lines per cm and blazed for 10 μ in the first-order spectrum. The elimination of the higher order spectra of shorter wave-lengths was achieved by the use of an indium antimonide filter with an anti-reflection coating of lead chloride (**9**). This remarkable filter has an extremely sharp cut-off at 7 μ, with maximum

transmission of 98·5 per cent at 10·2 μ, falling to 90 per cent at 8·2 μ and 13·5 μ. The detector was a Golay cell (Unicam) with a phase-sensitive rectifier and a Honeywell–Brown potentiometer recorder. The radiation falling on the Golay cell was chopped at 11 c/s. Fig. 3 shows the resolution obtained in the solar spectrum and illustrates the efficacy of the combination of gratings with semiconducting filters in a small and relatively inexpensive instrument.

Two careful tests for stray light from shorter wave-lengths showed this to be an entirely negligible factor. One test was to intercept the solar radiation with metal and glass shutters alternately, the glass shutter admitting radiation below 2·5 μ only. The other test was to compare the solar radiation directly with that from a metal shutter in a region of very strong atmospheric absorption. In both tests the scattered radiation was found to be less than 0·05 per cent.

It is advantageous in photometry to employ a null method, making the brighter beam equal to the weaker by some form of calibrated attenuator, so that the measurements are independent of the properties of the detector. In practice, however, a continuously variable and accurately calibrated attenuator is notoriously difficult to realize (**10**). In the present work a compromise has been made. The intensity of the solar beam was brought into approximate equality ($\pm$ 1 db) with that of the black body by the use of one of a set of four rotating sector disks with transmissions of 0·6227, 0·3991, 0·2504 and 0·1568. These sector disks were accurately machined and calibrated by geometric measurement. They were placed in front of the chopper and interrupted the beam at a frequency of 100 c/s. Since the time constant of the Golay cell is of the order of 0·1 sec, the sectors should produce the theoretical attenuation independently of the 11 c/s chopper; this has been confirmed experimentally by showing that there was no detectable variation in output with sector speeds between 50 and 100 c/s. The measurement of the ratio of intensities of the two nearly-equal beams now places far less stringent demands on the detector linearity. As a further precaution a calibrated electrical attenuator, which can be switched into the circuit to replace the normal gain control of the amplifier, was used to eliminate non-linearity in subsequent stages.

A careful test of the detector linearity was carried out using a constant signal from the black body and the fast rotating choppers as a means of changing the applied signal in a known way. This tested the linearity of the Golay cell and the amplifier combined. The linearity of the amplifier alone was found using the electrical attenuator as a means of changing the applied signal. From these tests it was concluded that errors in the measurements due to lack of linearity were entirely negligible.

3. *Reflectivity measurements.* (*a*) *Collimator mirror for black body* (M_1).—The absolute reflectivity of mirror M_1 was measured by setting it up on a special mount in the laboratory so as to form an image of a large vertical Nernst filament F at I (Fig. 4). Images of F and I were formed in the plane of the spectrometer entrance slit by M_3 and M_4, and by adjustment of the latter either of these may be made to fall on the slit. A good quality flat was used for M_3 to avoid errors arising from the use of slightly different parts of its surface for the two images. An aperture stop S was placed at the image of M_1 by M_4. Possible non-uniformity of temperature over the Nernst filament was allowed for by repeating the measurements after rotating it through 180°.

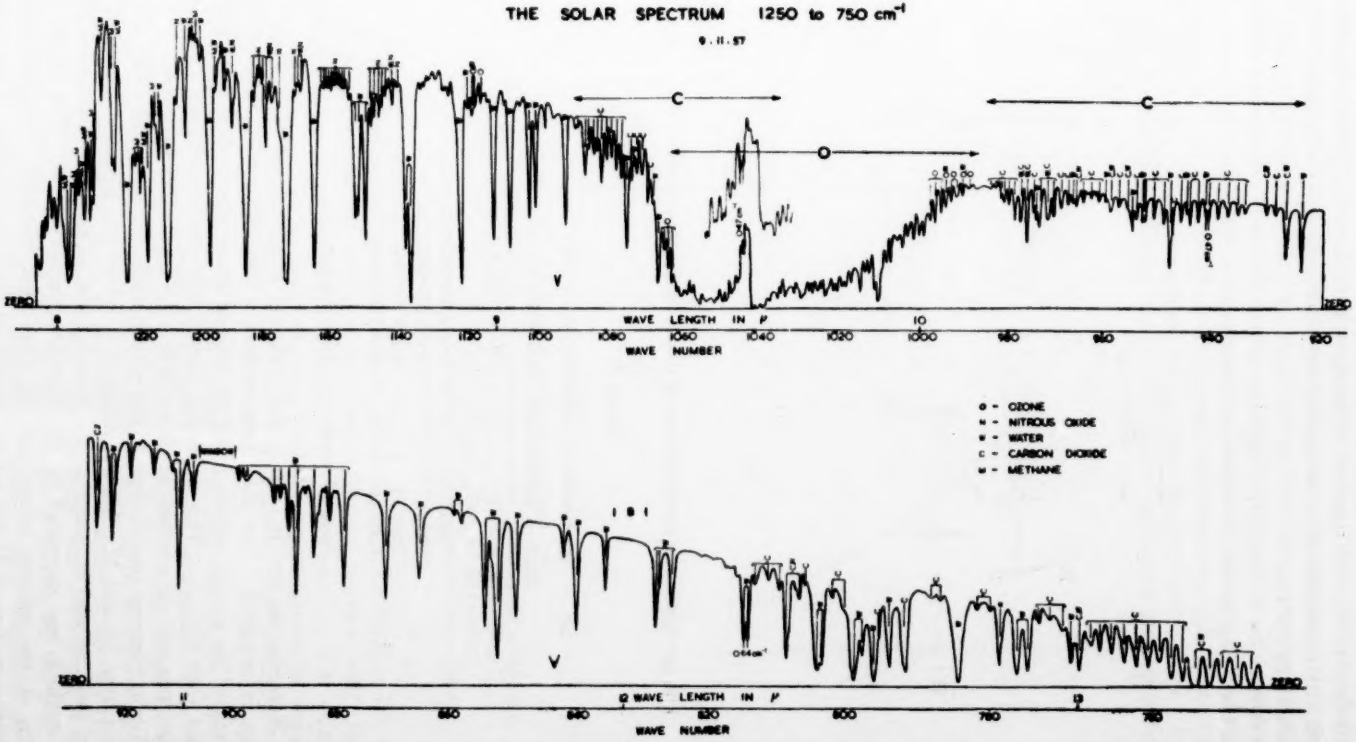

FIG. 3.—*Solar spectrum. The main scale refers to the complete spectrum recorded with unbloomed InSb filter. The small section shows the increased resolution achieved when a bloomed filter was fitted. The* 901 cm^{-1} (11·10 μ) *window used for these observations is marked. The* 832 cm^{-1} (12·02 μ) *window mentioned in the text is indicated by the letter* B.

The holder of M_1 was attached to its stand by a kinematic device, enabling the reflectivity measurement to be made at intervals with minimum disturbances to the observing system.

The reflectivity of this mirror appears to have remained effectively constant over the observing period, as shown by the results in Table I.

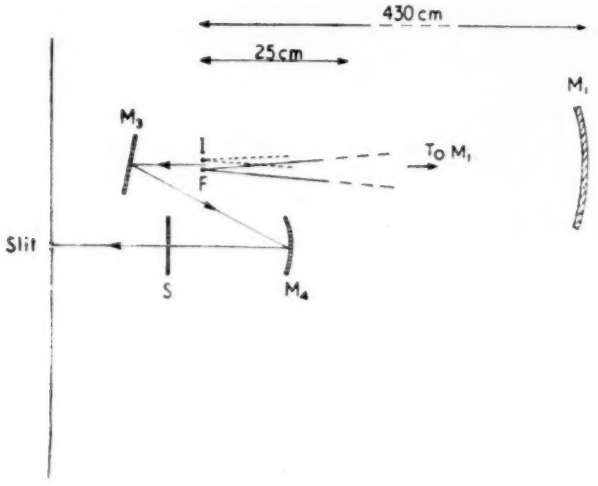

FIG. 4.—*System used for measurement of reflectivity of collimator mirror* M_1.

TABLE I

Reflectivity of collimator mirror M_1

Date of aluminizing: 1958 February 20

Date 1958	Reflectivity
March 21	0.979 ± 0.004
May 7	0.979 ± 0.005
June 23	0.976 ± 0.004
June 30	0.983 ± 0.005
Adopted mean:	0.979 ± 0.003

(*b*) *Siderostat mirror M.*—Only the variation of reflectivity with angle of reflection is required. For this measurement a subsidiary plane mirror M_5 was mounted on an arm which could be rotated about the vertical axis of the siderostat (see Fig. 1). The siderostat mirror was also constrained to rotate about this axis and the azimuth angle could be read from a divided circle.

A Nernst filament placed close to the spectrometer slit sent light to M_5 after reflection from M_2 and M. M_5 was adjusted to return this light along an almost identical path, so that an image of the filament was on the slit. The sensitivity of the method was improved by the double reflection at M. The angles of reflection at the mirrors other than M were kept constant. Unfortunately the reflecting surface of M was 2·5 cm off axis, so that lateral motion of the image

of M_5 occurred for different reflecting angles. A small stop was therefore placed at the image of M_5 by M_2 to ensure that the same reflecting area of M was used for any angular setting (this stop, inside the spectrometer, is not shown in Fig. 1).

Results are shown in Fig. 5 from which a table was drawn up for correcting observational results to a constant angle of reflection, namely that of the black body beam: 37°·5. The observed decrease of reflectivity with increasing angle of reflection may be expected from the presence of a thin layer of dust, which will obscure an increasing fraction of the aluminium surface as grazing incidence is approached.

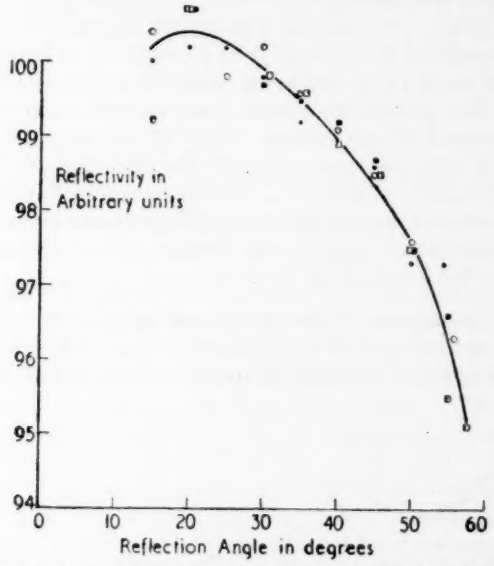

FIG. 5.—*Variation of reflectivity of siderostat mirror* M *with angle of reflection.*
Dates of measurements : 1958 *May* 24, ○ *to East,* ● *to West.*
1958 *July* 20, □ *to East,* ■ *to West.*
No change appears to have occurred over this period and the curve shown was used to correct all the observations.

4. *Observations.*—The observations reported here were made in the window at 11·10 μ (901 cm^{-1}); the slit was 7 mm high and 1·9 mm wide, the latter corresponding to a spectral slit width of 0·031 μ (2·5 cm^{-1}). The diameter of the solar image was 17 mm. Further series of observations in windows at 12·02 μ (832 cm^{-1}) and 8·63 μ (1159 cm^{-1}) are planned when weather conditions permit.

Observations were made from sunrise until deep convection started at 8^h or 9^h G.M.T.; this covered an adequate range of air masses for an accurate extrapolation to zero air mass. Alternate recordings were taken on the Sun and on the black body, using the sector disks and electrical attenuator to make the two deflections as equal as possible. The balancing of the two beams was made to within 2 per cent. When this condition was obtained, the electrical attenuator readings and the ratio of the recorder deflection for the Sun and the black body, together with the reflectivity measurements discussed above, the

transmission of the sector disk used and the temperature of the black body enable the mean solar intensity across the slit (I) to be found for each air mass.

A small correction, at most 0·6 per cent of energy, was applied to allow for the finite emission of the chopper, which was at room temperature. The gain of the electronics changes smoothly by approximately 10 per cent during a four hour run, but the change between any two observations of the black body did not exceed 0·3 per cent and a linear interpolation was used to obtain the black-body deflection at the time of the Sun observation.

The air-mass values calculated from the time were corrected for curvature of the Earth's surface and atmospheric refraction; for this purpose it was assumed from the work of Roach (**11**) that the atmospheric absorption in this part of the spectrum can be assigned to a thin layer at a height of 1·5 km (850 mb). The refractive index of air at 11·1 μ was taken to be $1{\cdot}0_5273$.

Log (I) was then plotted against air mass and the best straight line was obtained by the method of least squares. This line was then used to find log (I_0) by extrapolation to zero air mass. A correction for limb darkening must be applied to give the central intensity $I_\odot$. At this wave-length, and for the portion of the solar disk sampled, the correction is very small, and from limb darkening curves of Pierce, McMath, Goldberg and Mohler (**12**) at 10 μ and results of our own at 11·10 μ we find a correcting factor of 1·002.

5. *Results.*—The weather in the spring and summer of 1958 was so poor that a daily watch at dawn yielded only five useful runs. The plots for individual runs are given in Fig. 6 and the resulting intensities and temperatures in Table II.

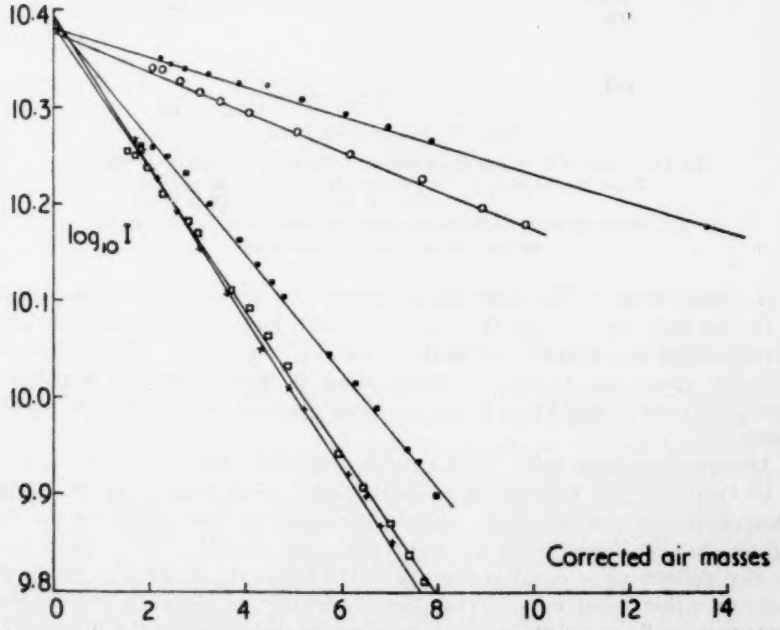

FIG. 6.—*Results of observations :* ● 1958 *April* 2. ○ 1958 *April* 12, □ 1958 *April* 30, ■ 1958 *May* 1, × 1958 *June* 18.

TABLE II

Results of observations of solar emission at 11·10 μ

Date (1958)	S per cent	$\log_{10}(I/B)_0$	T_b °K	w gm cm^{-2}	k (air mass)$^{-1}$	I_0 erg cm^{-2} ster^{-1} sec^{-1} (per cm wave-length range)	σ per cent
April 2	0·5	0·755	1321	0·95	0·0344	$2·408 \times 10^{10}$	0·81
April 12	0·0	0·757	1308	0·55	0·0471	$2·384 \times 10^{10}$	0·74
April 30	0·3	0·760	1312	1·8	0·169	$2·411 \times 10^{10}$	1·46
May 1	1·0	0·764	1313	1·5	0·138	$2·437 \times 10^{10}$	1·83
June 18	1·0	0·773	1307	1·6	0·179	$2·472 \times 10^{10}$	1·63

S = Maximum fraction of slit area covered by sunspots.
k = Extinction coefficient of atmosphere, base e.
T_b = Temperature of black body.
B = Intensity of black body at T_b.
I_0 = Average solar intensity over the slit outside the Earth's atmosphere.
σ = Standard deviation of I_0.
w = Atmospheric water-vapour content in the zenith.

An evaluation of the standard deviation of the regression lines enabled the standard deviation of $\log I_0$ to be found. Hence the standard deviation of I_0 was deduced and is included in Table II.

The values of the sunspot area (S) in Table II have been estimated from photographs kindly supplied by the Astronomer Royal. Their effect on the measurements is probably negligible, since the brightness contrast between spot and photosphere is likely to be small at this wave-length. The atmospheric extinction coefficient (k), deduced from the slope of the lines in Fig. 6, is also included in Table II, and so is an estimate from Meteorological Office Daily Aerological Records of the water-vapour content of the atmosphere, with which it shows a rough, not necessarily direct, correlation. The origin of this extinction is of considerable meteorological interest and is being further investigated.

Taking a mean of the intensities in Table II with weights proportional to the inverse square of the standard deviation, and applying corrections for limb darkening and deviation of the black body from a perfect enclosure, we obtain $I_\odot(11·10\mu) = 2·408 \times 10^{10}$ erg cm^{-2} ster^{-1} sec^{-1} (per cm wave-length range).

6. *Discussion.*—The standard deviation of the weighted mean of the five measurements of $I_\odot$ is 0·52 per cent. This includes indirectly the effect of errors in the measurements of the records, and any rapid changes of the atmospheric transmission. There are also possible systematic errors of measurement as follows: reflectivity of M (0·3 per cent); temperature of the black body (0·2 per cent); variation of reflectivity of M (0·2 per cent); attenuation of the sector disks (0·04 per cent). Combining these, an estimate of the error of $I_\odot$ was found to be ±0·67 per cent. Hence,
$I_\odot(11·10\mu) = 2·408 \pm 0·016 \times 10^{10}$ erg cm^{-2} ster^{-1} sec^{-1} (per cm wave-length range).
Using the data of Allen (14) this intensity corresponds to a black-body temperature of

$$T_\odot(11·10\mu) = 5036 \pm 30 \text{ °K}.$$

This result taken together with those of Peytureux (**2**) at 1·55, 2·03, 2·31 μ where $T_{\odot}$ was found to be 6330, 6045 and 5880 °K respectively (the results of Pierce (**3**) are in excellent agreement) is in line with the expected decrease of temperature with increasing wave-length. It also fits in with an effective temperature of 4500 °K at 6 mm as measured by Whitehurst *et al.* (**4**). There is however a possible discrepancy with the measurements of Coates (**13**) who gives a temperature of 6962 °K at 4·5 mm.

Acknowledgments.—We are indebted to Dr C. D. Walshaw for help with the observations and the composition of the paper; to Professor C. W. Allen for his interest and advice in the astrophysical questions involved; and to Dr W. T. Roach for designing the black body and some other preliminary work.

Department of Meteorology,
Imperial College,
*London, S.W.*7 :
1959 *February* 19.

References

(1) Minnaert, M., *The Sun*, ed. G. P. Kuiper, p. 88, University of Chicago Press, 1952.
(2) Peyturaux, R., *Ann. d'Astrophys.*, **15**, 302, 1952.
(3) Pierce, A. K., *Ap. J.*, **119**, 312, 1954.
(4) Whitehurst, R. N., Copland, J. and Mitchel, F. H., *J. App. Phys.*, **28**, 295, 1957.
(5) Migeotte, M., Neven, L. and Swenson, J., *The Solar Spectrum from* 2·8–23·7 *Microns*, Pts. 1 and 2, Mém. Soc. Roy. des Sciences de Liège, Special volumes Nos. 1, 2; Sections 85 and 86, 1956.
(6) Shaw, J. H., Oxholm, M. L. and Claassen, H. H., *Ap. J.*, **116**, 554, 1952.
(7) Roach, W. T. and Goody, R. M., *Quart. J. R. Met. Soc.*, **84**, 319, 1958.
(8) Tingwaldt, C., *Z. Instr.*, **65**, 7, 1957.
(9) Smith, S. D. and Moss, T. S., *J. Sci. Inst.*, **35**, 105, 1958.
(10) Normand, Sir C. and Kay, R. H., *J. Sci. Inst.*, **29**, 33, 1952.
(11) Roach, W. T., A quantitative study of the atmospheric infra-red absorption and emission properties in the region 8–13 μ. Dissertation, London University, 1957.
(12) Pierce, A. K., McMath, R. R., Goldberg, L. and Mohler, O. C., *Ap. J.*, **112**, 289, 1950.
(13) Coates, R. J., *Ap. J.*, **128**, 83, 1958.
(14) Allen, C. W., *Astrophysical Quantities*, p. 100, London (Athlone Press), 1955.

THE MAGNETIC AND DYNAMICAL FIELDS OUTSIDE A PROTO-STAR

L. Mestel

(Received 1959 March 7)*

Summary

A contracting proto-star formed in a magnetic cloud conserves its magnetic flux provided the plasma density does not become too low. In this paper the structure of the external field is studied, together with its effect on the flow of matter. Centrifugal force is assumed always negligible, and the star is supposed at rest in the cloud. The fields in the star and at infinity are both taken as uniform, and the flow is assumed isothermal.

Possible equilibrium fields include :

(i) A poloidal field, with all the lines of force extending to infinity, but with a small toroidal component strong enough to keep the centrifugal field small in spite of the inflow of matter. The field is weak at the equator, but the lines of force make sharp hairpin bends there, yielding a pinched equatorial discharge.

(ii) A poloidal field, with some of the stellar field lines finite, separated by a ring of X-type neutral points from the infinite field lines, which have a structure similar to field (i).

(iii) A twisted, torque-free, and approximately force-free field confined within a finite surface S, and an approximately curl-free field beyond S.

If the cloud field initially contains toroidal flux threading poloidal loops, then type (iii) will result; otherwise, types (i) and (ii) are the relevant equilibrium fields, applying respectively to earlier and later stages in the star's contraction.

The presence of the field alters the accretion problem somewhat. Solutions exist with supersonic and subsonic velocities at infinity, yielding respectively an increased or diminished accretion rate. In the absence of an external strong pressure field at infinity, the system is likely to approach the state with the lower rate, so that the presence of the field reduces the accretion rate substantially below Bondi's value.

Introduction.—The problem of star formation in a strongly magnetic gas cloud was discussed in a recent paper (1). If the cloud field is assumed to have the strength required by current theories of interstellar polarization, cosmic-ray acceleration, and synchrotron radiation, the cloud must have a mass at least of order $10^3 \odot$ if it is to withstand the magnetic and thermal pressures. If, further, the field is frozen into the cloud, this lower limit is hardly reduced if the cloud contracts, and it is difficult to see how masses of stellar order could spontaneously form. The difficulty is resolved when it is recognized that the magnetic field in an H I cloud is tied to the plasma rather than to the gas as a whole, so that if the frictional coupling between plasma and neutral gas is weak enough, the bulk of the cloud can contract without dragging the field with it. In a dense dust cloud, obscured from galactic ionizing radiation, the plasma density can

* Received in original form 1958 May 16

decay rapidly to a value low enough—approximately one per cent of the equilibrium value—for the two gases to be effectively uncoupled; neutral matter condenses across the magnetic field, high densities are built up without a corresponding high magnetic energy, and stars can form without magnetic impedance.

We now suppose that a proto-star has been formed, and that effective freezing-in of the magnetic field into the stellar matter has been re-established. This is certainly the case when the internal temperatures exceed 10^4 °K, the ionization temperature of hydrogen, while at lower temperatures the plasma–hydrogen friction for normal plasma densities is enough to prevent any sensible drift of plasma plus field through the neutral gas (1). In this paper attention is focused on the magnetic field external to the star, and its interaction with the flow of matter due to the star's gravitational field. Thus we are interested to know whether an initially poloidal field remains so, or whether it acquires a toroidal component; at what stage the stellar lines of force break off from the galactic field; and whether the field affects substantially the rate of accretion of matter by the star.

We consider the case of a contracting proto-star at rest in a cloud. Although we expect the cloud to be lightly ionized (an H I region), we shall also discuss the simpler case of a fully ionized (H II) region. There is a third possibility: the cloud may be lightly ionized beyond a critical surface, but wholly ionized within it. This could be due to compressional or frictional heating of inflowing neutral hydrogen, or, if the star is massive and has reached the main sequence, to stellar ultra-violet radiation. This case, which will demand study of the hydromagnetic shock at the critical radius, is postponed for separate treatment.

The magnetic field at large distances from the star ($\mathbf{H}_0$) is supposed uniform, it being a part of the local galactic field, and maintained by currents that flow in dimensions large compared with the relevant part of the cloud. For simplicity, the stellar contraction is taken as approximately homologous, so that within the star the field ($\bar{\mathbf{H}}$) is uniform and parallel to $\mathbf{H}_0$, except in a narrow surface region (cf. Section 2). The name "stellar flux tube" will be given to the tube generated by those lines of force that cut the star.

In the absence of a magnetic field, the velocity–density field of all the cloud matter (neutral and ionized) would approach the spherically-symmetric, temperature-limited pattern discussed by Bondi (2). For simplicity, let us suppose that initially the magnetic forces are weak, so that the field does not impede the flow, but rather the ionized matter distorts the field until it begins to exert forces comparable with gravity. Clearly a steady state is approached, in which no further dragging of the field takes place, the flow of ionized matter across the field being just the rate permitted by the high conductivity. The magnetic force is then balanced by the components across the field of the non-magnetic forces, including inertial forces, acting on the plasma—a familiar situation in steady state hydromagnetics. In particular, we shall find that in some regions the magnetic force compresses the plasma so as to build up a pressure gradient strong enough to balance it, just as in the well-known laboratory "pinch effect".

Simultaneously, the flow pattern approaches a steady state. Except in regions of very low field strength, the flow of plasma across the field is negligible; but along field lines of infinite length, there will be a steady flow of plasma, either

directly into the star, or towards the equator outside the star. The plasma density at the equator will grow until the rate of influx down the field lines is balanced by the rate of recombination, so that the neutralized plasma can drift across the field into the star*. If the cloud were fully ionized all the flow would be of this type; however, in a lightly ionized cloud neutral matter can drift across the field, but its motion is restricted by the frictional drag of the plasma. Although neutral matter does flow across the field into the star, Bondi's spherically symmetric velocity field will be distorted even for the neutral gas by the indirect effect of the magnetic field, acting through plasma–hydrogen collisions.

We are assuming implicitly that rotation in the cloud is never rapid enough to yield a centrifugal field comparable with gravity. If this is so at any time, then a strong enough magnetic field will ensure that the inflow of matter does not lead to the subsequent build-up of a strong centrifugal field. However, if the star is rotating it will tend to set the cloud rotating as well; we require that this transfer of angular momentum from the star to the cloud is rapid compared with the rate of contraction of the star, so that the stellar angular momentum is quickly distributed over the cloud, and no important centrifugal field arises. This at once shows the importance of knowing in detail the structure of the stellar magnetic field: clearly, if many lines of force have broken off from the galactic field and so do not extend to infinity, the field will be much less efficient in removing angular momentum.

Although the discussion of this paper is in terms of a *proto-star* containing a frozen-in magnetic field, similar conclusions could apply on a larger scale. Thus consider a freely-falling gas cloud of say 10^3 solar masses, and with a strong frozen-in magnetic field: the rather special conditions discussed in (1) for uncoupling of the field and the bulk of the cloud may not obtain, so that the frozen-in field prevents break-up into smaller masses. Then if the scale of the local galactic field is large compared with the cloud's dimensions, the problem is essentially that of this paper. As long as most of the cloud field lines are of infinite length, magnetic transport of angular momentum will probably keep low the rotation of the cloud, and no strong centrifugal field, either internal or external, will be built up. However, once the cloud field is mainly broken off from the galactic field, again we may expect much less efficient removal of angular momentum, and the probable build-up of a strong centrifugal field within the cloud; this will slow up or halt the cloud's contraction, and in particular allow more time for the strong internal magnetic field to leak out, as discussed in (1). In this way excess magnetic energy may be lost, at the cost of leaving a rapidly rotating cloud with a weak magnetic field. Further discussion is beyond the scope of this paper, but we may anticipate that the further evolution of the cloud would be in part determined by the slow interaction of the magnetic field with the rotation field (3).

Part I

The magnetic field

1. *The equations to the field outside the star.*—Although the boundary conditions imposed on the field refer only to the poloidal components, we allow for the possibility that the field has both a poloidal component H_p and a toroidal

* The probable importance of recombinations in this context was pointed out to the author by Dr A. Schlüter.

component $\mathbf{H}_t$, both assumed symmetric about an axis. The magnetic force density can then be written

$$\frac{(\nabla\wedge\mathbf{H})\wedge\mathbf{H}}{4\pi} = \frac{[(\nabla\wedge\mathbf{H}_p)\wedge\mathbf{H}_p+(\nabla\wedge\mathbf{H}_t)\wedge\mathbf{H}_t]}{4\pi} \text{ (poloidal component)}$$

$$+\frac{(\nabla\wedge\mathbf{H}_t)\wedge\mathbf{H}_p}{4\pi} \text{ (toroidal component)}, \tag{1}$$

the term $(\nabla\wedge\mathbf{H}_p)\wedge\mathbf{H}_t/4\pi$ vanishing identically.

The poloidal part of the magnetic force has a component

$$-\left[(\nabla\wedge\mathbf{H}_t)\wedge\mathbf{H}_p.\mathbf{H}_t\right]\frac{\mathbf{H}_p}{4\pi H_p^2} \tag{2}$$

in the direction of $\mathbf{H}_p$, and a component

$$\left[\nabla\wedge\mathbf{H}_p-\frac{(\nabla\wedge\mathbf{H}_t).\mathbf{H}_p}{H_p^2}\mathbf{H}_t\right]\wedge\frac{\mathbf{H}_p}{4\pi} \tag{3}$$

across $\mathbf{H}_p$. Let the poloidal non-magnetic forces (including inertial forces) acting on the plasma have a density $\mathbf{F}_p$, so that they have a component $\mathbf{H}_p\wedge(\mathbf{F}_p\wedge\mathbf{H}_p)/H_p^2$ across $\mathbf{H}_p$. As remarked in the Introduction, the distortion of the field ceases when the magnetic forces become strong enough, so that the equation defining the steady-state field is

$$\nabla\wedge\mathbf{H}_p-\frac{(\nabla\wedge\mathbf{H}_t).\mathbf{H}_p}{H_p^2}\mathbf{H}_t=4\pi\frac{\mathbf{F}_p\wedge\mathbf{H}_p}{H_p^2}. \tag{4}$$

It is convenient to introduce the following representation (4) in spherical polar coordinates (r,θ,ϕ) for a field symmetric about the axis $\theta=0$:

$$H_r=-\frac{1}{r^2\sin\theta}\frac{\partial P}{\partial\theta}, \qquad H_\theta=\frac{1}{r\sin\theta}\frac{\partial P}{\partial r}, \qquad H_\phi=-\frac{T}{r\sin\theta}, \tag{5}$$

where the scalars P and T are functions of r and θ only. The condition $\nabla.\mathbf{H}=0$ is automatically satisfied, and P is constant along a line of force. The current density $\mathbf{j}=(c/4\pi)\nabla\wedge\mathbf{H}$ is given by

$$\left.\begin{aligned}\frac{4\pi}{c}j_r&=-\frac{1}{r^2\sin\theta}\frac{\partial T}{\partial\theta}, \qquad \frac{4\pi}{c}j_\theta=\frac{1}{r\sin\theta}\frac{\partial T}{\partial r}\\ \frac{4\pi}{c}j_\phi&=\frac{1}{r}\left\{\frac{\partial}{\partial r}\left(\frac{1}{\sin\theta}\frac{\partial P}{\partial r}\right)+\frac{1}{r^2}\frac{\partial}{\partial\theta}\left(\frac{1}{\sin\theta}\frac{\partial P}{\partial\theta}\right)\right\}.\end{aligned}\right\} \tag{6}$$

We now discuss in general terms the different fields satisfying (6) and the boundary conditions. The simplest field is everywhere poloidal, so that $T=0$, and

$$\nabla\wedge\mathbf{H}_p=4\pi\frac{\mathbf{F}_p\wedge\mathbf{H}_p}{H_p^2}. \tag{7}$$

Such a field demands that the flow of matter be strictly in meridian planes—each element of matter in the cloud must have zero angular momentum about the axis of the field.

Next, we allow the field to have a toroidal component, but restrict the poloidal currents $\mathbf{j}_p$ to flow everywhere parallel to $\mathbf{H}_p$, so that the field exerts no torque about the axis of symmetry. By (5) and (6) this yields the condition

$$T=f(P), \tag{8}$$

so that T is constant along a line of force; also

$$\nabla \wedge \mathbf{H}_t=f'(P)\mathbf{H}_p. \tag{9}$$

In this case the toroidal field contributes to the equation (4) for $\mathbf{H}_p$ through the term

$$-\frac{(\nabla \wedge \mathbf{H}_t)\cdot \mathbf{H}_p}{H_p^2}\mathbf{H}_t=\frac{f(P)f'(P)}{r\sin\theta}\mathbf{t}, \tag{10}$$

$\mathbf{t}$ being a unit vector in the ϕ-direction. We can now see that such a field, with poloidal currents flowing strictly parallel to $\mathbf{H}_p$, cannot have lines of force extending to infinity. We are assuming that $\mathbf{H}_p$ reduces at infinity to the uniform field $\mathbf{H}_0$, corresponding to

$$P\to -\tfrac{1}{2}H_0r^2\sin^2\theta. \tag{11}$$

Let us consider the field line, assumed of infinite length, defined by a particular value of P, so that far from the star

$$(r\sin\theta)\simeq\left(-\frac{2P}{H_0}\right)^{1/2}. \tag{12}$$

The toroidal component $H_\phi=-T/r\sin\theta$; hence if we assert that the field remains untwisted at infinity, then T must vanish at infinity, and so everywhere along the line of force considered. Alternatively, if we assume that the cloud has uniform density and temperature at infinity, so that the pressure gradient vanishes, we need not require *a priori* that H_ϕ vanishes at infinity; for as $r\to\infty$ along the field line P, $(r\sin\theta)$ approaches (12), and the equation (4) to $\mathbf{H}_p$ will not hold unless $f(P)f'(P)=0$ at infinity, and so all the way along the line P. If $f(P)=0$, then $H_\phi=0$, while the case $f(P)=$ constant is ruled out as it yields a singularity on the axis.

The strictly torque-free field must therefore consist of two parts: an inner region, bounded by a surface S, with a toroidal field component maintained by poloidal currents flowing parallel to the poloidal field, and an outer region with the field purely poloidal. Within S the field lines are closed loops, but they may or may not enter the star. There can be no continuous flow of plasma within S, as no lines of force cross S. Plasma initially within S will flow down the field lines but will not be replenished. Depending on the geometry of the field line considered, it will either be swallowed up by the star, or it will flow towards the equator to form "dead" zones; some will be neutralized and flow into the star across the field, but there would probably remain a nucleus of "dead" plasma, drifting across the field only at the rate permitted by the high conductivity.

The torque-free field is therefore self-consistent; if there were a steady flow of plasma, it would in general require a toroidal magnetic force to keep the angular momentum of the plasma at the correct value for the flow to follow the field. As a further consequence of the depletion of plasma, the field within S will approximate to the *force-free* field, in which all the current flow is parallel to the field; for as the plasma drains away, the non-magnetic force $\mathbf{F}_p\to 0$, and so only in the dead zones will the steady-state magnetic field exert a force. (However, it is pushing the argument too far to assert that a complete vacuum results, with zero currents and a curl-free field. A minute electron density is quite capable of carrying the currents required to maintain fields of cosmical scale.)

We have explicitly excluded centrifugal force as an important contribution to the non-magnetic force $\mathbf{F}_p$. However, the matter in the cloud will certainly have some angular momentum about the axis of the field. We may expect a continuous inward flow of matter down infinite field lines, each element tending to conserve its angular momentum, and an initially poloidal field $\mathbf{H}_p$ will therefore be twisted by differential rotation. The torque so generated opposes the increase of angular velocity, but a weak field $\mathbf{H}_p$ would still be unable to prevent the ultimate build-up of a centrifugal field balancing gravity. The magnetic field would certainly play a role in the subsequent evolution of the system, but clearly the problem is quite different from that considered in this paper. On the other hand, if $\mathbf{H}_p$ is strong, a very slight twist will generate a torque strong enough effectively to cancel out the increase in centrifugal force. This is assumed to be the case; it remains to verify that the slight toroidal field $\mathbf{H}_t$ generated by the inflow exerts a poloidal force weak compared with that exerted by $\mathbf{H}_p$.

We obtain as follows a rough criterion for centrifugal force to remain negligible. Suppose an element of gas flows a distance $\delta\varpi$ towards the axis, with velocity v_ϖ, in time $\delta\varpi/v_\varpi$. If the cloud is fully ionized, or, although lightly ionized, sufficiently dense for both components to flow closely together, then non-uniformities in rotation between two points will be magnetically removed in the time that a hydromagnetic wave takes to travel from one point to the other. Our criterion is therefore:

$$\frac{\delta\varpi}{v_\varpi} \gg \frac{\delta\varpi}{H_p/(4\pi\rho)^{1/2}}$$

(ρ being the density), or

$$\frac{H_p^2}{8\pi} \gg \tfrac{1}{2}\rho v_\varpi^2; \tag{13}$$

the poloidal magnetic energy density should exceed the energy density of the inward motion.

We shall return to this condition in Part II, after the magnetic and dynamical fields have been studied. For the moment let us assume condition (13) holds for field lines of infinite length, along which there is a continuous flow of matter, and note the effect on the equations to the magnetic field. The magnetic torque generated by the inflow will be of order

$$\varpi\left|\frac{(\nabla\wedge\mathbf{H}_t)\wedge\mathbf{H}_p}{4\pi}\right| \simeq \rho\mathbf{v}\,.\,\nabla(\Omega\varpi^2) \simeq \rho\varpi v_\varpi\Omega, \tag{14}$$

where Ω is the angular velocity, and ϖ the distance from the axis. Thus the order of H_t is

$$H_t \simeq \frac{4\pi\rho v_\varpi\varpi\Omega}{H_p}. \tag{15}$$

Poloidal currents perpendicular to $\mathbf{H}_p$ make no contribution to the correcting term, involving $\mathbf{H}_t$, in the equation (4) to $\mathbf{H}_p$. However, by continuity there must also be a component of $\mathbf{j}_p$ parallel to $\mathbf{H}_p$, or comparable order, otherwise there would have to be current sources on the axis of symmetry; hence the ratio of the correcting term in (4) to $\mathbf{F}_p$ is by (13), (14) and (15) of order

$$\frac{\rho v_\varpi\Omega H_t}{F_p H_p} \sim \frac{(\rho v_\varpi\Omega)(4\pi\rho v_\varpi\varpi\Omega)}{F_p H_p^2} \ll \frac{\rho\Omega^2\varpi}{F_p} \ll 1. \tag{16}$$

We may therefore conclude that if the poloidal field is strong enough to keep the centrifugal force density small compared with $\mathbf{F}_p$—i.e. if (13) is satisfied—then the magnetic field has a poloidal part, hardly differing from the solution of (4), together with a small toroidal component. A flow of current along $\mathbf{H}_p$, much greater than that across it, would again not be consistent with the conditions at infinity, and so is not relevant to the case of infinite field lines with continuous flow of matter.

2. *The boundary conditions.*—At infinity the poloidal function P must reduce to (11); this takes care of both components of the field. One more condition may be imposed on (4); the continuity of the normal component of the field at the stellar surface yields

$$H_r = \bar{H} \cos\theta \tag{17}$$

at $r = R$, where $\bar{H}$ is the magnitude of the frozen-in, uniform field within the star, given by (21) below. However, there will in general result a discontinuity in the tangential component, as there is no reason why H_θ given by the solution of (4) should equal $-\bar{H}\sin\theta$. Such a discontinuity demands a finite surface current and an infinite force density, and so is clearly forbidden. The field lines within the star must be distorted near the surface so as to link up smoothly with the external field. As a rough estimate of the distortion, suppose the field remains straight within most of the star, but bends in a surface layer of thickness l. The resulting magnetic force cannot exceed the gravitational force; let us estimate l by equating them:

$$\frac{\bar{H}^2}{4\pi l} \simeq \left(\frac{GM}{R}\right)\left(\frac{M}{\frac{4}{3}\pi R^3}\right)\left(\frac{1}{R}\right). \tag{18}$$

Hence if the stellar magnetic energy is small compared with the gravitational, $l \ll R$, and the distortion is limited to the surface. The change in H_r through the surface zone is found from the divergence condition to be $\simeq lH_r/R$, so that the condition (17) remains accurate. But in a star with the magnetic energy, comparable with the gravitational—so that the field is at the limit for the star to be gravitationally bound—the distortion of the field spreads through the whole star. Condition (17) ceases to be accurate, and the more complicated boundary condition will react on the external field. Discussion of the internal field requires study of the equilibrium of the star and the progressive distortion of the field as the star contracts, and is beyond the scope of this paper. However, it is reasonable to assume that the star retains an internal dipole component of field, of strength approximately $\bar{H}$, so that (17) is a fair approximation to make in studying the main features of the external field at different stages of the star's contraction.

If the external field is twisted, there must be a toroidal component within the star. Consider first the force-free fields. As the lines of force emanating from the star are of finite length, they cannot steadily transfer angular momentum to the galaxy (4, 5); hence in a steady state the field must be torque-free within the star as well as without. If initially the internal field exerts a torque, it will oscillate about the torque-free state; there will be a periodic redistribution of angular momentum along the lines of force, but no continuous net transfer of angular momentum outwards. By contrast, field lines of infinite length can transfer angular momentum steadily out of the star into the cloud, and the internal

field could very well exert a permanent torque. Further discussion must await detailed study of the problem of a rotating magnetic system.

3. *The curl-free and force-free approximations.*—We have arrived at the following possibilities:

(i) A poloidal field with $\mathbf{H}_p$ satisfying (7). The lines of force are of infinite length, and there is a continuous flow of matter, strictly in meridian planes.

(ii) The field approximately as in (i), but with a small toroidal component superimposed, exerting a small toroidal force sufficient to keep the centrifugal field small, and making a small contribution to the equation (4) to $\mathbf{H}_p$.

(iii) The partially force-free fields, in which the current flow is strictly parallel to the field within a surface S, but which is of type (i) or (ii) outside S.

We arrived at case (iii) by showing that a torque-free field must be broken off from the local galactic field; no continuous flow of plasma can result, and so the plasma density must become very small nearly everywhere within S. However, as pointed out by Lüst and Schlüter (**6**), if the magnetic field is strong, very small currents across the field will yield forces comparable with the non-magnetic forces acting; the term on the right of (4) will therefore be small compared with the largest terms on the left, even if the plasma density were maintained by flow from outside S. This argument applies as well to the case (i), so that as a first approximation it is tempting to drop the term in $\mathbf{F}_p$ in (7). The untwisted force-free field is the *curl-free* field; but this case should be clearly distinguished from the *vacuum* field, for which the curl vanishes through there not being any charges present to carry current. In our case the current density is not zero, but is given by (7). In using $\nabla \wedge \mathbf{H}_p = 0$ to compute the field, we are asserting that for large H_p, the term $4\pi|\mathbf{F}_p \wedge \mathbf{H}_p|/H_p^2$ is small compared with $\partial(rH_\theta)/r\partial r$ and $-\partial H_r/r\partial\theta$ which together make up $\nabla \wedge \mathbf{H}$, so that these two terms are approximately equal.

We now discuss the untwisted and twisted force-free fields.

(*a*) *The untwisted field.* The curl-free field reducing to $\mathbf{H}_0$ at infinity, and continuous with $H_r = \bar{H}\cos\theta$ at $r = R$, has components

$$\left.\begin{aligned} H_r &= \left[H_0 + (\bar{H} - H_0)\left(\frac{R}{r}\right)^3\right]\cos\theta, \\ H_\theta &= \left[-H_0 + \tfrac{1}{2}(\bar{H} - H_0)\left(\frac{R}{r}\right)^3\right]\sin\theta, \\ H_\phi &= 0, \end{aligned}\right\} \tag{19}$$

and scalar function

$$P = -\tfrac{1}{2}H_0 r^2 \sin^2\theta\left[1 + \left(\frac{\bar{H}}{H_0} - 1\right)\left(\frac{R}{r}\right)^3\right]. \tag{20}$$

The internal stellar field $\bar{H}$ is given by

$$\bar{H} = H_0\left(\frac{R'}{R}\right)^2, \tag{21}$$

where R' is the radius at which the freezing of the field into the contracting proto-star is considered to have begun. If $\bar{H} > 3H_0$ the field (19) has a neutral point on the equator at the radius

$$r = R\left(\frac{\bar{H} - H_0}{2H_0}\right)^{1/3}. \tag{22}$$

Hence once $R < R'\sqrt{3}$, the general shape of the field will be as in Fig. 1 so that many, though not all, of the lines of force in the stellar flux tube are of finite length.

(*b*) *The class of twisted fields.* The boundary conditions on the field restrict P to be proportional to $\sin^2\theta$ at the star and at infinity; for simplicity, we consider only fields with $P \propto \sin^2\theta$ everywhere. We have seen in Section 1 that the torque-free condition $T = f(P)$ implies that twisted lines of force cannot extend to infinity. Hence beyond a certain surface S, the toroidal function $T = 0$, and again the field is approximately curl-free, with

$$P = -\tfrac{1}{2}H_0 r^2 \sin^2\theta\left(1 - \frac{A}{r^3}\right), \tag{23}$$

A being a constant. Within S, $T = f(P)$ and from (4) and (9) P satisfies

$$\frac{\partial^2 P}{\partial r^2} + \frac{(1-\mu^2)}{r^2}\frac{\partial^2 P}{\partial \mu^2} = -f(P)f'(P), \tag{24}$$

with $\mu = \cos\theta$; hence $f(P)f'(P) \propto P$, and so $T = f(P) = \alpha P$, with α constant. On S, T must vanish; hence P also vanishes on S, which must therefore from (23), be a sphere of radius r_c, with $A = r_c^3$.

Thus outside the sphere r_c, the field has the form

$$\left.\begin{aligned} H_r &= H_0\cos\theta\left(1 - \left(\frac{r_c}{r}\right)^3\right), \\ H_\theta &= -H_0\sin\theta\left(1 + \tfrac{1}{2}\left(\frac{r_c}{r}\right)^3\right), \\ H_\phi &= 0. \end{aligned}\right\} \tag{25}$$

Within r_c, the twisted force-free field is of the simple type discussed by Lüst and Schlüter (6) and Chandrasekhar (7), in which the scalar of proportionality between current density and field is constant not only along each twisted line of force, but over the whole region considered. P satisfies

$$\frac{\partial^2 P}{\partial r^2} + \frac{(1-\mu^2)}{r^2}\frac{\partial^2 P}{\partial \mu^2} = -\alpha^2 P, \tag{26}$$

and so is of the form (7)

$$P = -r^{1/2}(1-\mu^2)[AJ_{3/2}(\alpha r) + BJ_{-3/2}(\alpha r)], \tag{27}$$

where $J_{\pm 3/2}$ are the Bessel functions of order $\pm 3/2$, and A and B are constants. The field components are

$$\left.\begin{aligned} H_r &= \frac{2\cos\theta}{r^{3/2}}[AJ_{3/2}(\alpha r) + BJ_{-3/2}(\alpha r)], \\ H_\theta &= -\frac{\sin\theta}{r}\frac{d}{dr}\{r^{1/2}[AJ_{3/2}(\alpha r) + BJ_{-3/2}(\alpha r)]\}, \\ H_\phi &= \frac{\alpha\sin\theta}{r^{1/2}}[AJ_{3/2}(\alpha r) + BJ_{-3/2}(\alpha r)]. \end{aligned}\right\} \tag{28}$$

The continuity of H_r at R and of H_r, H_θ and H_ϕ at r_c gives

$$\left.\begin{aligned} &AJ_{3/2}(\alpha r_c)+BJ_{-3/2}(\alpha r_c)=0,\\ &\bar{H}=\frac{2}{R^{3/2}}\left[AJ_{3/2}(\alpha R)+BJ_{-3/2}(\alpha R)\right],\\ &\tfrac{3}{2}H_0=\frac{\alpha}{r_c^{1/2}}\left[AJ'_{3/2}(\alpha r_c)+BJ'_{-3/2}(\alpha r_c)\right]. \end{aligned}\right\} \tag{29}$$

Thus once $\bar{H}$ and H_0 are given, there is a single infinity of solutions, depending on the choice of r_c. The condition of continuity of j_r at r_c is satisfied, as $(\nabla\wedge\mathbf{H})_r=\alpha H_r$ vanishes as r_c is approached from within.

The general shape of the poloidal field is shown in Fig. 2. It is seen that between R and r_c there is another sphere r' on which $H_r=H_\phi=0$. This is a consequence of the fields $\mathbf{H}_0$ and $\bar{\mathbf{H}}$ having identical senses. At r_c and r' there are neutral points on the axis in both hemispheres. The poloidal part of the field vanishes on the equator between r_c and r' at the ring of points given by

$$[r^{1/2}(AJ_{3/2}+BJ_{-3/2})]'=0,$$

but the toroidal field is non-zero there. Clearly Fig. 2 is the simplest of type (*b*) fields; any number of pairs of zones, each similar to the zone between r' and r_c, may be included within the final sphere, beyond which the field is curl-free and untwisted.

An essential feature of the field (*b*) is the presence of linked lines of force within r_c. The total magnetic flux across a closed loop of the field $\mathbf{H}_p$ does not vanish: as the lines of $\mathbf{H}_p$ are also the lines of $\mathbf{j}_p$, this follows from elementary magnetic theory. In the present case, we have

$$\int_A \mathbf{H}_t\,.\,d\mathbf{A}=\frac{c}{4\pi\alpha}\int_A(\nabla\wedge\mathbf{H}_p)\,.\,d\mathbf{A}=\frac{c}{4\pi\alpha}\oint_C\mathbf{H}_p\,.\,\mathbf{ds}\neq 0, \tag{30}$$

where A is the area in a meridian plane bounded by C, a closed loop of $\mathbf{H}_p$. This is the vital distinction between these fields and those which are just poloidal fields with a toroidal component generated by non-uniform rotation, without any linked flux (cf. the following note).

A different choice of $f(P)$ (subject to the condition that $H_\phi=-f(P)/r\sin\theta\to 0$ on the axis) yields a non-linear equation for P within the surface S (which will not be a sphere in general). The resulting fields will be much more difficult to express mathematically but will not differ qualitatively from the special field given by (25) and (28).

4. *The limitations of the curl-free and force-free approximations.*—An immediate test of the validity of either approximation can be made by computing the neglected term $4\pi\mathbf{F}_p\wedge\mathbf{H}_p/H_p^2$, with the previously computed field $\mathbf{H}_p$ substituted, and comparing it with the other terms in (7). The non-magnetic forces $\mathbf{F}_p$ are given when the density–velocity field is known. This problem is postponed until Part II but we may anticipate that the plasma density along infinite field lines —maintained by continuous inflow—will not in general give rise to large pressure gradients normal to field lines, so that the force density $\mathbf{F}_p$ is at most of the order of the total gravitational force density; also, the densities do not exceed the

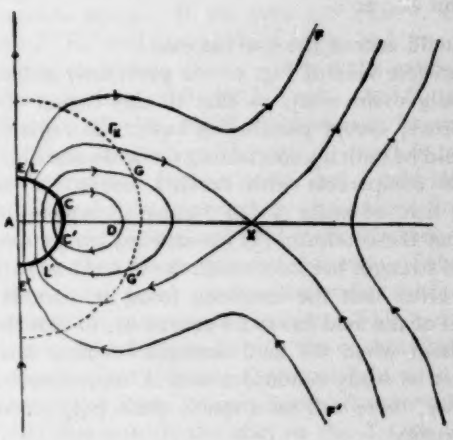

FIG. 1.—*Type (a).*

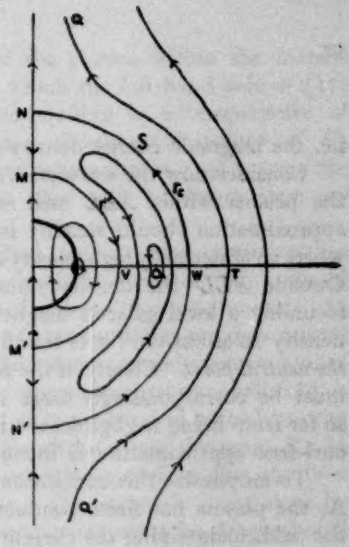

FIG. 2.—*Type (b).*

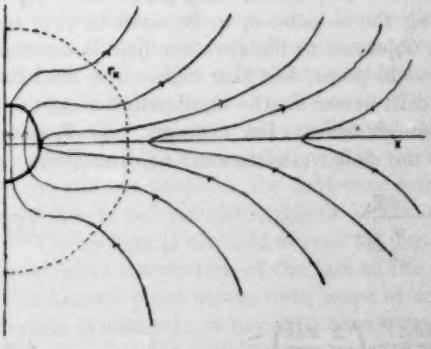

FIG. 3.—*Type (a').*

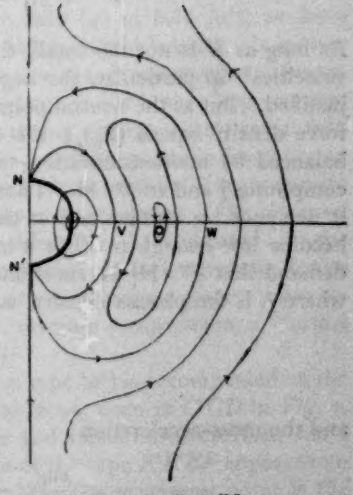

FIG. 4.—*Type (b').*

order of the densities in Bondi's spherical flow pattern, except in the equatorial zone. To order of magnitude, the condition is

$$\frac{4\pi\rho GM}{r^2 H_p} \ll \frac{H_p}{r}, \tag{31}$$

or

$$\frac{H_p^2}{8\pi} \gg \frac{GM\rho}{2r}; \tag{32}$$

i.e. the magnetic energy density should exceed the gravitational.

Consider now the untwisted, curl-free field of Fig. 1. As previously noted, the plasma within XLL' will rapidly drain away, so that in this region the approximation should steadily improve, except possibly in equatorial regions, where an abnormally high density could be built up, so affecting the field somewhat. Outside XLL' the density remains comparable with Bondi's values. Then assuming a local galactic magnetic field of order 5×10^{-6} gauss in regions of density 10 atoms/cm^3, it is found that the condition (32) is satisfied *except near the neutral point*. Clearly, if the field strength becomes small, the current density must be correspondingly large in order that the magnetic force be sizeable; so far from being negligible, the curl of the field has to be enormous, so that the curl-free approximation is inconsistent when the field strength becomes low.

To emphasize this conclusion, let us study conditions near X more closely. As the plasma has finite conductivity, there will be a steady drift $(\mathbf{v}_i)_\perp$ across the field, maintaining the current density

$$\mathbf{j} = \sigma\left(\frac{\mathbf{v}_i \wedge \mathbf{H}}{c}\right), \tag{33}$$

so that by (7),

$$(\mathbf{F}_p)_\perp = -\frac{\mathbf{j} \wedge \mathbf{H}}{c} = \frac{\sigma}{c^2}(\mathbf{v}_i)_\perp H^2. \tag{34}$$

As long as H is not too small, then $(\mathbf{v}_i)_\perp$ is very small compared with free-fall velocities; in particular, the neglect of the plasma inertia in (7) is completely justified. But as the neutral point is approached $(\mathbf{v}_i)_\perp$ increases until the inertial force density equals $(\mathbf{F}_p)_\perp$; the magnetic force is then negligible and $(\mathbf{F}_p)_\perp$ is balanced by mass-acceleration, yielding the velocity $\mathbf{v}_i$ to be used in (33) for computing $\mathbf{j}$ and so $\nabla \wedge \mathbf{H}$. Thus the objection to the curl-free field is not that it demands an infinite curl at the neutral point, but that before the field has become low enough to allow a large drift across it, the equilibrium conditions demand that $|\nabla \wedge \mathbf{H}|$ be enormous, though finite. For example, take $\mathbf{F}_p = \rho_i \mathbf{g}$, where ρ_i is the plasma density, and $\mathbf{g}$ the stellar gravitational field, so that

$$(\mathbf{v}_i)_\perp = \frac{\rho_i \mathbf{g}_\perp}{\frac{\sigma}{c^2} H^2}, \tag{35}$$

and the mass-acceleration

$$\rho_i v_i \frac{dv_i}{dr} \simeq -\frac{\rho_i (\rho_i g)^2}{\left(\frac{\sigma}{c^2}\right)^2 H^2}\left(\frac{2}{H^3}\frac{dH}{dr}\right). \tag{36}$$

This becomes comparable with $\rho_i g$ when

$$\frac{2\rho_i(\rho_i g)}{\left(\frac{\sigma}{c^2}\right)^2 H^5}\left|\frac{dH}{dr}\right| \simeq 1; \tag{37}$$

the force $\rho_i \mathbf{g}_\perp$ is balanced by an acceleration of the plasma within the narrow region, on either side of the neutral point, in which the left-hand side of (37) exceeds unity. If we take $\sigma/c^2 \simeq 10^{-10}$, corresponding to a temperature of $\simeq 10^2$ °K, and $\rho_i = 10^{-4}\rho(m_i/m_H)$, and the same simultaneous values of H_0 and ρ_∞ as before, then e.g. when the neutral point in solution (19) is near the star's surface, $r|\nabla \wedge \mathbf{H}|/H \simeq 10^9$. As F_p may very well be larger than $\rho_i g$ (Section 8), $r|\nabla \wedge \mathbf{H}|/H$ could be even larger.

Thus long before the neutral point is reached, the curl-free approximation has completely broken down, and a field initially of the shape of Fig. 1 would be immediately distorted by the inward flow of plasma towards the star. As long as the plasma and field move together—and this condition requires careful study—then the progressive distortion of the field must certainly continue until the neutral point reaches the stellar surface, where the gravitational field is balanced by a pressure gradient. This motion of the neutral point reduces the density of field lines cutting the equator between the star and the point X; in order to yield a strong force the field must have a large curl, so that the field lines make sharp hairpin bends at the equator. The magnetic force must be finite just outside the star, so the X-type neutral point must be dragged well below the surface; it is possible it may coalesce with and so annihilate the O-type neutral point that field (a) must possess within the star. The general shape of this field (a') is given in Fig. 3. It should be noted that well away from the equator, and also beyond X, the curl-free approximation remains good, and the lines of force are similar to the corresponding lines in Fig. 1.

However, in discussing the transition from field (a) to field (a'), we have dealt only with the requirement that the *radial* forces should balance. It is clear that the distortion of the field must introduce new transverse magnetic forces. The sharp curving of the field lines near the equator yields both a large current density, in the positive toroidal direction, and a strong, approximately radial field on either side of the equator. Hence there is a strong magnetic force acting towards the equator, which must compress the plasma, and build up a density gradient of the right magnitude to withstand the magnetic force. The situation is very similar to the well-known "pinch-effect". As indicated in the Introduction, although in equilibrium the magnetic and non-magnetic forces must balance, it does not follow that the magnetic field plays a passive role: as in the present problem, the field may *build up*, through compression, a thermal field able to balance the magnetic forces.

The motion of the field of type (a) into one of type (a') is accompanied by the progressive destruction of the flux of the closed loops, such as $C'CD$ in Fig. 1. The neutral point moves onto loops of smaller and smaller area until the star's surface is reached; at the same time more lines of the type $F'E'EF$ appear from the neutral point. This destruction of flux at an X-type neutral point is the reverse of the process discussed by Dungey (8) in another context. Near an O-type neutral point the drift of plasma through the field, due to the finiteness of the conductivity, is always such as to destroy magnetic flux: this is the gist

of Cowling's argument against the dynamo maintenance of fields containing O-type neutral points (9). Near an X-type neutral point, however, the ohmic field may either create or destroy flux, according to circumstances. For example, if another strong non-magnetic force were brought into play, acting away from the star, and stronger than gravity, the field would evolve in the reverse direction, new closed lines of force being produced as the neutral point moved outwards with the plasma.

In fact, the field in our problem would never take on the structure of Fig. 1. As the star contracts from the initial state with $\bar{\mathbf{H}} = \mathbf{H}_0$, the neutral point would appear near the surface of the star when $R = R'/\sqrt{3}$, but in the absence of a strong force overcoming gravity there is nothing to drive plasma and field outwards. A state of equilibrium, with the field having a topology similar to that in Fig. 1, could be maintained with the help of a plasma pressure gradient near the neutral point, and an equatorial dent in the field lines of finite length so that they can hold up the plasma*. Quite apart from the question as to how it could arise, such a field would be unstable against lateral perturbations, which would enable the plasma to flow down the finite field lines into the star, so that again the neutral point would be dragged into the star. But this possibility serves to emphasize that the field adopts the structure (a') rather than (a) because of the absence, all the way to infinity, of a non-magnetic force able to balance gravity; we may anticipate, for example, that if there is a strong centrifugal field in the cloud, one of the effects will be to break off the stellar field from the galactic field, through the appearance of a neutral point.

Further discussion of field (a') is postponed until Section 6. We now turn to fields of type (b), with twisted field lines with a sphere S of radius r_c, and an untwisted curl-free field beyond S (Fig. 2). There are four neutral points, all on the axis, at $r = r_c, r'$, and $\theta = 0, \pi$. Along the axis the plasma can flow straight into the star, but near the neutral points at N, N' the flow beyond S must be deviated so as to follow the lines of force such as $Q'TQ$, which swerve away from the axis. Hence again the field beyond S and near N and N' must have a large curl in order that the magnetic force may overbalance gravity and deviate the flow as required, the drift across the field due to the finiteness of the conductivity being again too slow for inertia to be important. The field (b) is therefore inconsistent with the equilibrium conditions, and the star's gravitational field drags inwards the plasma and field; the neutral points N and N' coalesce with M and M' respectively and a steady state is reached when the field has acquired a structure as in Fig. 4, with the two neutral points at the stellar poles. The distorted field lines will exert a force towards the axis, so compressing the plasma flowing down towards the star.

Plasma initially within the sphere r' (MVM' in Fig. 2) will flow directly into the star and will not be replenished, but plasma initially between r' and r_c flows down the field to the equator. Some will be neutralized there and flow into the star, but there will probably be formed an equatorial zone of dead plasma, unable to flow into the star except at the very slow rate allowed by the finiteness of the conductivity. A negative outward pressure gradient in this zone will supply a force opposing gravity and friction, and could get over a difficulty at the O-type neutral point of the poloidal field (cf. Fig. 4). At O, not only $(\nabla \wedge \mathbf{H}_p) \wedge \mathbf{H}_p = 0$, but also $(\nabla \wedge \mathbf{H}_t) \wedge \mathbf{H}_t = f'(P)\mathbf{H}_p \wedge \mathbf{H}_t = 0$, and the magnetic

* This suggestion was made by Mr D. Lynden-Bell.

force would seem unable to balance the non-magnetic forces. However, in fact the difficulty near O is not very serious and can be got over even without the help of a pressure gradient; whereas in the two previously discussed cases the neutral point problem led to striking changes in the fields, a very slight change in the toroidal field will yield a finite magnetic force. We write, instead of $T=\alpha P$,

$$T=P[\alpha+\beta(P-P^*)^{1/2}], \tag{38}$$

where P^* is the value of P at O, and β is a function of P, finite at O, and dropping rapidly to zero as P deviates from P^*. Then we find

$$|\nabla\wedge\mathbf{H}_t|\simeq P^*\beta P_{rr}^*, \tag{39}$$

which is finite near O, and so yields with $\mathbf{H}_t$ a finite magnetic force. In an accurate treatment of the field this extra twist would need to be included in the equation for P; for our purposes it suffices to remark that Fig. 4 remains an adequate picture of the poloidal field.

The correction to field (*b*) is less drastic than to field (*a*). Figs. 2 and 4 are alike in the topology of their lines of force; whereas in Fig. 3 all finite lines of force have disappeared, and the whole of the stellar flux-tube extends to infinity.

5. *The origin and stability of the twisted and untwisted fields.*—The fact that we can construct, besides the unique purely poloidal field, a whole class of twisted fields that satisfy the conditions of equilibrium and the boundary conditions. shows that the steady state condition is not in itself adequate to determine the field uniquely. This is because it is only the component of current *across* the field that enters explicitly into the magnetic force; currents parallel to the field enter only through the condition $4\pi\mathbf{j}=c\nabla\wedge\mathbf{H}$ that holds for all components.

In the time-dependent hydromagnetic problem there is no indeterminacy. The rate of change of the magnetic field is given by $\partial\mathbf{H}/\partial t=\nabla\wedge(\mathbf{v}_i\wedge\mathbf{H})$, where $\mathbf{v}_i$ is the velocity of the plasma (1); together with the equation of motion of the plasma this determines the magnetic and velocity fields at subsequent times in terms of the fields at the initial time. This is not altered if at some points the drift of plasma across the field is not negligible, due for example to the curl of the field becoming very large. Hence when steady-state solutions have been found the attempt must be made to discriminate between them either through a stability criterion, or through a qualitative argument showing that one or other steady state could not have been reached from the initial state through a physically allowed motion of the lines of force.

Suppose, therefore, that the local galactic field from which the stellar field has arisen is unbroken initially, so that its lines of force extend to infinity. (This assumption has been implicit in the discussion so far.) Clearly such a field can approach an untwisted equilibrium state as in Fig. 3. However, the transition from Fig. 3 to Fig. 4 is forbidden, because it demands creation of flux from an O-type neutral point. Creation or destruction of flux is dependent on the relative drift of plasma and field, which arises through departures from the relation $\mathbf{E}+\mathbf{v}_i\wedge\mathbf{H}/c=0$. The correct analogue of Ohm's law for a gas is

$$\mathbf{E}+\frac{\mathbf{v}_i\wedge\mathbf{H}}{c}=\frac{c\nabla\wedge\mathbf{H}}{4\pi\sigma}-\mathbf{E}^i, \tag{40}$$

where σ is the conductivity in e.s.u., and $\mathbf{E}^i$ represents the "impressed" e.m.f.s due to the electron partial pressure, the Hall field and other effects tending to cause drift of electrons relative to the ions. These extra effects are small, and

in any case take far too long to build up to their maximum, and so the only important cause of flux creation or destruction is the Ohmic field $c\nabla\wedge\mathbf{H}/4\pi\sigma$; and as previously remarked, at an *O*-type neutral point this always acts so as to destroy flux, in contrast to its behaviour at an *X*-type point. In order to reach Fig. 4 from Fig. 3 a circle of neutral points would have to be formed in each meridional plane, which would then have to separate into the two bounding curves NVN' and NWN'. This requirement is enough to dispose of the possibility.

However, it is possible that the local galactic field may have initially a poloidal component as in Fig. 3, with a broken-off part separating the lines of the stellar field and those stretching to infinity. Even so, the field cannot take up the modified force-free structure (*b'*) unless there is also a non-vanishing toroidal flux across a region bounded by a closed loop of $\mathbf{H}_p$. The distortion of $\mathbf{H}_p$ by non-uniform rotation will not generate such flux. Closed toroidal loops as are required must be generated on the axis of the field, where $\mathbf{H}_t=0$. Again, Cowling's argument shows that dynamo action near a neutral point is unable to overcome the destruction of energy and flux by Joule dissipation. To generate flux from the axis we require a poloidal "battery", represented by $\mathbf{E}^i$ in (40); but again the time-scale is far too long for the process to be relevant, even if $\mathbf{E}^i$ exists.

Hence if the poloidal field has initially the structure of Fig. 3, but there is no toroidal flux, it cannot approach the equilibrium state (*b'*); any toroidal field component within the surface *S* must exert a torque, and along each loop of force toroidal hydromagnetic oscillations will be set up about a mean state with $\mathbf{H}_t=0$. Consider then the equilibrium of the mean field. Field lines within the star are gripped by the pressure and gravitation fields; their external parts adjust themselves to the external forces, if any. But the part of the field between NVN' and NWN' has an intrinsic tendency to contract, for $(\nabla\wedge\mathbf{H})\wedge\mathbf{H}/4\pi$ is directed inwards in the general direction of the neutral point *O*. If there is a thermal field present, of energy comparable with the magnetic energy, then this contraction will be prevented by thermal pressure, and the rate of disappearance of the poloidal field loops into *O* will be controlled simply by the very slow Joule decay. This is a possibility if the region considered is at a distance not small compared with the Bondi sphere, at which the scale height is comparable with radial distance (cf. Part II, Section 7). But if the region considered is well within the Bondi sphere, any plasma originally within $NWN'VN$ will drain away either into the star or towards an equatorial zone of thickness comparable with the scale height, and moreover it cannot be replenished from outside. Hence the contracting flux-tubes cannot build up a pressure field able to withstand them, and there is nothing to prevent the continuous contraction of lines of force into loops of smaller and smaller area around *O*. Simultaneously, the field lines within NVN' and outside NWN' will move towards each other. Clearly if there were no plasma between NVN' and NWN', even in an equatorial zone, the flux-tubes would just disappear into *O*, NVN' and NWN' would coalesce, forming a neutral line, field lines on either side of this line would link up, and the system would ultimately settle down into an untwisted field of type (*a'*). However, if there were enough equatorial plasma, the collapse of the flux-tubes would be halted once a sufficiently strong pressure gradient had been built up near *O*. The equilibrium state would then be similar to type (*a'*), but containing as well a

tube of broken-off flux surrounding O and pinching the plasma within it. Such a tube would steadily decay through resistance; but in any case, it is unlikely to persist for long, as the highly compressed plasma will recombine rapidly, and it cannot be supplemented from outside. As the plasma is neutralized, its partial pressure decreases, the pinching magnetic force becomes unbalanced and compresses the plasma still further, so accelerating the rate of recombination, and the disappearance of the flux-tubes into O. Hence the field would approach configuration (a') in a comparatively short time-scale.

The last possibility is that the poloidal galactic field has initially a structure as in Fig. 3, but with toroidal flux linking the field $\mathbf{H}_p$, so that the modified force-free structure (b') is the relevant equilibrium state. This equilibrium field is likely to be stable against perturbations that are not too violent, even if there is no thermal pressure field; for there is no hydromagnetic motion that can remove the toroidal field, so leaving an unstable poloidal field. Contraction of the poloidal loops towards O is resisted by the toroidal field. If a loop of $\mathbf{H}_p$ contracts towards O, then H_p increases roughly as $1/l$, where l is a mean distance from O to the loop considered; whereas the toroidal field dragged with it increases like $1/l^2$. Similarly, contraction of a toroidal tube into the axis is prevented by the poloidal field.

Given enough time, Joule dissipation will cause a simultaneous contraction of the loops of $\mathbf{H}_p$ into O and the toroidal loops into the axis, so that again the field would be approached. (Quite generally, it is clear that no dynamo action can prevent the slow decay of a strictly force-free field, in which there is no current flow across the field.) This drift is very slow, but violent enough motions could so distort the field as to accelerate the decay.

In all the discussion it has been assumed that the stellar field is approximately uniform and given by equation (21)—it is just an isotropic compression of the field $\mathbf{H}_0$, assumed originally the uniform field of the whole cloud. We have seen that the equilibrium fields arising during the contraction of the proto-star are of type (a'); fields such as (b') are not relevant unless the initial cloud field contained toroidal flux. However, if more complicated cloud fields are allowed, then equally there is no compulsion to adopt (21) for the stellar field, so that one boundary condition can be relaxed. For example, the twisted force-free field (b') may extend from the surface S to the centre of the star. Or the stellar field could be uniform, but with a sense opposite to that of the field at infinity $\mathbf{H}_0$. If the external field is purely poloidal, then it has a structure similar to Fig. 3, except that the region between NVN' and NWN' is not present, and the field within NVN' has the opposite sense. The corresponding field (b') would have a similar poloidal part, and toroidal flux within NVN'.

6. *The untwisted field.*—The computation of field (a') is a formidable problem, and is postponed for separate treatment; however, anticipating some results of Part II on the velocity-density field, we may supplement the conclusions of Section 4 with some semi-quantitative arguments.

Plasma flows down the field lines, at a rate dependent on the structure of the field, and concentrates in the "equatorial zone" in approximate mechanical equilibrium. There is a strong tendency for the neutral matter to be dragged by the plasma into the zone. Neutral matter in the zone (including recombined plasma) drifts inwards across the field under gravity, but resisted by the plasma–hydrogen friction; this friction is thus approximately equal to the

gravitational force acting on the *neutral* gas. Hence in the equatorial zone the equation to the equilibrium of the plasma is

$$\frac{(\nabla\wedge\mathbf{H})\wedge\mathbf{H}}{4\pi}-\nabla p_i+\rho\nabla\phi=0, \tag{41}$$

where ϕ is the gravitational potential GM/r. The plasma pressure $p_i=2n_ikT$, n_i being the ionic number density, k Boltzmann's constant, and T the absolute temperature, the factor 2 arising from assuming singly ionized matter. We write $n_i=\eta n_{\mathrm{H}}$, where n_{H} is the number density of neutral atoms (mainly hydrogen); the factor η is given by a balance between the rate of inflow of matter into the zone, the rate of drift of neutral matter inwards, and the rate of plasma recombination. Thus η will be a complicated function of radial distance from the star, but as a first approximation we shall assume it varies slowly enough for it to be taken as constant.

Taking the curl of (41), we have

$$\nabla\wedge\left[\frac{(\nabla\wedge\mathbf{H})\wedge\mathbf{H}}{4\pi}\right]+m_{\mathrm{H}}\nabla n_{\mathrm{H}}\wedge\nabla\phi=0. \tag{42}$$

Also, (41) can be rewritten as

$$\frac{(\nabla\wedge\mathbf{H})\wedge\mathbf{H}}{4\pi}-2\eta kT\nabla n_{\mathrm{H}}+\rho\nabla\phi=0, \tag{43}$$

so that

$$\frac{[(\nabla\vee\mathbf{H})\wedge\mathbf{H}]\wedge\nabla\phi}{4\pi}=2\eta kT(\nabla n_{\mathrm{H}}\wedge\nabla\phi). \tag{44}$$

Equations (42) and (44) combine to give

$$[(\nabla\wedge\mathbf{H})\wedge\mathbf{H}]\wedge\nabla\phi+\frac{2\eta kT}{m_{\mathrm{H}}}\nabla\wedge[(\nabla\wedge\mathbf{H})\wedge\mathbf{H}]=0, \tag{45}$$

which is the equation to the field in the equatorial zone. Besides the same boundary conditions as before, we impose the restriction that H_θ should be negative all the way from the star to infinity, so that there is no neutral point outside the star. The equation (45) requires one more boundary condition; this may conveniently be taken as the value of H_θ at the star's surface. Assuming a plausible value for η, (45) can in principle be solved by substituting for $\mathbf{H}$ in terms of the scalar P, given by (5). Equation (43) then yields n_{H}, and so also the plasma density n_i. The densities in the zone should strictly be consistent with those given by the rate of flow down the field lines into the zone (cf. Part II), the drift of neutral matter inwards, and the rate of recombination. In practice, one can only hope, by a trial and error method, to choose value of η and $(H_\theta)_{\mathrm{R}}$ which yield density fields consistent as to order of magnitude.

Even so the solution of the problem remains formidable. Although the field outside the zone is approximately curl-free, its analytic form will not be simple because of its having to fit on to the rather eccentric zone field.

However, in the discussion of Section 4 it was pointed out that the field and plasma do not move strictly together, the drift of plasma across the field being given by (34). With low field strength and high current densities this drift can become important: as discussed in Section 4, once the inertia of plasma

drift becomes equal to the inward-pulling forces on the plasma, then the objection to the existence of a neutral point disappears. At this stage the structure of the field becomes (a''), a combination of fields (a) and (a'). Within the field line passing through the external neutral point the field will be nearly curl-free, for plasma drifting through the neutral point is soon forced to follow the field lines, so that most of this region has a low plasma density as well as a high field strength. Outside this limiting field line, the field will be similar to field (a'), with hairpin-shaped field lines at the equator, but curl-free field lines away from the equator and far enough away along the equator.

We may anticipate that the appearance of a neutral point will be assisted by the pinching effect of the magnetic field. The more distorted the field becomes, the greater the compressive force of the field, and the higher the plasma density required to balance it. Again at high densities the plasma recombination rate goes up. Unlike the case of the pinch effect discussed in the last section, there is now an external supply of plasma, as the field lines are of infinite length; but, as shown in Part II, the more distorted the field, the greater is the inhibiting effect it has on the flow of gas from infinity. Hence at some stage in the contraction of the star, further distortion of the field demands for equilibrium a plasma density greater than can be maintained. The plasma density decays, and the field lines contract laterally; this accelerates still further the recombination of the plasma, and at the same time inhibits still more the replenishment from outside. Thus the plasma density must steadily decrease, so that the frictional coupling with the neutral gas diminishes, until the dominant inward force on the plasma is just the gravitational force $\rho_i \mathbf{g}$. Again, the curl of the field, at the point where inertial force takes over from magnetic force as the principal opponent of gravity, is given by (33) and (35), with H satisfying (37); hence at this point $|\nabla \wedge \mathbf{H}|$ is approximately proportional to $\rho_i^{1/2}$. Thus as ρ_i decreases, with the consequent lateral motion of the field lines and increase in $|\nabla \wedge \mathbf{H}|$, simultaneously the value of $|\nabla \wedge \mathbf{H}|$ required to allow substantial plasma drift across the field decreases. Once, therefore, this lateral instability sets in, there is nothing to prevent the appearance of an X-type neutral point and broken-off field lines. It is hoped that a subsequent paper will determine at what stage in the star's contraction the neutral point appears.

It is of interest to note the evolution of the field, assuming that the present theory were relevant to a magnetic star that has reached the main sequence, and so stopped contracting. The field within the star is not curl-free, and so would gradually decay; lines of force would slip out of the star, and the external field would steadily adjust itself to the changing boundary condition. Ultimately, the field would be given by the solution of (7), reducing to $\mathbf{H}_0$ at infinity, and continuous in *both* components at $r = R$ with the ultimately uniform, curl-free field within the star: the solution of (7) would determine the amount of flux of the original galactic field retained by the star.

Part II

The dynamical problem

7. *The flow of gas in a fully ionized cloud.*—Although we are mainly interested in a star embedded in a lightly ionized H I cloud, we begin by considering a fully ionized cloud. The problem could be relevant to the case of a bright star surrounded by an H II region, but the main reasons for studying it are its

comparative simplicity, and because even in a lightly ionized gas the plasma and neutral components flow close together if the density is high enough. We shall assume that the flow is isothermal. In an H II zone compressional energy generated is rapidly absorbed by a slight increase in the already high degree of ionization (**10**); while in a dense H I cloud a high concentration of dust grains acts as an efficient cooling mechanism. The magnetic field assumed is of type (a') or (a'').

Although the plasma flow is along the field, it should be noted that there will not be a continuous flow along all lines of force. This can be seen by comparison with Bondi's spherically symmetric non-magnetic problem (**2**). There exists a critical sphere, of radius $r_c = GM/c_\infty^2$, where M is the stellar mass, G the constant of gravitation, and c_∞ the constant velocity of sound. The stellar radius must be less than r_c, otherwise the star could not hold itself together against thermal pressure. Within r_c the gravitational energy per gram exceeds the thermal energy per gram, so that in a hypothetical state of hydrostatic equilibrium the scale height would be small compared with the radial distance; this results in the impossibly large densities near a fully contracted star found by Bondi for the case $\lambda = 0$ (zero accretion), and also in his solutions with subsonic velocities near the star. Hence once the stellar radius is well below r_c, matter within r_c must flow in radially at approximately free-fall (supersonic) velocities. Beyond r_c continuity demands a radial, subsonic flow; departure from hydrostatic equilibrium is very slight, and the density is nearly constant.

Now consider the present problem. If a line of force is part of the star's field, the gravitational pull of the star must again lead to flow down the line of plasma within r_c, and by continuity the flow extends itself outwards beyond r_c. Similarly, if the line does not cut the star, but crosses the equator well *within* r_c, there will be a continuous flow down the line into the equatorial zone. Hydrostatic equilibrium along such a line of force would not be reached until the density at the equator is enormous. Quite apart from the loss of plasma from the zone through recombinations and inward drift across the field, there will not be enough matter in the cloud to supply the density field necessary for hydrostatic equilibrium. Hence the picture is as outlined in the Introduction: steady flow down the field lines into an equatorial zone containing both plasma and neutral matter, their densities being determined by the inflow of plasma, the rate of recombination, and the dynamics of the drift of neutralized gas across the field into the star.

By contrast, if a line of force cuts the equator *beyond* r_c, hydrostatic equilibrium along such a line is soon reached by a slight drift of plasma towards the equator, and no continuous flow will result (provided that the source of radiation keeping the cloud ionized is maintained). Hence there is a critical tube of flux that crosses the equator near the Bondi radius; outside it the gas is at rest, but within it there is a continuous flow down the field lines.

We now discuss the dynamics of the flow. Once a steady state has been reached, the plasma velocity $\mathbf{v}$ is parallel to the field:

$$\mathbf{v} = \kappa \mathbf{H}, \tag{46}$$

with κ a scalar function of position. If ρ is the plasma density, the equation of continuity yields

$$0 = \nabla . (\rho \mathbf{v}) = \nabla . (\rho \kappa \mathbf{H}) = \mathbf{H} . \nabla (\rho \kappa), \tag{47}$$

so that

$$\rho\kappa = \text{constant along a line of force} = \rho_\infty \kappa_\infty. \tag{48}$$

Hence in a steady state there is a non-vanishing velocity field $v_\infty = \kappa_\infty H_0$ far from the star: even if initially the gas is at rest at infinity, the flow will asymptotically approach a state with v_∞ finite. This is because the magnetic field prevents flow of gas from one flux-tube to another; if the field does not vanish at infinity, each flux-tube remains of finite width, with continuity demanding a finite velocity everywhere along the flux-tube.

The equation to the steady flow along a field line is just Bernoulli's equation, with the gravitational field as a body force:

$$c_\infty^2 \log \frac{\rho}{\rho_\infty} - \frac{GM}{r} + \tfrac{1}{2}v^2 = \tfrac{1}{2}v_\infty^2. \tag{49}$$

In a steady state the magnetic field does no work, as the flow is parallel to the field. Introducing non-dimensional variables x, z, y and h, defined by

$$r = \left(\frac{GM}{c_\infty^2}\right)x, \qquad \rho = \rho_\infty z, \qquad v = c_\infty y, \qquad H = H_0 h, \tag{50}$$

we have from (48) and (49)

$$\frac{yz}{h} = y_\infty, \tag{51}$$

and

$$-\frac{1}{x} + \log z + \tfrac{1}{2}y^2 = \tfrac{1}{2}y_\infty^2. \tag{52}$$

Eliminating z, we get

$$\phi(y) - \psi(x) = \gamma, \tag{53}$$

where

$$\phi(y) = \tfrac{1}{2}y^2 - \log y, \qquad \psi(x) = \frac{1}{x} - \log h, \qquad \gamma = \tfrac{1}{2}y_\infty^2 - \log y_\infty. \tag{54}$$

Equations (51) and (53), applying to each line of force, replace Bondi's equations

$$x^2 yz = \lambda, \qquad (\tfrac{1}{2}y^2 - \log y) - \left(\frac{1}{x} + 2\log x\right) = -\log\lambda \tag{55}$$

for spherically symmetric flow.

The discussion of (53) follows closely Bondi's discussion of (55). The minimum value of $\phi(y)$ is 0·5, and it is attained for $y = 1$; hence the parameter γ must be chosen so that for all x along the line of force considered

$$\gamma + \psi(x) \geqslant 0{\cdot}5. \tag{56}$$

Now $\psi(x) \to 0$ as $x \to \infty$; also, for all physically relevant fields, $\psi(x) \to \infty$ as $x \to 0$. Hence along each line of force ψ must have a finite minimum value. Suppose first that $\psi > 0$ everywhere along the line except at infinity. Then (56) is satisfied for $\gamma \geqslant 0{\cdot}5$, and so $\phi(y) \geqslant 0{\cdot}5$. By inspection of the graph of $\phi(y)$ against y, we have

if	$y_\infty > 1$,	then	$y > 1$	for all finite x.
if	$y_\infty < 1$,	then	$y < 1$	
and if	$y_\infty = 1$,	then	either $y > 1$ or $y < 1$	

If ψ is non-negative for all x, but has a zero for $x = x'$, then the solution with $y_\infty = 1$ will by (53) attain the sonic velocity again at x'; hence a solution supersonic beyond the zero may change over to a subsonic solution at x', and *vice versa*.

Now suppose ψ becomes negative for some range of x along the line of force considered, and let x_m be the point at which it attains its minimum. Depending on how far the star has contracted and on the line of force considered, x_m may be a true minimum and off the equator; or just at the equator; or not a true minimum, but the point where the line enters the star's surface. The inequality (56) will hold everywhere along the line provided it holds at x_m. Thus if $\gamma+\psi(x_m)=0{\cdot}5$, then $y(x_m)=1$, and the flow on either side of x_m may be supersonic or subsonic. The velocity at infinity is then given by

$$\phi(y_\infty)=\gamma=[0{\cdot}5-\psi(x_m)]; \tag{57}$$

approximately,

$$y_\infty=[1-2\psi(x_m)]^{1/2} \text{ if the flow is supersonic at infinity,} \tag{58}$$

or

$$y_\infty=\exp[\psi(x_m)-0{\cdot}5] \text{ if the flow is subsonic at infinity.} \tag{59}$$

All values of y_∞ yielding $\phi(y_\infty)$ larger than (58) are allowed, for then $\phi=\psi+\gamma>0{\cdot}5$ at x_m, and so for all other values of x; but values of y_∞ between (58) and (59) will not yield steady state solutions. If y_∞ is less than (59), the flow is subsonic everywhere; if greater than (58), it is supersonic everywhere. For either of the two values (58) and (59) the flow is just sonic at x_m, and so flow supersonic for $x>x_m$ may become subsonic for $x<x_m$ or, by a discontinuity in the velocity gradient at x_m, may remain supersonic for $x<x_m$. Similarly, flow subsonic for $x>x_m$ may become supersonic or remain subsonic for $x<x_m$.

However, not all steady state solutions are physically plausible. As ψ gets large for small x, by (53) the velocity in the solutions subsonic near the star becomes very small for small x, and leads by (51) to very large densities. This is again due to the smallness of the scale height well within the Bondi sphere: for low velocity solutions, the equation of motion approximates to the equation of hydrostatic support. Such solutions may be relevant when the star's radius is near r_c, but once $R\ll r_c$ they can be ignored, along with the zero flow solution.

Assuming, then, that the flow near the star is supersonic, the problem arises as to which of the allowed steady-state solutions will arise in practice. Let us suppose that initially the cloud is at rest at infinity. Within the Bondi sphere the gravitational field causes inward flow, and the region of flow is gradually extended outwards by continuity. Once the system has reached that velocity field, supersonic near the star, consistent with the equations of motion and continuity, and with the *least energy per gram of matter*, there is no reason why the velocities should increase above this level. Hence we expect the system to approach the flow with the minimum allowed velocities: if $\psi\geqslant 0$ everywhere along a field line, we take $y_\infty=1$, while if ψ has a negative minimum at x_m, we take $y(x_m)=1$, and adopt the solution that is subsonic for $x>x_m$. The point x_m on each line of force plays the role of the point $x=\frac{1}{2}$ in Bondi's spherically symmetric solution (**2**): beyond it the dynamical pressure is small, and approximate hydrostatic equilibrium holds.

However, it should be emphasized that the equations of motion and continuity do not forbid all higher velocities at infinity, with correspondingly greater flow along the field lines. If $\psi\geqslant 0$, all supersonic velocity fields are allowed; while

if $\psi<0$ for some range of x, all values of y_∞ greater than (58) are allowed. Solutions of this type, with y_∞ greater than the minimum allowed, will be relevant to the case of a cloud not initially at rest at infinity, but having matter being driven in rapidly enough by an external pressure field (e.g. by an external H II region). This result is in striking contrast to Bondi's spherically symmetric flow, and is again due to the confining effect of the magnetic field. If Bondi's spherically symmetric cloud had a non-vanishing inward velocity at infinity, the radial flow would rapidly build up a high pressure gradient and dam back the flow, which would asymptotically approach the steady pattern with zero velocity at infinity. In the present problem the magnetic field prevents the build-up of such a pressure gradient, by restricting the flow to be along the lines of a field that is *finite* at infinity. The flow along each infinitesimal flux-tube is analogous to flow through a pipe of variable but finite cross-section: not only are there low velocity solutions, in which the pressure controls the flow until it becomes sonic, but there are also high velocity solutions in which the pressure gradient is negligible everywhere. These results are analogues of well-known results in laboratory gas dynamics, the reciprocal of the field-strength playing the part of area of cross-section of the pipe.

In Bondi's spherically symmetric problem there is a definite upper limit to the total rate of accretion by a star:

$$A \simeq 4\pi\left(\frac{GM}{c_\infty^2}\right)^2 c_\infty \rho_\infty = 4\pi r_c^2 c_\infty \rho_\infty. \tag{60}$$

Again, a higher rate of inflow would lead to a large pressure gradient beyond the sphere r_c, which would dam back the flow. In the present problem, the rate of inflow across a sphere S surrounding the star, with outward unit normal $\mathbf{n}$, and of radius less than r_c, is

$$-\int_S \rho \mathbf{v}\,.\,\mathbf{n}\,dS = 2\int_{S'} |\kappa|\rho \mathbf{H}\,.\,\mathbf{n}\,dS = \frac{2\rho_\infty}{H_0}\int_{S'} |\mathbf{v}_\infty|(\mathbf{H}\,.\,\mathbf{n})dS, \tag{61}$$

where S' is the northern hemisphere. We have seen that there exist steady state solutions with v_∞ supersonic; these yield a rate of flow across S greater than

$$\frac{2\rho_\infty c_\infty}{H_0}\int_{S'} \mathbf{H}\,.\,\mathbf{n}\,dS = 2\pi L_\infty^2 \rho_\infty c_\infty, \tag{62}$$

where L_∞ is the radius at infinity of the flux-tube containing S. The total accretion rate is given by taking for S the Bondi sphere; hence if L_∞ for this sphere exceeds $\sqrt{2}r_c$, the accretion rate exceeds Bondi's maximum (60). Even if L_∞ were less than $\sqrt{2}r_c$, high enough velocities at infinity would still lead to enhanced accretion.

However, supersonic velocities at infinity will arise only if there is an external pressure field driving the matter in. We have seen that a cloud initially at rest at infinity will spontaneously approach a state with at most the sonic velocity at infinity. If the freezing of the field into the proto-star starts at a radius $R_0>\sqrt{2}r_c$, then $L_\infty>R_0>\sqrt{2}r_c$, and so the "cross-section" for capture of material will be greater than the area of Bondi's sphere; but this will not lead to an enhanced accretion rate unless the velocities at infinity are of sonic order.

Thus the crucial question as to whether a magnetic field can assist spontaneous accretion of matter by a star (still assuming that centrifugal force is negligible)

depends critically on the structure of the field, as determined by equation (7); for it is the field-strength which determines the variation of ψ along a line of force. If ψ remains positive along the line considered, then $y_\infty = 1$ for that line; but if the field-strength increases too rapidly inwards along the line (implying a sharp decrease in the area of the flux-tube along which the gas flows), ψ becomes negative, and y_∞ is by (59) strongly subsonic. Although an accurate estimate of the spontaneous accretion rate must await detailed computation of the fields (*a*) and (*a'*), our qualitative discussion of the field suggests strongly that the accretion rate will be well below Bondi's value. Those lines of force that approach the equator are crowded together, as illustrated in Fig. 3; the large radial component of $\mathbf{H}$ will yield a negative value for $\psi(x_m)$, and a consequent large reduction in the accretion rate.

It should be noted that field (*a*) would also cut down the accretion rate. Only a few infinite field lines reach the star; the rest cutting the equator beyond the neutral point X. Now the position of X in the curl-free field (*a*) is near the radius at which the freezing-in of the field commenced, and this is likely to be at least as great as r_c. Hence most of the infinite field lines cut the equator beyond r_c, and so there will be no continuous flow of plasma down them.

If the steady state theory is to be relevant, the time for the system to approach its asymptotic state should not be too long. Once the flow has extended outwards to a distance x_0 at which the field lines are nearly straight, we can expect the flow to approximate to the steady state pattern: the gas confined by the straight field lines will just expand into the partial vacuum created by the inflowing matter. For a rough estimate, let us suppose that before the asymptotic state is reached the matter flows in with Bondi velocities: the time for the flow to reach x_0 is then $\simeq \frac{1}{3}x_0^3(GM/c_\infty^3) \simeq 6 \times 10^{10}\bar{M}x_0^3$ where $\bar{M} = M/\odot$. Now x_0 is the distance at which the freezing of the field into the star may be considered to have started. If $x_0 \simeq 1$, the time-scale is very short; and even for $x_0 \simeq 10$ (near the upper limit if the star is not to contain too much magnetic flux for stability), the time-scale is still short compared with the Kelvin–Helmholtz time-scale, and of the same order as the time of free-fall.

8. *The flow of gas in a lightly ionized (H I) cloud.*—As in the fully ionized case, we must distinguish between lines of force that cut the star or cross the equator within Bondi's sphere r_c, and those that cross the equator beyond r_c. Again there is no continuous flow of plasma down the distant field lines, but instead hydrostatic equilibrium is reached after a slight drift of plasma towards the equator. By contrast, there is a continuous flow of plasma along the field lines within r_c, towards the star or the equator, and the plasma velocity field extends outwards, leading asymptotically to a finite velocity field at infinity.

In addition there is the problem of the flow of the neutral gas. In the absence of the magnetic field, all the matter would flow in radially with Bondi velocities, but in the present problem, with the plasma tied to the field, the flow of neutral gas across the field is resisted by the frictional drag. The density of the mutual friction between the two gases is (1):

$$\pm n_{\mathrm{H}} n_i \sigma m_{\mathrm{H}} V(\mathbf{v}_{\mathrm{H}} - \mathbf{v}_i), \tag{63}$$

where n_{H}, n_i are the number densities of hydrogen and ions, $\mathbf{v}_{\mathrm{H}}$, $\mathbf{v}_i$ are the velocity vectors of the two gases, σ is the mutual collision cross-section, taken as $10^{-16}\,\mathrm{cm}^2$, m_{H} is the mass of the hydrogen atom, and $V = |\mathbf{v}_{\mathrm{H}} - \mathbf{v}_i|$ or c_∞, whichever is the

larger. If the hydrogen is to flow across the field essentially as in Bondi's theory, the component across the field of the friction, with Bondi's radial velocity field substituted, must be small compared with the gravitational force on the hydrogen:

$$n_H r^2 (v_H)_\perp \left(\frac{n_i}{n_H}\right)\left(\frac{\sigma V}{GM}\right) = x^2 \left(\frac{V}{c_\infty}\right)\left(\frac{(v_H)_\perp}{c_\infty}\right) n_H (1{\cdot}6 \times 10^{-4} \bar{M}) \ll 1. \qquad (64)$$

We have assumed $n_i/n_H = 10^{-4}$, a standard value for the ratio of the densities of ionized metals to neutral hydrogen in an H I cloud.

Beyond r_c ($x = 1$), the Bondi velocity is $\simeq c_\infty/x^2$ so that $V = c_\infty$ and $n_H \simeq (n_H)_\infty$. Condition (64) is then independent of x, and yields

$$(n_H)_\infty \ll \frac{6 \times 10^3}{\bar{M}}. \qquad (65)$$

Within r_c, however, Bondi's velocity $\simeq c_\infty/x^{1/2}$ is supersonic; V is then $|\mathbf{v}_H - \mathbf{v}_i|$, which is of the same order as $\mathbf{v}_H$ except for regions where the field is nearly radial (where in any case both gases flow parallel to the field). The ratio (64) is then $\propto 1/x^{1/2}$, and so friction increases more rapidly than gravity as the star is approached. Whenever the frictional drag on Bondi flow exceeds gravity, the transverse flow must in fact be given by a balance between friction and gravity, and is therefore cut down to well below Bondi's velocity.

When friction cancels the transverse component of gravity, the neutral matter is effectively forced to follow the field lines. Hence for densities above the limit (65), the two gases flow together down the field, and the theory of the last section applies to the gas as a whole. In particular, both gases have asymptotically a finite velocity parallel to the field at great distances from the star. As Bondi's spherical velocity field vanishes at infinity, and the transverse drift of the neutral gas is reduced below Bondi's field by friction, the approximation of taking the neutral gas flow as parallel to the field improves at great distances.

However, although for $(n_H)_\infty \gg 6 \times 10^3/\bar{M}$ the flow of neutral matter within the critical flux-tube is everywhere closely parallel to the field, there is a slight transverse drift, such that the frictional drag on the neutral gas balances gravity. This flow will be maintained by drift of neutral matter across the field from the "dead" plasma zone outside the critical flux-tube. If the flow within the tube were strictly parallel to the field, the neutral matter in the "dead" zone would reach hydrostatic equilibrium as well as the plasma; as it is, continuity demands some inward flow. Thus the neutral matter that reaches the equatorial zone consists mainly of matter that has flowed down the field lines within the flux-tube, but includes some that has drifted in from the "dead" plasma region.

If $(n_H)_\infty$ satisfies (65), frictional resistance to flow across the field is negligible beyond a radius $r_1 < r_c$; in particular, neutral gas will flow into the critical flux-tube from the "dead" region, and will continue radially with Bondi velocities until r_1, after which it will flow closely parallel to the field lines. Within the critical flux-tube the plasma builds up its finite velocity field far from the star, and this flow is gradually transferred to the neutral gas by mutual friction. Hence ultimately both gases flow nearly parallel to the field far from the star; but the time-scale for this state to be built up is probably longer in this case.

Assuming $n_i/n_H = 10^{-4}$, we find the friction everywhere exceeds the gravitational force on the *plasma* if $(n_H)_\infty > 0{\cdot}6/\bar{M}$; for lower densities friction dominates near enough to the star. Depending on the density at infinity, and the distance from the star, the correct non-magnetic force $\mathbf{F}_p$ to be used in (7)

for an accurate computation of the field is the gravitational force on the plasma or the frictional drag on the plasma, whichever is the greater; but the friction cannot exceed the gravitational force on the *neutral* gas.

9. *The centrifugal field.*—Consider finally the condition (13) for the magnetic field to be able to keep the centrifugal force small compared with gravity. Beyond the Bondi sphere r_c, the spontaneous velocity field is at most sonic, so that (13) certainly holds if the magnetic energy density is large compared with the thermal, as is the case for the galactic magnetic field usually assumed in H I clouds. Within the Bondi sphere the inflow is approximately free-fall; $v_\varpi^2 \sim GM/\varpi$, and (13) is just the condition (32) for the magnetic energy density to exceed the gravitational. Again, the magnetic field is strong enough for this to hold in general: in fact it is the condition which would imply the curl-free approximation, if this did not lead to a neutral point. If the cloud field were somewhat weaker than is usually assumed, then the two energy densities would be roughly equal —the initially straight field lines would be distorted by the inflowing matter until a rough equipartition of energy is built up.

Acknowledgments.—The work of this paper and of the following note was done in part while the author was visiting Yerkes Observatory, with a grant from Commission 38 of the I.A.U. He wishes to thank Professor B. Strömgren for his hospitality, and to acknowledge helpful discussions with Professor S. Chandrasekhar and Dr K. Prendergast. He is also grateful to the referee for suggesting how to improve the presentation of the arguments.

St John's College,
Cambridge:
1959 *March* 6.

References

(1) L. Mestel and L. Spitzer, Jr., *M.N.*, **116**, 503, 1956.
(2) H. Bondi, *M.N.*, **112**, 195, 1952.
(3) L. Mestel, Article in *Vistas in Astronomy*, Vol. 3 (in press).
(4) R. Lüst and A. Schlüter, *Z. f. Ap.*, **38**, 190, 1955.
(5) L. Mestel, *M.N.*, **119**, 249, 1959.
(6) R. Lüst and A. Schlüter, *Z. f. Ap.*, **34**, 263, 1954.
(7) S. Chandrasekhar, *Proc. Nat. Acad. Sci.*, **42**, 1, 1956.
(8) J. W. Dungey, *Phil. Mag.*, **44**, 725, 1953.
(9) T. G. Cowling, *M.N.*, **94**, 39, 1933.
(10) L. Mestel, *M.N.*, **114**, 437, 1954.

A NOTE ON THE MAGNETIC BRAKING OF A ROTATING STAR

L. Mestel

(Received 1959 March 7)*

Summary

A poloidal magnetic field connecting a rapidly rotating star and a slowly rotating envelope will be twisted so that it transports angular momentum across the intermediate region of low density. The field exerts equal and opposite torques on the star and envelope. In the intermediate region the field will probably not exert strong compressive forces, but will be approximately force-free. By contrast with the *completely* force-free fields of the previous paper, which cannot be generated by distortion of a poloidal field, there is no toroidal flux linking a poloidal loop, and current does not flow in the same sense at every point of a loop.

In a recent paper (1) Lüst and Schlüter have discussed the magnetic braking of a rotating star, in the context of the von Weizsäcker cosmogony. It is assumed that a star has been formed in a rotating cloud; a magnetic field emanating from the star ensures that a sphere of radius r_K surrounding the star rotates with it (the Ferraro–Alfvén effect). If Ω_0 is the star's angular velocity, r_K is taken as of the order of the "Kepler" radius, at which gravity and centrifugal force balance:

$$\Omega_0^2 r_K^3 = GM, \tag{1}$$

M being the stellar mass. Beyond r_K each sphere has the appropriate Keplerian angular velocity Ω, where

$$\Omega^2 r^3 = GM = \Omega_0^2 r_K^3. \tag{2}$$

The non-uniform rotation is supposed to lead to turbulence, and the consequent rapid dissipation of energy to a simultaneous outward transport of mass and angular momentum.

The form of the magnetic field beyond r_K is not discussed by the authors, as they assume that turbulent friction is the dominant toroidal force responsible indirectly for the outward flow of mass and angular momentum. They concentrate attention on the torque-free field between the star and r_K; the field is supposed to have both poloidal and toroidal components, the twist being sufficient to transport from the star to r_K just that amount of angular momentum that the turbulence beyond r_K is transporting to infinity. The rate of loss of angular momentum by the star is estimated as a function of the decaying turbulence, but not of the magnetic field, which plays a subsidiary role: the turbulence beyond r_K disperses the envelope, and generates just the right twist in the field.

The authors also discuss the possibility that the edge of the uniformly rotating zone may be given not by (1), but by r_m, defined by the condition of equality of magnetic and turbulent energy densities. In this case the magnetic field does appear in the formula for the loss of angular momentum, but only through the

* Received in original form 1958 May 16.

quantity r_m; the picture is still of a turbulent transport beyond r_m, and a torque-free field between the star and r_m, its twist being determined by conditions beyond r_m.

The authors give an elegant discussion of the conditions under which a torque-free field may transport angular momentum. If T_{ij} is the magnetic stress tensor, and k_j the magnetic force density, then

$$T_{ij} = -\frac{1}{4\pi}(H_iH_j - \tfrac{1}{2}H^2\delta_{ij}), \tag{3}$$

and

$$k_j = -\frac{\partial}{\partial x_i}T_{ij}. \tag{4}$$

T_{ij} may be interpreted as the rate of flow in the i-direction of the j-component of linear momentum, and the integral $\int_S T_{ij}n_i\,dS$ as the total flow of j-momentum across a closed surface S with outward normal n_i. Similarly the authors introduce a tensor density describing the torque-density of the magnetic field:

$$d_{ij} = (x_jk_i - x_ik_j) = -\frac{\partial}{\partial x_k}D_{ijk} = -\frac{\partial}{\partial x_k}(x_jT_{ik} - x_iT_{jk}), \tag{5}$$

where D_{ijk} is the density of flow of angular momentum. The index-pair (i,j), (with $D_{ijk} = -D_{jik}$) gives the direction of the angular momentum component, and k the direction of flow. The integral $\int_S D_{ijk}n_k\,dS$ over a closed surface S gives a unique value for the net rate of transport of the (i,j) component of angular momentum out of the volume enclosed. For an axially symmetric field defined by scalars P and T as in (2), the total flow out of a sphere of the component parallel to the axis is

$$\frac{1}{2}\int_{-1}^{1} T\frac{\partial P}{\partial \mu}\,d\mu = \tfrac{1}{2}[F(P(r,1)) - F(P(r,-1))], \tag{6}$$

where $\mu = \cos\theta$, and $F(P)$ is defined by the torque-free condition

$$T = f(P) = \frac{dF(P)}{dP}. \tag{7}$$

It follows from the condition that the field be source-free that this flow is independent of r, as must be the case in a steady state.

The relevance of Lüst and Schlüter's work does not necessarily depend on the correctness of the cosmogony with which it is linked. Certainly, if the Keplerian velocity field does not give rise to turbulence, then an important feature of their process will be missing. However, the magnetic field beyond r_K can play a role analogous to turbulence, in that constant twisting by the Keplerian field will generate toroidal forces and lead equally to a radial transport of matter and angular momentum. Even if one does not picture a star as being born in a medium which already possesses a strong rotation field, the magnetic field will transfer angular momentum from the proto-star to the cloud and in time will probably build up a rotation field similar to that assumed by Lüst and Schlüter. If the loss of angular momentum from the star is not rapid enough, compared with the rate of contraction, the star will take up a disk-like structure, symmetrical about the rotation axis. The subsequent evolution of the disk may very well be determined by the magnetic redistribution of mass, the inner parts contracting

and the outer parts dispersing with excess angular momentum (3). The relevant feature is that there will again arise a zone in which the magnetic field exerts no torque and so does not accelerate or decelerate the matter in the zone (which will be of low density), but acts as a means of transport of angular momentum from an inner to an outer region—just the problem discussed by Lüst and Schlüter.

The purpose of the present note is to criticize the particular field chosen in (1) and to suggest more plausible alternatives. The authors choose

$$F(P) = \mp \frac{T_0}{P_0}\left(\frac{P}{P_0}\right)^{1/2}\left(\frac{P^2}{5} - \frac{PP_0}{3}\right), \tag{8}$$

where $P_0 = P(r, \pm 1)$ (assumed non-zero), and T_0 is a constant to be determined by the conditions at r_K. The toroidal function T is then

$$T = F'(P) = \mp \tfrac{1}{2} T_0 \left(\frac{P}{P_0}\right)^{1/2}\left(\frac{P}{P_0} - 1\right). \tag{9}$$

T can have no discontinuities, and $F(P)$ must have opposite signs at the poles if the field is to transport angular momentum; hence there must be a line of force $P = 0$ so that $F(P)$ can change sign. The simplest function satisfying this condition and the other conditions for a real non-singular field is

$$P = P_0 \cos^2\theta. \tag{10}$$

Hence the field chosen, and the currents maintaining it, have components

$$\left.\begin{aligned} H_r &= \frac{2P_0}{r^2}\cos\theta, & j_r &= -\frac{c}{8\pi}\frac{T_0}{r^2}(3\cos^2\theta - 1), \\ H_\theta &= 0, & j_\theta &= 0, \\ H_\phi &= -\frac{T_0}{2r}\sin\theta\cos\theta, & j_\phi &= \frac{c}{2\pi}\frac{P_0}{r^3}\sin\theta. \end{aligned}\right\} \tag{11}$$

This field transports angular momentum $\frac{2}{15} T_0 P_0$ per second from the star to the radius r_K. The meridional lines of force are straight lines through the origin.

It should be noted that the field (11) is not force-free; the authors point out that in some cases considered the magnetic forces are far larger than the gravitational, and if the conditions of equilibrium (equation (4) of (2)) is to be satisfied, it must be through a large plasma pressure gradient, built up by the magnetic forces themselves. It was pointed out in (2), Section 5, that there is a limit to the amount of compression a plasma can tolerate, especially if neutralized plasma cannot be replenished from outside, as will be the case with a Keplerian rotation field beyond r_K. Further, field lines that are to assist in decelerating a star must be part of the stellar field, and there is nothing to prevent plasma initially within r_K from flowing into the star. Hence a field such as (11), with lines of force having opposite senses on either side of the equator, is likely to approach a state with an X-type neutral point and broken-off field lines. The high conductivity of the plasma is no argument against such a transformation, any more than in the work of (2). The value of the conductivity merely determines the scale of the distortion required for relative drift of plasma and field to be noticeable; if either the magnetic or non-magnetic forces produce a field with a large enough curl, the theorem of the freezing of the field is no longer valid.

In fact, the reasons for adopting the rather eccentric field (11), with its singularity, are not very compelling. The authors justify their choice by appeal to an "economy-principle". They suggest that the field is determined by the transport of angular momentum, in the sense that the field adjusts itself to transport angular momentum "with least expense": the field lines link the origin and r_K in the simplest way, without being anywhere retrograde. But this principle can hardly be more fundamental than the condition of equilibrium. If the equilibrium condition and the boundary conditions at r_K do not suffice to fix the field, then the remaining arbitrariness may be removed by appeal to the economy-principle; but the choice of the field (11), in spite of the forces it exerts, rather puts the cart before the horse.

Without denying that cases may arise in which the magnetic forces are balanced by gas pressure, it is certainly plausible to look for a force-free field that can transport angular momentum across the region of probable low density between the star and r_K. The equation to the field is (4) of (2), with $\mathbf{F}_P \simeq 0$. The field is also torque-free, but it should be noted that relation (7) holds only between the star and r_K; within the star (7) cannot hold, as the field must exert a decelerating torque. In particular, a line of force (defined by a constant P) which enters the star at θ ($> \pi/2$), travels through the star and leaves it at $(\pi - \theta)$ is *not* forbidden in its external parts to have associated toroidal components of opposite sign in northern and southern hemispheres, as is required if the line is to assist in the transport of angular momentum. Outside the star the field is torque-free up to r_K, and so T must be constant along each segment of the line of force within r_K and outside the star. Within the star, however, T will gradually change its sign as the line traverses the star. Similarly, beyond r_K, T will vary along a field line in such a way that the field exerts on the matter a torque equal and opposite to the torque exerted on the star. Lüst and Schlüter's difficulty in finding a force-free field capable of transporting angular momentum seems to arise from their demanding that T be the same function of P along the *whole* length of a line of force.

In the preceding paper we discussed force-free fields, with T constant along each field line, and hence with toroidal flux across loops of the poloidal field. Such fields cannot be maintained by dynamo action against Joule decay, nor can they be generated by distortion of a poloidal field by non-uniform rotation: any linked flux must be primeval. However, for the present problem this type of force-free field is irrelevant, as we do not demand that T be constant along the whole length of a field line. As there must be currents across the field within the star and beyond r_K, in order that the field may exert a torque, the equation of continuity of charge can be satisfied without T having the same sign everywhere along a field line. Hence even if there are closed field lines C of $\mathbf{H}_P$, $\int_C \mathbf{j}_P \cdot \mathbf{ds}$ can vanish, so that there need not be any linked toroidal flux: nor is there any contradiction in picturing the field as arising by toroidal distortion of an initially poloidal field. Further, dynamo maintenance of the field against Joule decay cannot be ruled out *a priori*. In the regions where the field exerts a torque, dynamo action can drive the transverse currents, while as the currents parallel to the field need not flow in the same sense at every point of a line of force, they can be driven by an electrostatic field. (Of course general arguments such as Cowling's theorem apply to forbid maintenance of certain types of field; but

the breakdown in dynamo action is due to the induced currents being too weak near an O-type neutral point, not to their having the wrong direction).

It is of course possible that the initial field is not poloidal, but for example is one of the twisted fields of (2), with toroidal flux. In that case non-uniform rotation will superpose a further toroidal component, and the problem is essentially unchanged. However, we shall consider only the case of an initially poloidal field, with axis identical with the axis of rotation, and with a toroidal part imposed by the condition at r_g, where either turbulent friction or a magnetic torque begins to act on the matter. Suppose, for example, that the poloidal field in the star and in the torque-free region were as in Fig. 3 of (2), up to the sphere r_g, and let P^* be the value of P on the line of force that just grazes the star at the equator. Consider the following function T defining the toroidal field:

$$T=\begin{cases} T_0\left(\frac{P}{P^*}\right)\left(\frac{P}{P^*}-1\right) & 0\geqslant P\geqslant P^* \\ 0 & P^*>P \end{cases} \text{ and } \theta\leqslant\pi/2$$
$$\begin{cases} 0 & P^*>P \\ -T_0\left(\frac{P}{P^*}\right)\left(\frac{P}{P^*}-1\right) & 0\geqslant P\geqslant P^* \end{cases} \text{ and } \theta\geqslant\pi/2. \qquad (12)$$

T vanishes at $\theta=0$ and on the line $P=P^*$. The function $F(P)$ (yielding $T=F'(P)$) is

$$F(P)=\begin{cases} \pm\tfrac{1}{6}T_0P^*\left(\frac{P}{P^*}-1\right)^2\left(\frac{2P}{P^*}+1\right) & 0\geqslant P\geqslant P^*, \\ 0 & P^*>P, \end{cases} \qquad (13)$$

and the angular momentum transported per second—by those lines of force for which $P>P^*$—is by (6) $\frac{1}{3}T_0P^*$. The poloidal current maintaining the toroidal field is

$$\mathbf{j}_P=\begin{cases} \pm\frac{c}{4\pi}\frac{T_0}{P^*}\left(\frac{2P}{P^*}-1\right)\mathbf{H}_P & 0\geqslant P\geqslant P^* \\ 0 & P^*>P. \end{cases} \qquad (14)$$

The poloidal force due to $\mathbf{H}_t$ is

$$\begin{cases} -\frac{T_0^2}{4\pi r\sin\theta P^*}\left(\frac{P}{P^*}-1\right)\left(\frac{P}{P^*}\right)\left(\frac{2P}{P^*}-1\right)\{H_\theta,-H_r,0\} & 0\geqslant P\geqslant P^* \\ 0 & P^*>P \end{cases} \qquad (15)$$

and the term in $\mathbf{H}_t$ in the equation to the field ((4) of (2)) is

$$\begin{cases} \frac{T_0^2}{P^*}\left(\frac{P}{P^*}\right)\left(\frac{P}{P^*}-1\right)\left(\frac{2P}{P^*}-1\right)\Big/r\sin\theta & 0\geqslant P\geqslant P^* \\ 0 & P^*>P. \end{cases} \qquad (16)$$

The equation to P within r_K is then

$$\frac{\partial^2 P}{\partial r^2} + \frac{\sin\theta}{r^2}\frac{\partial}{\partial\theta}\left(\frac{1}{\sin\theta}\frac{\partial P}{\partial\theta}\right) = -\frac{T_0^2}{P^*}\left(\frac{P}{P^*}\right)\left(\frac{P}{P^*}-1\right)\left(\frac{2P}{P^*}-1\right) \qquad (17)$$

for $0 \geqslant P \geqslant P^*$. For $P^* > P$ the equation is (17) with the right-hand side zero, provided the density is low in this region also. The boundary conditions are continuity of H_r at the stellar surface and at r_K, and also continuity of H on the field line $P = P^*$ (so that the magnetic pressures may balance). Numerical integration of the equations will decide whether the field can in fact have the postulated structure, with all the field lines infinite.

The conditions will be relaxed somewhat if there is a high plasma density for $P < P^*$, so that the field in this region is not curl-free, but exerts a compressive force balanced by the plasma pressure gradient. As the lines with $P < P^*$ are not linked with the star, this plasma will not rapidly drain away. However, too great a compression would again lead to recombinations and decay of the plasma density unless it were replenished from beyond r_K. This in turn requires that the Keplerian velocity field beyond r_K is restricted to the region $P > P^*$.

If T_0 is small enough (corresponding to a slow dispersal of the envelope beyond r_K), the term on the right of (17) is small, so that for $P > P^*$ the field is effectively curl-free. If also the pressure gradient is negligible for $P < P^*$, the field as a whole is nearly curl-free within r_K; its structure will then certainly not be as in Fig. 3, but rather as in Fig. 1. Along loops such as CDC' which lie within r_K, the function T must be zero, as there is no toroidal flux; hence no net angular momentum transport can occur, as is physically obvious. But lines that cross r_K, whether they form closed loops or go off to infinity, will again not be torque-free beyond r_K, but will be twisted by the non-uniform rotation so that they exert a torque of sign opposite to that exerted on the star; hence T will have opposite signs at points such as G and G'. The toroidal function (12) can now be applied to this field, provided P^* is defined as the parameter of the limiting loop of force that just grazes the sphere r_K. In contrast to the previous case, only a fraction of the stellar field lines assist in the transport of angular momentum.

Clearly there are many generalizations of (12). If the field has no toroidal flux (i.e. it is just a twisted poloidal field), the toroidal component is determined if the conditions beyond r_K are completely known. It may be that in no case of interest does the field have the structure of Fig. 3, and that the transport of angular momentum is primarily from the parts of the star near to the rotation axis, a result of possible importance during the contraction of the star to the main sequence. This note is merely concerned to show that the general theory of Lüst and Schlüter can be applied to the type of field that naturally arises from equilibrium conditions, and no special fields such as (11) need be postulated.

St John's College,
Cambridge:
1959 *March* 6.

References

(1) R. Lüst and A. Schlüter, *Z. f. Ap.*, **38**, 190, 1955.
(2) L. Mestel, *M.N.*, **119**, 223, 1959.
(3) L. Mestel, Article in *Vistas in Astronomy*, Vol. 3 (in press).

STELLAR GROUPS, IV. THE GROOMBRIDGE 1830 GROUP OF HIGH VELOCITY STARS AND ITS RELATION TO THE GLOBULAR CLUSTERS

Olin J. Eggen and Allan R. Sandage

(Communicated by the Astronomer Royal)

(Received 1959 March 4)

Summary

The available proper motions and radial velocity data have been used to establish the existence of a moving group of subdwarfs (Groombridge 1830 group) which includes RR Lyrae. On the basis of the relationship between the observed ultra-violet excess and displacement below the normal main sequence, the subdwarfs in the Groombridge 1830 group are identified with main sequence stars in the globular clusters. This identification gives a modulus of $m-M=14^{m}\cdot2$ for the globular cluster M13 with the result that $M_V\sim+0^{m}\cdot5$ for the 2 RR Lyrae variables and $M_V=-2^{m}\cdot3$ for the brightest stars in the cluster. RR Lyrae itself, for which we derive $M_V\sim+0^{m}\cdot8$ from the moving cluster parallax, is shown to obey the period–amplitude relation for the variables in M3 and to be reddened by $0^{m}\cdot05$ with respect to those variables. By equating the luminosity of RR Lyrae to the mean of the variables in M3 we obtain a modulus of $m-M=15^{m}\cdot0$ for the cluster. We have not derived this modulus in the logical way of fitting the M3 main sequence to the main sequence of the Groombridge 1830 group because the colour observations of the M3 main sequence stars may contain a systematic error.

Because the presence of RR Lyrae variables in stellar groups may provide the only accurate calibration of the luminosities of these stars, it is important to make a systematic search for such groups. We have tabulated the available information for (1) all stars classified as subdwarfs on the basis of their spectral features, (2) stars that are probably extreme subdwarfs, on the basis of their observed ultra-violet excesses, although classified as normal main sequence objects, and (3) stars that may be globular cluster giants, subgiants or horizontal branch stars. Space motions of objects in these three categories have been computed from parallaxes derived by fitting them to the $(M_V, B-V)$-diagram of M13, which was calibrated by the Groombridge 1830 group. It is shown that there is a high probability that several of these stars are travelling together in space and that, when additional material becomes available, several groups similar to the Groombridge 1830 group will be found. Also, the space motions of 4 RR Lyrae variables with relatively well-determined proper motions are identified with those for some nearby subdwarfs with a resulting $M_V\sim+0^{m}\cdot6$ for the four variables.

In previous papers of this series (Eggen 1958a, b, c; Papers I, II and III) several groups of stars have been discussed on the basis of the apices and total amounts of the stellar motions. Aside from the interesting dynamical questions raised by the existence of these groups (Woolley 1959), the resulting $(M_V, B-V)$-diagrams are of importance in supplementing the available material from galactic clusters. This is especially true if stellar groups can be found that contain stars for which a luminosity calibration is not available from

other sources. Of particular interest in this connection are the field RR Lyrae variables and subdwarfs that might be identified with globular cluster stars. In this paper we will discuss (1) the evidence for the existence of a group of very high velocity subdwarfs moving together in space and containing RR Lyrae (Groombridge 1830 group), (2) the use of this group in obtaining distance modulii for globular clusters by the identification of the main sequences of the clusters with those of the group stars, and (3) the possible existence of other similar groups.

1. *The Groombridge 1830 group.*—Among the stars known to be within 20 parsecs of the Sun, and for which radial velocities and proper motions are available, the object with by far the largest space motion is the subdwarf Groombridge 1830 (HR 4550). The relevant data are as follows:

$$\mu = 7''\cdot042/\text{yr}, \qquad U = -263 \text{ km/sec},$$
$$\rho = -98 \text{ km/sec}, \qquad V = -151 \text{ km/sec},$$
$$\pi = 0''\cdot116, \qquad W = -22 \text{ km/sec},$$

where the velocity vectors, relative to the Sun, are directed as follows: U, away from the galactic centre ($l = 148°$, $b = 0°$); V, in the direction of galactic rotation ($l = 58°$, $b = 0°$); W, toward the north galactic pole ($b = 90°$). Taking the velocity of the Sun, relative to the stars within 20 parsecs (Woolley 1958) as $U(\odot) = -11$, $V(\odot) = +17$ and $W(\odot) = +7$ km/sec, the space motion of Groombridge 1830 relative to the mean of these nearby stars becomes

$$U + U(\odot) = -274 \text{ km/sec},$$
$$V + V(\odot) = -134 \text{ km/sec},$$
$$W + W(\odot) = -15 \text{ km/sec}.$$

A search through a catalogue of 700 high velocity stars yielded the following stars which appear to share the large space motion of Groombridge 1830; the stars were chosen by the convergent point (i.e. moving cluster) method described in Papers I and II:

Star	θ_0	$\Delta\theta \sin\lambda$	μ	ρ km/sec	Q	$V_t = 285$ $\Delta\rho$	$V_t = 285$ π_g	$= 300$ km/sec $\Delta\rho$	$= 300$ km/sec π_g
	°	°	″				″		″
+72°94	309	+ 5	0·25	−266	d	−6	0·010	+ 7	0·0095
Gmb. 1830	145	0	7·042	− 98	b	−6	0·126	0	0·116
HD 163810	209	0	0·82	+192	c	−8	0·020	−18	0·018
RR Lyr	210	+ 4	0·24	− 72	a	−3	0·004	− 4	0·0035
HD 219617	203	−11	1·30	+ 15	var	−3	0·0225	− 4	0·0205

The values of $\Delta\theta$ were formed from the observed position angles of the proper motions, θ_0, and the position angles computed from the assumption that the stars are moving with Groombridge 1830 toward $A = 16^h\,19^m$ and $D = -54°\cdot4$; λ is the angular distance between the star and the point (A, D). The observed radial velocities, ρ, and their quality, Q, were taken from R. E. Wilson's catalogue and the computed values were obtained from the expression $V_t \cos\lambda$, with two values for V_t, the total velocity referred to the Sun, determined from two values for the parallax of Groombridge 1830; 285 km/sec for a parallax of $0''\cdot126$ and 300 km/sec for a parallax of $0''\cdot116$. The group parallaxes, π_g, were computed from the expression $\pi_g = 4\cdot74\mu/V_t \sin\lambda$.

The proper motion and radial velocity determinations for the group members are in Table I where the uncertainties in some of the data are apparent; the

proper motions of +72°94, HD 163810 and RR Lyrae, and, to a lesser extent the radial velocity of +72°94, HD 163810 and HD 219617, could be greatly improved by additional observations.

TABLE I

Proper motion and radial velocity determinations for members of the Groombridge 1830 group

Star	μ_α	PE	μ_δ	PE	S*	ρ	S*
	s	s	"	"			
+72°94	−0·240	0·010	+0·218	0·010	G	−266	Md (2)
	−0·195	10	+0·157	10	G		
Gmb. 1830	3·995	1	−5·800	1	GC	− 99	W (11)
						− 97	L (5)
						− 98	
HD 163810	−0·473	11	−0·673	12	Y	+187	W (3)
	−0·321	9	−0·746	6	C	+198	Md (2)
						+192	
RR Lyr	−0·122	8	−0·188	6	GC	− 70	Md (300)
	−0·121	8	−0·224	8	S	− 74	W (20)
						− 72	
HD 219617	−0·512	8	−1·186	7	GC	+ 8	W (8)
	−0·513	0·014	−1·200	0·010	Y	+ 23	Md (2)
	−0·512		−1·190				

* GC = General Catalogue, Y = Yale Zone Catalogues, C = Cape Observatory, G = Greenwich Observatory, and S = Sproul Observatory. The sources of the radial velocities are Md = McDonald, W = Mount Wilson, and L = Lick Observatories; the observatory abbreviations are followed, in parentheses, by the number of plates.

The space motions of the group members have been computed from the parallaxes derived above on the basis of the group motion and are listed in Table II. In those cases where there is a large difference between two values of the observed proper motion or radial velocity, space motions have been computed for both determinations to demonstrate the sensitivity of the three components of the space velocity to variations in the observed data. For example, because of its apparent place in the sky, the large observed difference in the distribution of the total proper motion of HD 163810 between the two coordinates is reflected almost entirely in the value of the *W*-velocity. From the spread of values of the space velocities in Table II it can be seen that, within the uncertainties in the data, the members of the Groombridge 1830 group can be considered to have isoperiodic galactic orbits (Woolley 1958) and, therefore, to form a kinematical group.

In Paper II an attempt was made to estimate, by the use of a synthetic convergent point, the number of spurious group members that might be present in groups of various velocities as a result of the method of selection. It was estimated that two or three spurious members would be included for groups

TABLE II

Space motions for members of the Groombridge 1830 group

μ	θ	ρ km/sec	$U+U(\odot)$	$V+V(\odot)$ km/sec	$W+W(\odot)$	π	V_E	$(B-V)$	M_V		Sp.
(+72°94)											
″	°					″	m	m	m	m	
0·32	312	−266	−294	−110	+39	0·0085	10·03	+0·44	+4·7–	+5·2	sdF2
0·32	312	−266	−276	−129	+22	0·0105					
0·25	309	−266	−265	−127	− 4	0·0085					
0·25	309	−266	−253	−139	−15	0·0105					
(Gmb. 1830)											
7·042	145	− 98	−288	−139	−13	0·110	6·44	+0·74	+6·6–	+7·0	sdG8
7·042	145	− 98	−268	−127	−20	0·120					
7·042	145	− 98	−247	−116	−26	0·130					
(HD 163810*)											
0·82	215	192	−255	−140	+37	0·018	9·62	+0·625	+5·9–	+6·1	sdF8
0·82	215	192	−247	−122	+29	0·020					
0·82	203	192	−253	−136	− 3	0·018					
0·82	203	192	−247	−117	− 2	0·020					
(RR Lyrae†)											
0·225	213	− 72	−246	−127	+18	0·004	7·81	+0·38	+0·5–	+1·1	...
0·225	213	− 72	−282	−138	+21	0·0035					
0·255	208	− 72	−250	−134	− 7	0·0045					
0·255	208	− 72	−283	−134	−11	0·004					
(HD 219617‡)											
1·300	206	8	−235	−178	−33	0·0205	8·17	+0·47	+4·7–	+4·9	sdF8
1·300	206	23	−238	−173	−46	0·0205					
1·300	206	8	−215	−160	−28	0·0225					
1·300	206	23	−225	−156	−40	0·0225					

* ADS 10938, $\Delta m = 1^m$.

† Mean magnitude and colour, obtained by planimetering the light curves converted into intensity units, are listed. No correction has been made for absorption.

‡ ADS 16655, $\Delta m = 0$. The luminosity was corrected for components of equal magnitude and colour before plotting in Fig. 1.

with a total space motion of 100 km/sec. The same material (FK_3) indicates that no spurious members will be included in groups with total space motions in excess of 150 km/sec, but because the stars in the FK_3, which were tested by the synthetic convergent point ($\delta = -90°$) have generally very low velocities compared to the subdwarfs, this result may not be applicable to the present case. On the other hand, the fact that relatively few stars have space motions near 300 km/sec makes it highly unlikely that spurious motions of this size will simultaneously (1) result from placing the stars on a definite sequence in the (M_V, $B-V$)-diagram, (2) have vectors U, V and W similar to those for Groombridge 1830, and (3) represent stars that have the same ultra-violet excess as Groombridge 1830 (Section 3). For example, there are 33 F-, G- and K-type subdwarfs in Tables VI and VII that have ultra-violet excesses comparable with those of Groombridge 1830 and the globular cluster stars. Only seven of these—the first three stars in Table VI, the second in Table VII and the three members of the Groombridge 1830 group for which $U-B$ values are available —are inbound toward the galactic centre with velocities greater than 200 km/sec. Since the values of $V+V(\odot)$ and $W+W(\odot)$ for these seven stars range, respectively, from -120 to -450 km/sec and from -140 to $+60$ km/sec, it seems unlikely that nearly fifty per cent of the stars would accidentally satisfy the requirements for membership in the Groombridge 1830 group. More quantitative statistical tests for spurious members of high velocity groups will be possible when extensive astrometric, photometric and spectroscopic observational programmes for subdwarfs, which are now in operation, are completed.

The magnitudes and colours, which were observed in either the $(P, V)_B$-system or, by Roman (1955), in the (B, V)-system, are listed in Table II together with the spectral types, also by Roman, and the range in luminosity resulting from the range of parallax shown in the table. The colours on the (B, V)-system are used here since our ultimate aim is to compare the group stars with globular cluster stars and the latter have mostly been observed on that system. The colours and luminosities of the group members are shown in Fig. 1 where the Pleiades–Hyades main sequence is also plotted. The estimated uncertainties in the luminosities of the group members, based on the extreme range of the parallaxes shown in Table II, are indicated by the length of the lines in Fig. 1. The trigonometric parallaxes of the group members, other than Groombridge 1830, are small and offer little check on the derived luminosities. The individual values are as follows; the observatory abbreviations and the weights, in parentheses, are those given by Jenkins (1952):

Star	π_i (unit = 0″·001)
+72°94	0 M(6)
Gmb. 1830	111 A(28), 107 M(8), 164 St(3) − mean = 116
HD 163810	26 M(7), 11 Y(12), 31 C(7) − mean = 20
RR Lyr	11 A(28), −12 Yk(6), 5 W(7), 25 S(7) − mean = 9
HD 219617	14 M(8), 39 Y(12), 43 D(4), 0 C(7) − mean = 24.

2. *The double stars.*—Fig. 1 shows that members of the Groombridge 1830 group are undoubtedly subdwarfs lying $1^m{\cdot}5$ below the Pleiades–Hyades main sequence in the (M_V, $B-V$)-diagram. The question of the existence of these and other subdwarfs in the (M_{Bol}, $\log T_e$)-diagram is discussed elsewhere in

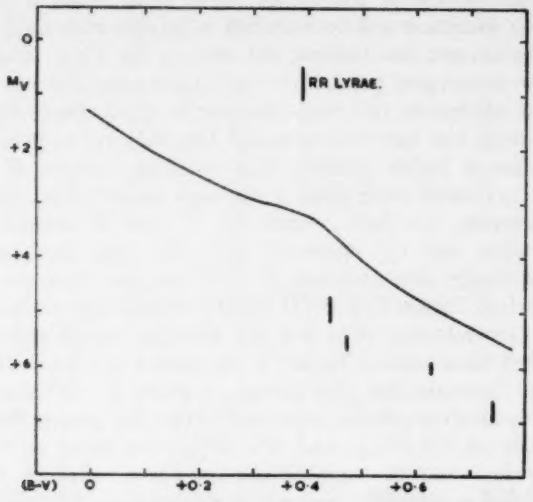

FIG. 1.—*The* (M_V, $B-V$)*-diagram for members of the Groombridge* 1830 *group. The length of the vertical lines indicates the range of luminosities for the various values of the parallax given in Table II. The continuous curve represents the Pleiades–Hyades main sequence.*

Monthly Notices (Sandage and Eggen 1959). From the equations developed in that discussion it is apparent that if subdwarfs do exist in the (M_{Bol}, log T_e)-diagram, they will violate the mass–luminosity relation for normal dwarfs and it is, therefore, very important that masses of subdwarfs be independently determined. As pointed out previously (Eggen 1956) there are very few known or suspected subdwarfs in binary systems. The best mass determination available is that for 85 Pegasi A, but since the derived mass depends upon the trigonometric parallax, there is necessarily considerable uncertainty in the value. On the other hand, membership of visual binaries in stellar groups permits the use of the group motion parallax in deriving the mass. Representative observations of the two binaries in the Groombridge 1830 group, ADS 10938 and 16644, are shown in Table III. Very few observations of ADS 10938 have been made since its discovery in 1900; the three listed in Table III show an angular motion of 1°/year and a fixed separation near 0″·5 but orbital elements obviously cannot yet be derived. The observations of ADS 16644 extend back to 1876 and more than one-half an orbital period may have elapsed since then, but unfortunately this system is seen nearly edge-on (inclination near 90°) and any orbital elements must depend mainly on the observed separations. The two components of the system are of nearly equal magnitude and are indistinguishable, but a double reversal of quadrant (180° of motion) has been assumed to have occurred between 1902 and 1929. The apparent orbit is nearly rectilinear with one end as yet unobserved. Using the observations to 1930, Parenago (1946) derived the value of $P=145$ years and $a=0''\cdot52$ from the observed rate of change of the observed separations and the assumption that van den Bos's observations in 1928 define one end of the rectilinear apparent orbit. These elements do not satisfy later observations and it doubtful whether even preliminary elements can be derived until it can be shown from observations made now that apastron has

TABLE III

Observations of ADS 10938 and 16644

ADS 10938					ADS 16644				
t	PA	Sep.	Obs.	*n*	*t*	PA	Sep.	Obs.	*n*
	°	″				°	″		
1900·47	218	0·48	Hu	3	1876·28	42	0·83	D	3
1923·36	198	0·47	VB	2	1891·59	49	0·63	*β*	3
1947·83	172	0·51	VB	4	1898·66	48	0·58	*β*	2
					1901·16	42	0·58	*β*	2
					1901·73	47	0·63	Doo	2
					1927·00	Too close		B	...
					1927·80	180	0·15	B	2
					1929·60	252	0·15	V	2
					1932·33	Too close		B	3
					1937·53	224	0·26	B	4
					1942·56	226	0·34	B	4
					1943·55	229	0·47	V	3
					1944·84	223	0·40	B	2
					1948·64	222	0·44	VB	2
					1949·85	224	0·42	B	2
					1955·62	226	0·72	Wor	4
					1957·90	223	0·68	Cou	2

been reached. An attempt to find the extreme range of periods and semi-major axes that will fit the available observations indicated that the total mass of the system is less than two solar masses, that is, the two (assumed) equal masses are both less than the mass of the Sun, but this result is very uncertain.

3. *Identification of the subdwarf group members with globular cluster stars.*—In addition to the dynamical questions raised by the possible existence of a moving group of subdwarfs near the Sun, the existence of RR Lyrae stars in this and possibly other stellar groups (Section 5) provides a powerful method of calibrating the luminosities of the cluster type variables themselves. Furthermore, since the Groombridge 1830 group shows that subdwarfs and cluster variables are related, it seems probable that the globular cluster main sequences should be compared to the subdwarfs rather than to the ordinary dwarfs near the Sun. In the past this has been a question of some importance because, as Fig. 1 indicates, an error of more than a magnitude can result in the luminosities of the globular cluster stars if the cluster main sequences are fitted to the Pleiades–Hyades main sequence rather than to the subdwarfs. In this section we use the main sequence of the Groombridge 1830 group (subdwarfs) to compare with the main sequence of M13 and discuss the resulting luminosities of the M13 stars. A similar discussion of the available M3 data is given in Section 4 but in this case greater reliance is placed on the absolute magnitude of RR Lyrae itself as determined from the assumption that it is moving with the Groombridge 1830 group than on available observations of the M3 main sequence stars. Justification for comparing RR Lyrae with the M3 variables comes from the similarity of the characteristics of these stars (Section 4). The divergence of the M3 main sequence from that of the Groombridge 1830 group, which results from this comparison (Fig. 8), is interpreted as an error of about $0^{m}\cdot1$ in the colours of the faint stars in M3.

The most reliable data for faint globular cluster stars are probably those published by Baum, Hiltner, Johnson and Sandage (1959) for M13. Earlier

results for M13 by Arp and Johnson (1955) provided accurate three-colour observations to visual magnitude 17·5 and the later results carried this to magnitude 20·5 in three colours and magnitude 22 in two colours. The two colour indices, $U-B$ and $B-V$, obtained from more than one photoelectric observation by Arp and Johnson for giant and subgiant members of M13 are shown in Fig. 2 as open circles. The filled circles in the figure represent the photoelectric colours obtained for main sequence stars in the cluster by Baum, Hiltner, Johnson and Sandage. The continuous curve represents the relationship between $U-B$ and $B-V$ for the Hyades stars (Sandage and Eggen 1959). The following values of $U-B$ are also available for three subdwarf members of the Groombridge 1830 group:

Star	$B-V$	$U-B$
	m	m
Gmb. 1830	+0·74	−0·17
HD 163810	+0·625	−0·06
HD 219617	+0·47	−0·20

these are shown in Fig. 2 as crossed circles. The faint companion to HD 163810 probably has little effect on the colour of the system: the equal components of HD 219617 probably have identical colours.

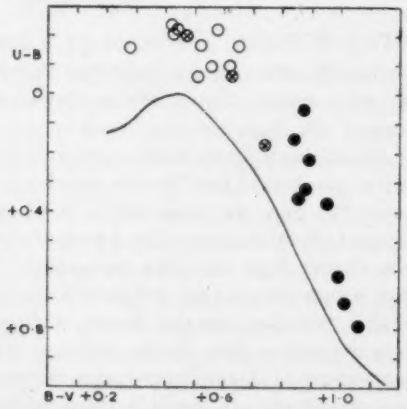

FIG. 2.—*Three colour diagram for the giant and subgiant members of M13 (filled circles), main sequence members of M13 (open circles) and Groombridge 1830 group members (crossed circles). The continuous curve represents the $(U-B, B-V)$-relation for the Hyades main sequence stars.*

It is evident from Fig. 2 that the observed ultra-violet excess of the Groombridge 1830 group members and the M13 stars is very similar. Since we have shown elsewhere (Sandage and Eggen 1959) that, at least to a first approximation, displacement below a standard main sequence in the $(M_V, B-V)$-diagram is directly correlated with the observed ultra-violet excess, we will fit the main sequence of M13 to that defined by the Groombridge 1830 stars. The result of this procedure is shown in Fig. 3. It has been assumed that M13 is free from reddening since the bluest stars are observed to be bluer than any stars known in the Galaxy. Arp (1955) and Arp and Johnson (1955) have derived a reddening of $0^m{\cdot}16$ and $0^m{\cdot}12$, respectively, but we believe that the procedures used in these derivations are probably unsatisfactory.

The filled circles in Fig. 3 represent mean points from the photographic observations by Baum, Hiltner, Johnson and Sandage (1959) for luminosities fainter than $M_V = +2^m$ and from those of Arp and Johnson to $+3^m$; the open circles represent the individual photoelectric results for cluster members observed

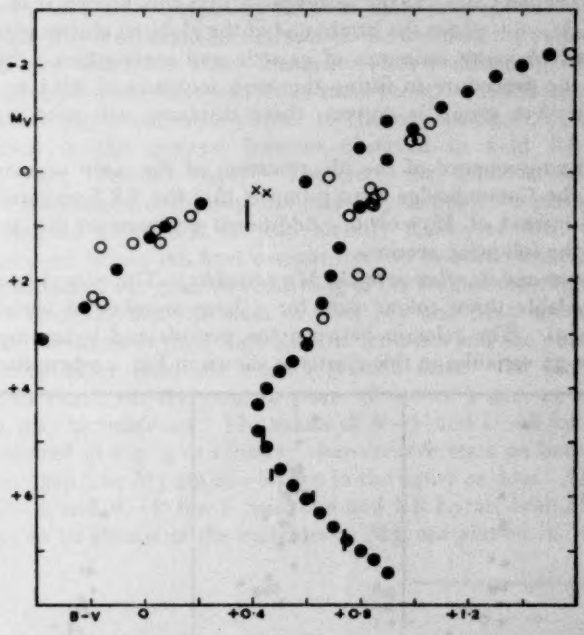

FIG. 3.—*The $(M_V, B-V)$-diagram for M13 (circles) and the Groombridge 1830 group (vertical lines). The filled circles represent photographic mean points and the open circles individual photoelectric results. The two crosses represent the RR Lyrae variables in M13. The modulus of M13 was determined as $m-M=14{\cdot}2$ by fitting the main sequence of the cluster to the subdwarf members of the Groombridge 1830 group. M13 is assumed to be unreddened.*

by Arp and Johnson. A mean, colour–luminosity relation for the stars fainter than $M_V = +5^m$ in Fig. 3 is tabulated in Table IV based on a distance modulus of $14^m{\cdot}2$ obtained from the above procedure.

TABLE IV

Mean colour–luminosity relation for the main sequence of M13

$(B-V)$	$(P-V)_E$	M_V
m	m	m
+0·45	+0·565	+5·1
+0·50	+0·605	+5·5
+0·55	+0·655	+5·8
+0·60	+0·705	+6·05
+0·65	+0·75	+6·3
+0·70	+0·80	+6·55
+0·75	+0·85	+6·8
+0·80	+0·90	+7·0
+0·85	+0·945	+7·15
+0·90	+0·99	+7·4

One consequence of the above procedure is that the brightest stars in M13 are at $M_V = -2^m.3$. This value should be compared with the usually adopted one of -3^m which is based on (1) the observed fact that in most globular clusters the brightest giants are three magnitudes brighter than the horizontal branch (RR Lyrae variables) and (2) the assumption that this branch is at $M_V = 0^m.0$. The value of $M_V = -3^m$ for the bright end of the globular cluster giant sequence has been used in many estimates of galactic and extra-galactic distances and therefore, if the procedure in fitting the main sequence of M13 to that of the Groombridge 1830 group is correct, these distances will need a substantial revision.

A second consequence of the identification of the main sequence of M13 with that of the Groombridge 1830 group is that the RR Lyrae variables have $M_V \sim +0^m.5$ instead of $M_V \sim 0^m.0$. Additional evidence on this point will be discussed in the following sections.

4. *RR Lyrae and its relation to the M3 variables.*—The only cluster for which there are available three colour data for a large number of variables is M3 (Sandage 1959). The relation between the periods and light amplitudes, *B*, *V*, and *U*, for 33 variables in this cluster is shown in Fig. 4 where the separation

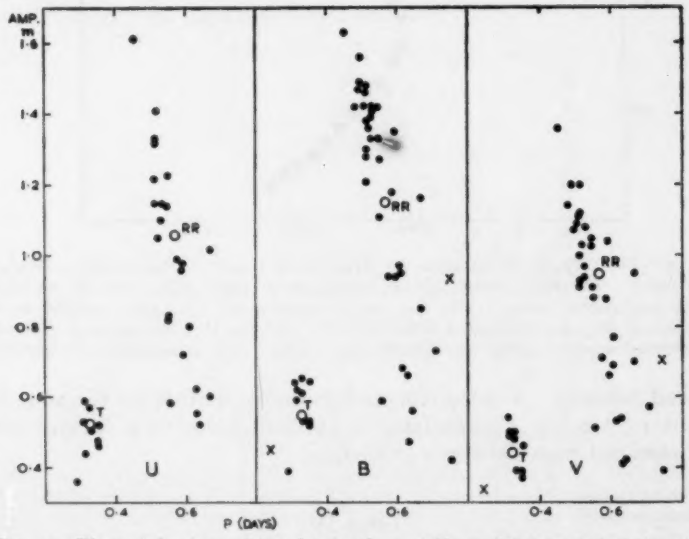

FIG. 4.—*The period–colour relationship for the variables in M3 more distant than 180″ from the cluster centre. The position of RR Lyrae and T Sextantis and of two variables in M13 (crosses) are also shown.*

of the Bailey type *a* and type *b* stars (large amplitudes) and the type *c* stars (small amplitudes) is apparent. The three colour results for RR Lyrae (Hardie 1955) and for T Sextantis (Tifft and Smith 1958) are also plotted in the figure and indicate that, in light amplitude at least, these two field variables are very similar to the M3 stars. The results for RR Lyrae and T Sextantis are as follows:

	$U-B$	$B-V$	A_V	A_B	A_U
RR Lyr	+0·05	+0·38	0·95	1·15	1·08
T Sex	+0·06	+0·24	0·82	0·55	0·44

On the other hand, the available two-colour data for the M13 variables (Arp 1955), which are represented in Fig. 4 by crosses, show marked deviations from the mean period–amplitude relations for the M3 variables. Both of the M13 variables stand off, in opposite directions, from the mean period–amplitude relations for the *ab* and the *c* type M3 variables more than any individual variable in M3. This result is a particular example of the fact that the period–amplitude relation can vary markedly from cluster to cluster (Belserene 1954). This variation is probably related to the fact that small variations in the mean luminosity of the variables may occur from cluster to cluster (Sandage 1958) and to the great variation in the spectral features observed in field RR Lyrae stars (Iwanowski 1953, Preston 1958). Therefore the field variables probably represent an inhomogeneous group and it is only through the period–amplitude relations discussed above that we can identify RR Lyrae with the variables in M3. However, before the final comparison can be made between RR Lyrae and the M3 variables, the possible reddening of the former must be investigated.

We have assumed that the stars in both M3 and M13 are unaffected by absorption on the basis of their high galactic latitudes and the presence of stars observed to be bluer than any known galactic stars. On the other hand, RR Lyrae lies nearly in the galactic plane ($b = +11°$) and, at a distance of 250 parsecs, may be reddened. The values of $B-V$ and $U-B$ for the variables in M3 are plotted in Fig. 5 as crosses; non-variable stars on both sides of the variable star "gap" in M3 are also shown in the figure as dots. Also, the mean values of $U-B$ and $B-V$ for T Sextantis and RR Lyrae, both of which were shown above to be similar to the variables in M3, are plotted in Fig. 5 as large

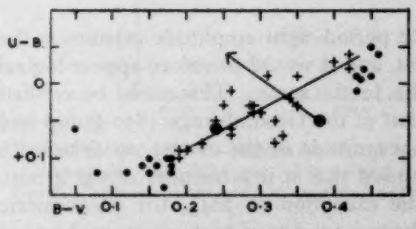

FIG. 5.—*Three colour diagram for the M3 variables in Fig. 4. T Sextantis falls on the mean relation for the cluster stars but RR Lyrae needs to be moved* $0^m{\cdot}04$ *in* $U-B$ *and* $0^m{\cdot}05$ *in* $B-V$ *along the reddening line indicated by the arrow. Non-variable horizontal branch stars are indicated by filled circles.*

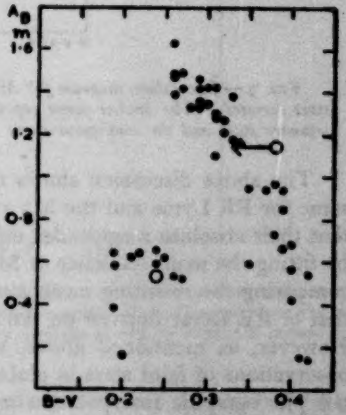

FIG. 6.—*Colour–(blue) amplitude relation for the M3 variables in Fig. 4. T Sextantis (unreddened) and RR Lyrae (with a reddening of* $0^m{\cdot}05$ *indicated by an arrow) are plotted as open circles.*

filled circles. There appears to be little or no reddening affecting T Sextantis, because it falls on the mean $(U-B, B-V)$-line defined by the M3 stars, but RR Lyrae needs to be moved $0^m{\cdot}05$ in $B-V$ and $0^m{\cdot}04$ in $U-B$ along the reddening line $(U-B)=0{\cdot}74(B-V)$ (Lindholm 1957). The value of

$E_{(B-V)} = +0^{m}.05$ derived in this way differs considerably from $+0^{m}.12$ derived previously (Sandage 1956) but, within the framework of the assumptions that RR Lyrae is similar to the M3 variables and that the latter stars are unreddened, the present value is undoubtedly more reliable. The previous determination rests on the questionable assumption that the intrinsic colour of RR Lyrae is the same as that of the supposed unreddened, non-variable stars with which it was compared. The consistency of the result that RR Lyrae is reddened by $+0^{m}.05$ and the assumption that it is similar to the M3 variables is demonstrated in Fig. 6 which contains the colour (blue)–amplitude relation for the M3 variables. A correction for $+0^{m}.05$ reddening in this diagram puts RR Lyrae on the mean colour–amplitude relation of the cluster variables.

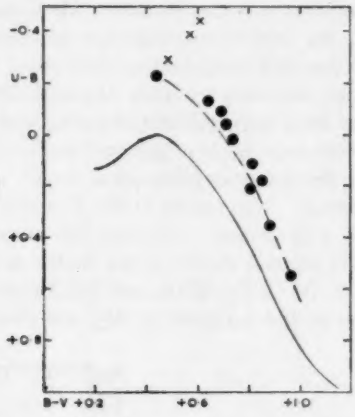

FIG. 7.—*Two colour diagram for M3 giants and subgiants (filled circles) and main sequence stars (crosses). The broken curve represents the mean relationship for M13 giants and main sequence stars and the continuous curve that for the Hyades main sequence stars.*

The above discussion shows that the period–light amplitude relation is the same for RR Lyrae and the M3 variables, and it would therefore appear logical that their absolute magnitudes might also be the same. This could be verified by fitting the main sequence of M3 to that of the Groombridge 1830 group and comparing the resulting mean absolute magnitude of the cluster variables with that of RR Lyrae derived on the assumption that it is a member of the group. However, as mentioned above, with the exception of M13, the photometric observations of faint stars in globular clusters are not of high precision because the photographic interpolation usually depends on very few photoelectrically calibrated standard stars and it is difficult, in the photographic interpolation method, to control the colour indices at faint light levels with an accuracy greater than $0^{m}.1$. This is particularly true of M3 (Johnson and Sandage 1956) where only 8 photoelectric standards were observed fainter than $V = 19^{m}$ whereas 23 such standards were obtained for the investigation of M13. Because an error of only $0^{m}.1$ in the colour indices of the faint M3 stars will cause an error of $0^{m}.4$ in the position of the main sequence, the M3 data are considered to be of insufficient accuracy to compare main sequences. A further indication of possible difficulties in the M3 photometry is the anomalous $U-B$ values derived for M3

main sequence stars shown in Fig. 7. The accurate M13 data show that the main sequence stars have an excess of about $\delta(U-B)=0^{m}\cdot2$ whereas the observed M3 values rise to $0^{m}\cdot4$ to $0^{m}\cdot5$.

Therefore, instead of fitting the main sequence of M3 to that of the Groombridge 1830 group, we have fitted the mean magnitude of the M3 variables to that of RR Lyrae in Table II, after correction for the absorption discussed above. The resulting $(M_V, B-V)$-diagram for M3 is shown in Fig. 8 which also contains the colours and luminosities of the Groombridge 1830 group members; the colour and magnitude of RR Lyrae have been corrected for absorption before plotting in Fig. 8.

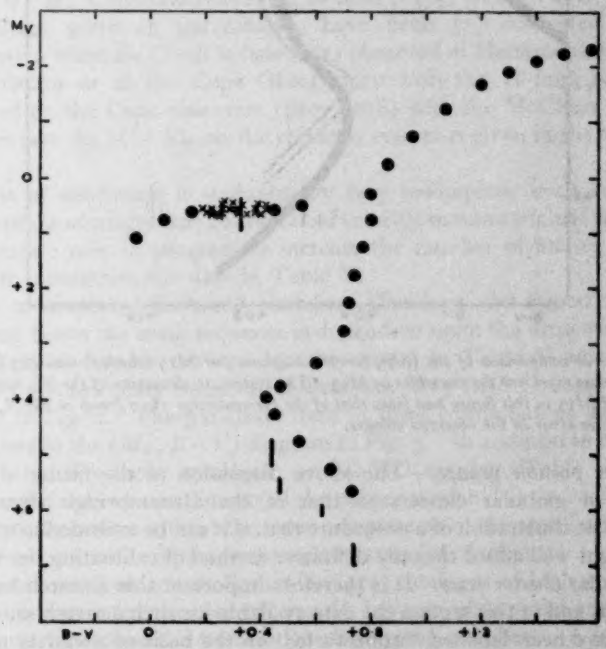

FIG. 8.—*$(M_V, B-V)$-diagram for M3. The modulus of $15^{m}\cdot0$ was derived from a comparison of the variables with RR Lyrae. The vertical lines represent members of the Groombridge 1830 group. The mean colour and luminosities of representative variables in M3 are plotted as crosses.*

The $(M_V, B-V)$-diagrams for M13 (shaded) and M3 (unshaded) are compared in Fig. 9 where the two variables in M13 are shown as crosses and the variable star gap in M3 by broken lines; the blue extension of the horizontal branch in M3, which is populated by only a few stars, is shown as a thin line. Figs. 8 and 9 show that the stars in M3 fainter than $V=19^{m}$ do indeed systematically deviate from the main sequence of the Groombridge 1830 group and of M13. This deviation is not considered to be real however, because of a possible error in the measured colour indices of the faint M3 stars. These same stars, fainter than $V=19^{m}$, also show an anomalous ultra-violet excess (Fig. 7) which may be caused by the same error.

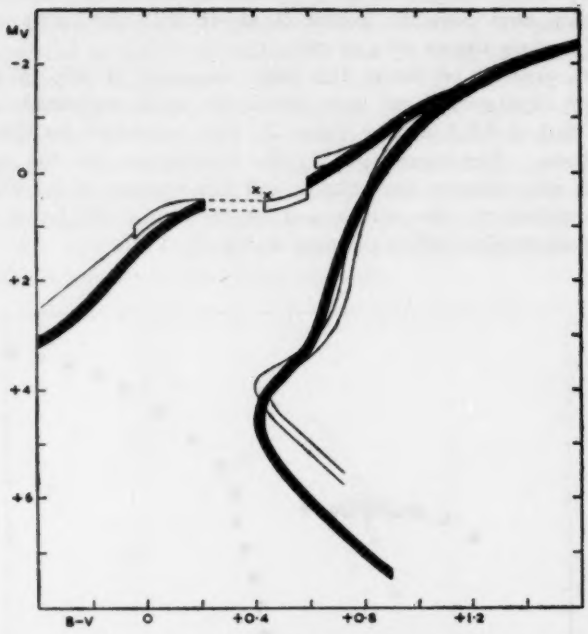

FIG. 9.—*A comparison of the* (M_V, $B-V$)*-diagrams for* $M13$ *(shaded) and* $M3$ *(unshaded). The two crosses represent the variables in* $M13$. *The systematic deviation of the* $M3$ *main sequence from that of* $M13$ *in this figure and from that of the Groombridge* 1830 *group in Fig.* 8, *is believed to be due to an error in the observed colours.*

5. *Other possible groups.*—The above discussion of the fitting of the main sequences of globular clusters to that of the Groombridge 1830 group is intended as an illustration of a procedure that, if it can be extended to other stellar groups, might well afford the only definitive method of calibrating the luminosity of the globular cluster stars. It is therefore important that a search be made for other groups and in this section the data available for such a search are discussed.

Stars have been labelled "subdwarfs" on the basis of a variety of criteria; for example, velocity, position in the HR diagram, the appearance of the spectrum, and the spectral type–colour relationship. The interrelations of some of these criteria are discussed elsewhere in *Monthly Notices* (Sandage and Eggen 1959) and we will deal here only with subdwarfs so classified by the appearance of their spectra, with some additional stars included on the basis of an observed ultra-violet excess in their colours. Stars for which radial velocity observations are available and which, as far as can be determined, have been classified as subdwarfs on the basis of their spectral features, are listed in Table V. The table contains the following information:

Wilson No.: The number in R. E. Wilson's (1953) catalogue of radial velocities. A few stars, not in that catalogue, are identified by their HD or BD numbers.

m_v: The visual magnitude taken from Wilson's catalogue except for stars observed photoelectrically, which are indicated by two decimal magnitudes.

Sp.: The spectral type assigned by the observer mentioned in the sixth column. Other classifications are noted at the end of the table.

ρ, Q: The radial velocity and its quality, *a*, *b*, *c*, *d*, taken from Wilson's catalogue. A few values not in that catalogue, or improved by more recent observations, are indicated by the observer; R = Roman (1955), E = Evans (1958), G = Greenstein (1954).

Ob.: The authority for the classification listed in the third column; P = Popper (1942, 1943), J = Joy (1947), R = Roman (1955), M = Münch (1944), E = Evans (1958) and G = Greenstein (1954).

μ, θ: The total annual proper motion and its position angle, taken from various sources.

$B-V$, $U-B$: Colours observed by Roman (1955) on the (U, B, V)-system A few values, given in parentheses, have been (1) converted from the $(P, V)_B$-system when no $U-B$ is listed, (2) observed at Herstmonceux with the 20-inch reflector or at the Cape Observatory with the 18-inch reflector, or (3) observed by the Cape observers (Stoy 1958) with the McClean refractor—in the latter case the $(U-B)_C$ on the refractor system is given in the notes to the table.

This list of subdwarfs is undoubtedly very incomplete, even among stars brighter than visual magnitude 10 and radial velocity, astrometric and photometric observations are now in progress to increase the number of known subdwarfs as well as to strengthen the data in Table V.

On the assumption, discussed elsewhere (Sandage and Eggen 1959), that displacement below the main sequence is dependent upon the ultra-violet excess, we have computed space motions for those stars in Table V whose $(U-B)$ and $(B-V)$ colours place them on or near the M13 (and Groombridge 1830 group) line in Fig. 2. The parallaxes used in these computations were derived by fitting stars to the $(M_V, B-V)$-diagram in Fig. 3. In addition to the number in Wilson's radial velocity catalogue, or BD/HD number, Table VI includes (1) the values of the two components of the proper motion, (2) the radial velocity, (3) the adopted parallax and (4) the three components of the space velocity freed of the solar motion with respect to the nearby stars (cf. Section 1).

There are several objects in Roman's (1955) catalogue of high velocity stars that, although not noted there as subdwarfs, have an ultra-violet excess similar to the globular cluster and Groombridge 1830 group members. A few of these stars are globular cluster giants. Others, although spectroscopically classified as luminosity class V, may be subdwarfs. Some of these stars are listed in Table VII where, in addition to the information supplied for the stars in Table VI, we have included the magnitudes, colours and spectral types; the parallaxes were obtained by fitting the giant or main sequence of the $(M_V, B-V)$-diagram in Fig. 3. Two A-type stars, which show an ultra-violet *deficiency*, are included in Table VII. The parallaxes of these stars have been computed on the assumption that they belong to the horizontal branch of the $(M_V, B-V)$-diagram for globular clusters since a similar deficiency has been observed for A-type stars in a globular cluster (Sandage and Walker 1955). Although there may be a range of $0^m{\cdot}3$ in luminosity of the horizontal branch from cluster to cluster (Sandage 1958), we have fitted these A-type stars to that of M13 in Fig. 3.

In Table VIII we have gathered together the stars in Tables VI and VII that appear to have similar space motions. It should be remembered that in

TABLE V

Stars classified as subdwarfs on the basis of their spectral features

Wilson No.	m_v	Sp.	ρ	Q	Ob.	μ	θ	$B-V$	$U-B$
91*	12·0	sdF4	−100	G	G	0·25	79	...	...
390	10·27	sdA9	−114	d	P	0·35	72	+0·36	−0·16
646*	5·20	G5 VI	− 97	a	R	3·76	115	+0·70	+0·11
987	10·08	sdF2	−266	d	P	0·32	...	(+0·44)	...
HD 16031	9·75	sdF4	+ 63	R	R	0·17	153	+0·45	−0·22
1735	8·06	sdF7	−139	R	R	0·82	194	+0·46	−0·24
1800	10·5	sdK5	−167	b	J	1·36	156	...	...
1828	10·18	sdA8	+154	c	P	0·3:	140:	(+0·46)	(−0·25:)
1892	10·8	sdF3	− 33	d	P	0·45	141	...	...
1904	10·6	sdK5	−173	c	J	1·58	135	...	...
HD 21543	8·22	G2 V–VI	+ 59	R	R	0·41	120	+0·62	+0·03
1919	9·7	sdF9	−160	c	P	1·63	131	...	...
2420	9·22	sdF5	+339	c	R	0·54	122	+0·44	−0·19
2851	6·97	G1 V–VI	+ 27	b	R	0·66	146	+0·60	+0·23
3314	11·5	sdF6	+543	c	J	0·45	126	...	...
3562	11·9	sdF7	− 4	c	P	0·60	170	...	...
3668	10·8	sdF9	+ 12	c	P	0·43	165	...	...
4005	8·08	sdGo	+167	b	J	0·08	225	+0·86	+0·22
4400	10·0	sdF2	+189	c	J	0·56	175	...	...
5058	11·6	sdG2	+ 89	c	P	0·62	141	...	...
5240*	8·34	G2 VI	−240	c	R	1·97	158	+0·60	−0·12
5494	9·69	sdF4	+ 59	c	P	0·66	182	+0·48	−0·19
5730	9·59	sdF6	+203	c	R	0·62	142	(+0·42)	(−0·25)
5757	11·5	sdF8	− 5	c	P	0·43	180	...	...
25°1981	9·35	sdF2	+ 47	R	R	0·35	197	+0·30	−0·12
5784*	8·74	sdGo	−168	b	J	0·09	149	+0·97	+0·53
5793	10·10	sdA5	+ 26	c	P	0·37	247	(+0·38)	(−0·24)
5815	10·8	sdG6	+276	c	P	0·64	155	...	...
5908	11·5	sdF7	+126	d	P	...	...	...	...
5909	9·8	sdF3	+ 25	c	J	0·79	138	...	...
5951	11·8	sdF5	− 51	c	P	0·47	180	...	...
+9°2190	10·5	sdA5	+265	G	G	...	...	...	...
6236*	11·0	sdA7p	− 59	c	P	0·54	160	...	...
6237	10·2	sdF5	− 19	c	P	...	...	...	...
6294*	8·24	sdA4	− 18	b	J	0·88	154	+0·41	−0·25
6296	10·6	sdA8	− 91	c	G	0·18	180	...	...
6704	10·3	sdF5	+ 74	c	J	0·83	165	(+0·49)	...
6728	12·6	sdGo	−128	d	P	0·38	118	...	...
6734	8·23	sdF8	+ 62	b	R	0·55	210	+0·47	−0·19
6869	10·8	sdG3	+ 68	c	P	0·82	230	...	...
6880	9·8	sdF3	−188	c	P	0·52	166	...	...
7017	11·3	sdGo	−108	c	P	0·60	171	...	...
7117	10·70	sdF5	+186	c	P	0·52	266	(+0·53)	...
7131	9·5	sdGo	+ 61	d	P	1·02	240	...	...
7170	6·49	G8 VI	− 98	b	R	7·04	145	+0·74	0·17
7266	10·1	sdA7	+ 56	c	P	0·34	226	...	...
7296	10·9	sdF2	+ 98	d	P	0·43	180	...	...
7308	10·18	F2 V–VI	+ 95	c	R	0·46	203	+0·48	−0·18
7464	9·68	sdF4	+159	c	P	0·48	180	+0·44	−0·25
7547	10·5	sdF6	− 40	e	P	0·35	283	...	...
7567	11·7	sdA6	− 57	c	P	0·35	250	...	...
7913	9·8	sdK5	+126	c	P	0·63	252	...	...
7923	12·8	sdA8	+252	d	P	...	...	...	...
7932	8·79	sdF4	+143	d	P	0·76	277	(+0·42)	...
7951	11·6	sdF2	− 34	d	P	0·18	279	...	...

TABLE V (*cont.*)

Stars classified as subdwarfs on the basis of their spectral features

Wilson No.	m_v	Sp.	ρ	Q	Ob.	μ	θ	$B-V$	$U-B$
8236	10·04	sdF3	−162	c	P	0·54	161	+0·42	−0·21
8246	11·6	sdG3	+ 16	d	P	0·88	164	...	...
8249	6·20	sdF5p	− 22	c	J	0·21	290	+0·90	+0·38
8296	9·7	sdF7	+126	c	J	0·50	215	...	...
8554	10·46	sdG2	−138	d	J	0·87	270	+0·70	+0·11
8603	9·74	sdF4	+ 34	c	R	0·35	185	+0·42	−0·22
8691*	8·5	sdA9	+167	c	P	0·75	229	...	...
8771*	9·06	Ko VI	+292	c	P	3·68	196	+0·80	0·15
9069	7·20	sdF5	−171	b	R	1·19	254	+0·48:	−0·10:
9236	10·0	sdF5	−157	c	P	0·51	213	...	...
9401	11·4	sdG2	+167	d	P	0·44	183	...	...
9840*	9·13	sdG1	− 51	c	P	0·29	229	+0·67	+0·10
+2°3375	9·95	sdF5	−389	R	R	0·37	281	+0·44	−0·20
10287	6·98	sdA2	−363	b	R	0·08	218	+0·16	+0·10
10289	10·8	sdF8	+ 91	c	M	0·44	148	...	...
10367	11·0	sdF8	−216	c	J	0·60	181	...	...
10404*	9·62	sdF8	+191	c	M	0·83	214	0·62	−0·06
11060	11·4	sdA5	− 68	G	G	0·26	184	...	...
HD 181743*	9·64	sdF	+ 18	E	E	0·82	180	(+0·46)	...
11949	10·20	sdF7	−172	c	R	0·53	183	+0·48	−0·12
+26°3578	9·36	sdF4	−128	R	R	0·17	180	+0·37	−0·23
12730	8·5	sdGo	−172	c	M	1·21	153	...	...
12754	10·6	sdFo	−319	c	M	...	...	...	...
13327	7·38	F9 VI	− 45	b	R	0·90	187	+0·51	−0·09
13543*	10·52	sdF	+103	d	M	0·48	188	(+0·40)	...
13782	11·7	sdF6	− 67	c	P	...	...	...	...
+17°4708	9·47	sdF6	−296	R	R	0·55	88	+0·43	−0·21
14122*	14·4	sdK5	−157	d	J	1·68	164	...	...
14539	10·00	sdG2	−113	b	P	1·29	189	(+0·48)	...
14568	10·62	sdF6	− 32	d	P	0·57	129	(+0·42)	...
14598*	8·17	sdF8	+ 10	b	R	1·29	203	+0·47	−0·20
14704	10·5	sdFo	−100	d	P	0·47	85	...	...
14884*	7·0v	sdF2	− 15	c	J	0·90	163	...	...
15042	8·92	sdA8	+ 50	d	M	0·34	204	(+0·33)	(−0·20)

Notes to Table V

91	LDS 1A.
646	μ Cas.
4005	Roman (1955) classifies this star as G2 III and states: "All lines are very weak".
5240	Roman (1955): "very weak lines".
5784	Roman (1955) assigns the classification G5 IV and states: "very weak lines and strong CH".
6236	Spectroscopic binary with a range of 83 km/sec.
6294	Roman (1955): sdF2.
8554	Roman (1955): G6 V.
8691	Astronometric binary, $P \sim 1300^d$.
8771	A companion, 300″ distant, has common proper motion and velocity.
9840	Roman (1955): G2 V.
10404	ADS 10938.
HD 181743	$(U-B)_C = +1^m.49$, which is roughly equivalent to $U-B = -0^m.17$.
13543	$(U-B)_C = +1^m.45$, which is roughly equivalent to $U-B = -0^m.20$.
14122	Spectroscopic binary with a range of 37 km/sec.
14598	ADS 16644.
14884	SX Phe.
15042	ADS 17173.

TABLE VI

Space motions of stars in Table V with observed ultra-violet excesses comparable to that of the M13 and Groombridge 1830 group stars

Wilson No.	μ_α	μ_δ	ρ	π_{pt}	$U+U(\odot)$	$V+V(\odot)$	$W+W(\odot)$
	"	"					
8771	−1·012	−3·544	+300	0·037	−282	−450	− 43
5240	+0·725	−1·836	−240	0·035	−273	−211	− 87
8236	+0·104	−0·438	−162	0·008	−204	−177	−140
1735	−0·203	−0·805	−139	0·026	−163	−103	− 57
6294	+0·370	−0·790	− 18	0·019	−160	−135	0
8603	−0·031	−0·347	+ 34	0·010	−130	−100	+ 29
7464	−0·012	−0·473	+159	0·012	−121	−195	+ 65
5784	+0·049	−0·082	−168	0·0017	−120	−272	+ 66
5730	+0·373	−0·488	+203	0·012	−125	−270	+ 67
13327	−0·112	−0·900	− 45	0·034	− 82	− 86	− 40
HD 16031	+0·078	−0·155	+ 63	0·012	+ 3	− 53	− 53
7308	−0·184	−0·430	+ 95	0·011	− 33	−202	+ 45
6734	−0·268	−0·465	+ 62	0·025	+ 21	− 98	+ 26
HD 181743	−0·077	−0·818	+ 18	0·013	+ 21	−275	− 44
HD 21543	+0·354	−0·204	+ 59	0·0395	+ 37	− 37	− 21
4005	+0·051	−0·056	+167	0·003	+ 38	−184	+ 6
8249	−0·203	−0·062	− 22	0·0055	+ 91	−132	+ 24
5494	−0·010	−0·648	+ 59	0·0135	+100	−187	+ 42
10287	−0·050	−0·064	−363	0·006	+160	−285	−125
+17°4708	+0·496	+0·071	−296	0·0135	+198	−250	+ 77
+ 2°3375	−0·368	+0·069	−389	0·011	+338	−213	+ 52
2420	+0·455	−0·283	+339	0·014	+344	−109	− 57

each case the space motion was computed on the assumption that the stars could be fitted to the dwarf (or giant) sequence of the (M_V, $B-V$)-diagram for M13 and the Groombridge 1830 group. This assumption is based on the observed ultra-violet excess in the colours of the stars. When more photometric and radial velocity material becomes available for subdwarfs, we believe that additional stars will undoubtedly be found to be members of these possible groups. In support of this view we include in brackets in Table VIII a few stars from Table V for which photoelectric, photometric data are not available. For these stars we have tried several parallaxes, guided by a rough spectral type–colour relationship, until one was found that gave space motion vectors similar to those for some star in Tables VI and VII. It should be emphasized that this method is exactly equivalent to the convergent point method described in Papers I and II since, for an individual star, a necessary and sufficient condition for group membership is that the components of the space motion be identical with those of the group. An illustration of the accuracy of the parallax which can be obtained by this method, on the assumption of group membership, is given below for Wilson Nos. 6294 (HD 84937) and 5909 (−3°2525). This illustration, as well as the discussion of the Groombridge 1830 stars given in Table II, also shows the sensitivity of the computed space motions to the accuracy of the fundamental data.

It should be noted that, although we have stated that group membership implies that the space vectors of the group stars are identical, this may not be precisely true. Deviations from this requirement can ocur, in U and V, of 1 to 2 km/sec/100 pc as a result of small differences in the eccentricities of isoperiodic

Wilson No. 6294

μ_α	μ_δ	
+0".380	−0".790	GC
+0".359	−0".791	Y
+0".370	−0".790	

ρ	
−18·1	W (5)
−15·3	Md (1)
−17·6	

No. 5909

μ_α	μ_δ	
+0".33	−0".58	Cape

ρ	
+20	W (6)
+40	Md (2)
+25	

π	$U+U(\odot)$	$V+V(\odot)$	$W+W(\odot)$
0".018	−168	−147	+10
[0·019	−160	−135	0]
0·020	−153	−128	−10

π	$U+U(\odot)$	$V+V(\odot)$	$W+W(\odot)$
0".010	−241	−202	−5
0·014	−172	−145	+1
[0·015	−159	−135	+2]
0·016	−148	−128	+4

orbits of widely separated stars (Woolley 1958). Also, if W is not tightly coupled with U and V, we would expect its value for the group members to be correlated with the height of the stars above or below the galactic plane because of the differences in the gravitational field at different Z-distances (Woolley 1957). However, an evaluation of this effect for the Z-distances involved here shows that extreme differences of only 10 to 15 km/sec in W will be encountered and in this preliminary investigation they will be ignored.

One of the most important uses of the possible groups discussed above is in calibrating the luminosities of field RR Lyrae variables. As is evident in Table I, even the available data for members of the Groombridge 1830 group are uncertain and this is true of subdwarfs and RR Lyrae variables in general. There are not more than a dozen RR Lyrae variables with well determined annual proper motions in excess of 0".05 and, perhaps, another dozen with relatively large but insufficiently observed motions. The same situation exists for the radial velocities which in many cases depend upon only one or two observations and often have a probable error as large as 25 km/sec. There is also an additional uncertainty in the radial velocities of the RR Lyrae variables caused by the uncertainty in the phase of the light variation.

We have tentatively identified the motions of a few of the field RR Lyrae variables, that have large and relatively well determined motions, with those of subdwarfs. These stars are listed in Table IX where various determinations of the proper motion and radial velocity and the space motions of the variables, for two values of the parallax are given. The mean absolute visual magnitude of the variables, determined by the group parallax method, together with RR Lyrae from the Groombridge 1830 group, is $M_V = +0^m.6$. This value must be considered as preliminary since accurate photometry is not yet available for most of the variables. This preliminary value of $+0^m.6$ should be compared with the usually adopted value of $0^m.0$ determined solely from a statistical discussion of the motions of these stars. It should also be noted that the most recent determination based on these statistics is $+0^m.5$ (Pavlovskaia 1953). But the agreement of $+0^m.6$ and $+0^m.5$ obtained by the two methods should

TABLE VII

Space motions for a few giant, horizontal branch and subdwarf stars in the solar neighbourhood

Wilson No.	μ_α	μ_δ	ρ	π_{pt}	$U+U(\odot)$	$V+V(\odot)$	$W+W(\odot)$	V	$B-V$	$U-B$	Sp.
	"	"		"				m	m	m	
6379	+0·144	−0·228	+ 13	0·0038	−253	−214	+ 42	7·99	+0·12	+0·16	A1 V
3785	+0·673	−0·633	−190	0·024	−228	−121	+ 60	9·32	+0·62	−0·08	G0 V
7708	+0·307	−0·792	+144	0·029	−157	−125	+ 10	8·38	+0·53	−0·11	F8 V
665*	+0·028	+0·046	−245	0·0028	−121	−193	+116	6·73	+1·18	+0·88	K1 III
13660	−0·374	−0·507	− 51	0·035	− 82	− 53	+ 10	9·41	+0·85	+0·29	K0 V
HD 221170*	+0·011	−0·045	−120	0·002	− 69	−207	+ 89	7·66	+1·13	+0·64	G2 IV
58	+0·334	−0·007	+ 80	0·0385	− 12	− 63	− 33	8·37	+0·65	−0·07	G2 V
12951	+0·044	−0·436	− 30	0·0295	− 8	− 75	− 15	8·21	+0·51	−0·13	F6 V
8433	−0·062	−0·298	− 47	0·022	+ 14	− 19	− 62	9·33	+0·60	−0·07	G2 V
HD 117880	−0·061	−0·135	− 45	0·0025	+ 21	−190	−185	9·08	+0·04	+0·06	A0 V
2302	+1·745	−1·348	− 30	0·050	+ 38	−190	+ 25	8·52	+0·88	+0·36	K1 V
4801	−0·499	+0·173	+ 60	0·0495	+ 58	− 2	− 26	7·73	+0·63	−0·01	G2 V
8754	−0·514	−0·058	− 60	0·0335	+ 61	− 43	− 4	8·27	+0·57	−0·06	F9 V
HD 63410	−0·026	−0·016	+ 81	0·004	+ 73	− 12	+ 9	6·78	+0·95	+0·59	G8 III
12767	+0·113	−0·549	−246	0·026	+ 85	−230	+ 12	8·36	+0·49	−0·14	F6 V
6038*	−0·147	+0·046	+ 56	0·008	+ 93	+ 36	− 12	5·97	+0·86	+0·37	G6 III
HD 5916	+0·106	−0·021	− 71	0·0030	+ 92	−138	+ 3	6·84	+0·90	+0·45	G8 III–IV
6120*	−0·090	−0·114	+135	0·0055	+ 99	−128	+ 26	6·56	+0·94	+0·55	G8 III
1428	+0·400	−0·060	+234	0·010	+200	−164	−134	10·42	+0·47	−0·17	dF1

* 665 Mt Wilson, dG5.

HD 221170 "The colour indicates a much later spectral type, but the strength of the hydrogen lines makes this unlikely. CH is strong; all other lines are weak." (Roman 1955.)

6038 Mt Wilson: sgG3.

6120 Mt Wilson: dG5. Roman (1955): "Strong CH and very weak lines",

not be stressed since the inherent inaccuracies of the traditional statistical parallax method make it inferior to the method demonstrated here.

TABLE VIII

Possible groups

Wilson No.	π	$U+U(\odot)$	$V+V(\odot)$	$W+W(\odot)$	V	$B-V$	Sp.	M_V
	"				m	m		m
6294	0·019	−160	−135	0	8·24	0·41	sdF2	+4·6
7708	0·029	−157	−125	+ 10	8·38	0·53	F8 V	+5·7
[5909	0·015	−159	−135	+ 2	9·8:	...	sdF3	+5·7:]
[6728	0·0105	−160	−126	0	12·2:	...	sdGo	+7·3:]
2302	0·050	+ 38	−190	+ 25	8·52	0·88	K1 V	+7·0
4005	0·003	+ 38	−184	+ 6	8·08	0·86	G2 III*	+0·5
HD 5916	0·0030	+ 92	−138	+ 3	6·84	0·90	†	−0·8
8249	0·0055	+ 91	−132	+ 24	6·20	0·90	†	−0·1
6120	0·0055	+ 99	−128	+ 26	6·56	0·94	†	+0·3
5730	0·012	−120	−270	+ 67	9·59	0·43	sdF6	+5·0
5784	0·0017	−120	−272	+ 66	8·74	0·97	‡	−0·2
[5058	0·015	−115	−198	+ 67	11·6:	...	sdG2	+7·5:]
7464	0·012	−121	−195	+ 65	9·68	0·44	sdF4	+5·1
8236	0·0075	−204	−177	−140	10·04	0·42	sdF3	+4·4
[6880	0·0105	−203	−174	−126	9·8:	...	sdF7	+6·0:]
[7017	0·020	− 71	−133	+ 47	11·2:	...	sdGo	+7·7:]
8296	0·015	− 74	−145	+ 50	9·7:	...	sdF7	+5·6:]
10287	0·006	+160	−285	−125	6·98	0·16	sdA2§	+0·9
[10367	0·009	+143	−303	−155	11·0:	...	sdF8	+5·8:]

* 4005. Roman (1955): " All lines are very weak ".

† HD 5916 and Wilson Nos. 8249 and 6120. HD 5916 has been classified as G8 III–IV by Roman (1955) and as dG2 at Mt Wilson (Wilson 1953); the observed colour is much too red for either classification. No. 8249 (HD 122563) has been classified Go VI by Roman and sdF5p by Wilson and Joy (1950) who state that the hydrogen and metallic lines are weak; the colour is much too red for either classification. No. 6120 (HD 81192) has been classified as G8 II by Roman, who states, " Strong CH and very weak lines ", and as G7 III+ by Keenan and Keller (1953), who state, " CN and metallic lines weak and 4172 slightly strong ". The parallaxes used in computing the space motions of all three stars were obtained by fitting the stars to the $(M_V, B-V)$-diagram of Fig. 3 near the bifurcation of the giant sequence.

‡ 5784. This star (HD 74462) has been classified as G5 IV by Roman with the statement, " very weak lines and strong CH ", and as sdGo by Wilson and Joy. The colour is too red for either classification and the space motion has been computed from a parallax derived on the assumption that the star is a globular cluster giant.

§ 10287. This high velocity A-type star (HD 161817) is probably a horizontal branch star. The spectra are described in detail by Slettebak (1952).

TABLE IX

Space motions for a few RR Lyrae variables compared with those for subdwarfs

Star	μ_α	μ_δ	S*	ρ	S*	π	$U+U(\odot)$	$V+V(\odot)$	$W+W(\odot)$	M_V
	″	″								
TU U Ma	−0.076 ± 6	−0.050 ± 6	1							
	−0.076 ± 6	−0.042 ± 7	1							
	−0.076 ± 5	−0.047 ± 5		+105	W (3)	0.0018	+155	−182	+ 54	
						0.0013	+193	−255	+ 35	+0.4
+17°4708	+0.510	+0.071	Y	−296	R (4)	0.0135	+198	−250	+ 77	+5.1
SU Dra	−0.035 ± 6	−0.068 ± 6	1							
	−0.025 ± 10	−0.075 ± 10	1							
	−0.044 ± 10	−0.071 ± 11	1							
	−0.035 ± 4	−0.070 ± 4		−180	W (8)	0.0013	− 21	−319	− 7	
						0.0016	− 13	−271	− 35	+0.8
W 5757	0.00	−0.43	H	− 5	Md (2)	0.007	− 18	−265	− 31	+6.0:
X Ari†	+0.091 ± 4	−0.075 ± 4	Y							
	+0.080 ± 6	−0.093 ± 6	1							
	+0.054 ± 10	−0.081 ± 10	1							
	+0.084 ± 3	−0.081 ± 3		− 40	W (1)	0.0020	+ 1	−261	+ 24	
				− 20	...	0.0019	+ 11	−275	+ 10	+0.8
HD 181743	−0.077	−0.818	C	+ 18	C (4)	0.013	+ 21	−275	− 44	+5.2
W CVn	−0.061 ± 13	−0.014 ± 13	1							
	−0.047 ± 9	−0.020 ± 9	1							
	−0.020 ± 13	−0.008 ± 13	1							
	−0.044 ± 6	−0.016 ± 6		+ 26.5	W (24)	0.0009	+ 95	−185	+120	
						0.0008	+126	−200	+127	+0.2
W 7932	−0.749	+0.096	C	+142	C (4)	0.016	+ 95	−205*	+120	+4.8

* 1 = *Variable Stars*, 9, 1955; Y = Yale; H = Hertzsprung; C = Cape; W = Mt Wilson and Md = McDonald.

† The radial velocity depends upon one Mt Wilson spectrogram. The dependence of the space motion vectors on the radial velocity is illustrated by assuming an alternative value of −20 km/sec.

Although the accuracy of the group parallax value of $M_v = +0.6$ should also not be emphasized at the present time, the potential accuracy of this method is so high that its exploitation promises to provide a definitive calibration of the luminosity of RR Lyrae variables when good astrometric and photometric data are available.

Royal Greenwich Observatory,
Herstmonceux Castle,
Sussex :
1959 *February* 27.

Mt Wilson and Palomar Observatories,
Carnegie Institution of Washington,
California Institute of Technology,
Pasadena, Cal., U.S.A.

References

Arp, H. C. and Johnson, H. L., 1955, *Ap. J.*, **122**, 171.
Arp, H. C., 1955, *A. J.*, **60**, 317.
Baum, W. A., Hiltner, W., Johnson, H. L. and Sandage, A. R., 1959, *Ap. J.*, in press.
Belserene, E. P., 1954, *A.J.*, **59**, 406.
Eggen, O. J., 1956, *A.J.*, **61**, 361.
—— 1958 a, *M.N.*, **118**, 65.
—— 1958 b, *M.N.*, **118**, 155.
—— 1958 c, *M.N.*, **118**, 560.
Evans, D. S., 1958, private communication.
Greenstein, J. L., 1954, *Pub. A.S.P.*, **66**, 126.
Hardie, R. H., 1955, *Ap. J.*, **122**, 256.
Iwanowski, W., 1953, *Torun Bull.* III, No. 2.
Jenkins, L., 1952, *General Catalogue of Trigonometric Stellar Parallaxes*, Yale Univ. Obs.
Johnson, H. L. and Sandage, A. R., 1956, *Ap. J.*, **124**, 379.
Joy, A. H., 1947, *Ap. J.*, **105**, 96.
Keenan, P. C. and Keller, G., 1953, *Ap. J.*, **117**, 241.
Lindholm, E. H., 1957, *Ap. J.*, **126**, 588.
Münch, G., 1944, *Ap. J.*, **99**, 271.
Parenago, P. P., 1946, *Astr. Jour. Soviet Union*, **23**, 31.
Pavlovskaia, P., 1953, *Variable Stars*, **9**, 349.
Popper, D. M., 1942, *Ap. J.*, **95**, 307.
—— 1943, *Ap. J.*, **98**, 209.
Preston, G., 1958, unpublished results.
Roman, N. G., 1955, *Ap. J. Supplement*, No. 18.
Sandage, A. R., 1956, *Ap. J.*, **123**, 278.
—— 1958, *Stellar Populations, Spec. Vat.*, **5**, 41.
—— 1959, *Ap. J.*, **129**, 596.
Sandage, A. R. and Eggen, O. J., 1959, *M.N.*, **119**, 278.
Sandage, A. R. and Walker, M., 1955, *A.J.*, **60**, 230.
Slettebak, A., 1952, *Ap. J.*, **115**, 576.
Stoy, R. H., 1958, *M.N.A.S.S.A.*, **17**, 142.
Tifft, W. and Smith, H. J., 1958, *Ap. J.*, **127**, 513.
Wilson, R. E., 1953, *General Catalogue of Stellar Radial Velocities*, Carnegie Inst. of Wash. Pub. No. 601.
Wilson, R. E. and Joy, A. H., 1950, *Ap. J.*, **111**, 221.
Woolley, R. v. d. R., 1957, *M.N.*, **117**, 198.
—— 1958, *M.N.*, **118**, 45.
—— 1959, *Vistas in Astronomy*, III, London.

ON THE EXISTENCE OF SUBDWARFS IN THE (M_{Bol}, LOG T_e)-DIAGRAM

Allan R. Sandage and Olin J. Eggen

(Communicated by the Astronomer Royal)

(Received 1959 March 4)

Summary

The effect of weakening the Fraunhofer lines on the observed colour indices of stars is examined. The blocking of the continuum radiation by the lines and the change in the temperature distribution of the solar atmosphere due to the lines is taken into account. If all of the lines were removed from the Sun, the change in the observed colour indices is predicted to be $\Delta(U-B)=0^m.32$ and $\Delta(B-V)=0^m.17$. These changes define a "blanketing line" in the $(U-B, B-V)$-diagram from which the correction to the observed $B-V$ colour due to line weakening can be found from the observed ultra-violet excess $\delta(U-B)$.

The magnitude and colour data for subdwarfs lying more than $0^m.25$ below the normal main sequence are given. Colour corrections derived from the observed ultra-violet excesses are applied to the observed $B-V$ colours. The corrections are sufficient to move the mild subdwarfs on to the Hyades main sequence. The conclusion is that most subdwarfs are below the main sequence in the $(M_V, B-V)$-diagram only because of the effect of the weak Fraunhofer lines on their observed colours. Members of the Groombridge 1830 moving group are not completely corrected to the main sequence and it is possible that these stars do in fact lie below the main sequence in the (M_{Bol}, log T_e)-diagram. Tentative conclusions from the data are (1) the internal opacity of subdwarfs is probably due to free-free transitions of H and He rather than the photoelectric opacity of the heavy elements, and (2) the H/He ratio in the Groombridge 1830 stars may differ slightly from that of the Hyades.

The blanketing model gives a relation between the magnitude difference of any star from the Hyades main sequence and the observed ultra-violet excess. The relation is applied to stars in different galactic clusters and to stars in the general field with the result that (1) the method of fitting main sequences to find distance moduli of galactic clusters is in error if corrections for the different ultra-violet excesses are not applied, and (2) the observed range of 0·10 mag. in the ultra-violet excesses of field stars which are usually called "main sequence dwarfs" shows that the total intrinsic width of the main sequence defined by these stars is at least $0^m.60$. Because the strong-line field stars, the subdwarfs, and stars in different galactic clusters form a continuum in the $(B-V)$, $(U-B)$-diagram, it seems probable that (*a*) the subdwarfs form a continuum in the $(M_V, B-V)$-diagram, merging into the more normal, strong-line stars and (*b*) differences in the heavy element abundance exist between individual field stars and between stars in different galactic clusters.

Introduction.—The presence of stars between the normal main sequence and the white dwarfs in the HR diagram has been known since the work of Adams and Joy (1922) and of Adams, Joy, Humason, and Brayton (1935). Modern

trigonometric parallaxes for the nearby stars leave no doubt that there are stars which lie as much as $1^m.5$ below the normal main sequence. However, because subdwarfs exist in the (M_V, spectral type)- and the (M_V, colour index)-diagrams does not guarantee that they exist in the (M_{Bol}, log T_e)-diagram. Different bolometric corrections and a different colour-effective temperature relation may apply to subdwarfs and main-sequence stars. The present paper is concerned with the observed ultra-violet excess for known subdwarfs with well determined absolute magnitudes. Following Strömgren (unpublished) and Schwarzschild, Searle and Howard (1955), this excess is interpreted as an effect of the Fraunhofer lines on the continuous spectrum. A "blanketing model"* is given using the blanketing coefficients for the Sun by Michard (1950). This model predicts that the change in $B-V$ for a given observed ultra-violet excess, $\delta(U-B)$, for F and G subdwarfs is just sufficient to move most of the subdwarfs with known M_V on to the Hyades main sequence.

The observational data on subdwarfs with well determined absolute magnitudes are given in Section 1, where the ultra-violet excess is discussed. The semi-empirical blanketing model giving the $\Delta(B-V)=f[\delta(U-B)]$ relation is derived in Section 2. Here the predictions of the model are compared with the observations. The model is applied to the observed $B-V$ values and the corrected positions of the subdwarfs in the (M_V, $B-V$)-diagram are shown. To interpret the observational results in terms of stellar structure, the well-known theoretical equations are then reviewed. Other applications of the theory are given in Section 3.

1. *Observational data for subdwarfs.*—The term subdwarf was first used by Kuiper in 1939 to describe stars lying between the main sequence and the white dwarfs. Subdwarfs had been found several years earlier in the Mt Wilson spectroscopic parallax programme when a list of 6 so-called "intermediate white dwarfs" was published (Adams, Joy, Humason and Brayton 1935). It is important to point out that most "subdwarfs" have been so termed not by definite knowledge of their position in the HR-diagram but rather by the peculiar spectral features or by large proper motions. For example, in the searches carried out by Kuiper from 1939 to 1942, the parallaxes of proper motion stars were inferred from the assumption that the tangential velocities were less than 474 km/sec, that is, that $\pi/\mu \prec 0''.01$. This procedure, and its justification, is described by Kuiper in the publication of the Paris Colloquium on white dwarfs (1941). Clearly the method can give only very approximate estimates of the real absolute magnitudes of these stars. Kuiper's early estimates placed the subdwarfs in a band extending to 3 magnitudes fainter than the main sequence in the HR-diagram (Kuiper 1941, Fig. 1).

P. P. Parenago later discussed the data available for subluminous stars in 1946. He used absolute magnitudes derived entirely from trigonometric parallaxes (Parenago 1946, Table 2) but only eight stars, other than white dwarfs, had $\pi \geqslant 0''.050$. Parallaxes smaller than this are usually so uncertain as to be of little individual value. The HR-diagram determined by Parenago shows a band of subdwarfs lying $2^m.5$ below the main sequence.

In recent years it has been pointed out that the subdwarfs are usually assigned an earlier spectral class than that compatible with their effective temperature.

* The nomenclature will be described in Section 2.

This misclassification, which is partly due to the weakness of the spectral lines, has the effect of placing the subdwarfs too far to the left in the HR-diagram and therefore introducing a false displacement from the normal main sequence. It has been pointed out by Greenstein (1956) that the colour-index is a better indication of the true temperature of subdwarfs than the spectral type. It has been shown, however, that the colour is also affected by the weakness of the spectral lines (Schwarzschild, Searle and Howard 1955). A fundamental question is whether a subdwarf sequence remains in the (M_V, $B-V$)-diagram when proper correction is made for the effect of the weak Fraunhofer lines on the observed colour.

To investigate this question we have selected all the stars, later than Fo, which fall more than $0^m.25$ below a standard main sequence (Eggen 1955 *b*, Table III). Only stars with photoelectrically determined magnitudes and colours and

TABLE I

Subdwarfs more than $0^m.25$ below the main sequence

Yale No.	HD	V	$P-V$	$B-V$	$U-B$	Sp	$\pi \pm$P.E. Unit $0''.001$	Wt.	M_V	Remarks
		m	m						m m	
3	55	8·51	0·94	...	...	Ko	72± 8	14	7·80± ·24	
219	6582	5·14	0·59	0·71	0·11	Go VI	136± 6	32	5·81± ·10	μ Cass
365	10700	3·50	0·62	0·72	0·20	G8Vp	275± 5	34	5·70± ·04	τ Cet
479	14412	6·32	0·62	0·72	0·17	G5V	88± 8	18	6·03± ·17	
599	17925	6·04	0·78	0·87	0·56	dKo	122± 6	25	6·46± ·11	
701	20766	5·51	0·52	0·64	0·06	G2V	106± 12	7	5·31± ·25	ζ^1 Ret
705	20807	5·22	0·46	0·58	−0·04	G1V	97± 12	7	5·02± ·27	ζ^2 Ret
887	25329	8·52	0·78	0·88	0·36	K1V	54± 5	36	7·18± ·20	
1002	...	8·32	0·80	0·89	0·65	K2V	56± 7	18	7·06± ·27	
1314	38230	7·31	0·73	0·83	0·51	dK2	77± 5	40	6·69± ·14	
1864	64379	5·02	0·34	0·44	−0·06	F5V	67± 7	19	4·11± ·23	SDS, 3″
1889	65583	7·01	0·59	0·70	0·18	G8V	56± 5	48	5·75± ·19	
2082	74377	8·53	0·84	...	...	dK5	59± 5	40	7·38± ·18	
2413	89125	5·82	0·39	0·50	−0·05	dF3	60± 5	35	4·70± ·18	39 Leo. ADS 7712A
2745	103095	6·41	0·64	0·74	0·17	sdG8	116± 5	36	6·72± ·09	Gmb 1830
2935	110897	5·98	0·42	0·54	−0·01	GoV	65± 7	23	5·04± ·23	10CVn
2974	112758	7·54	0·70	...	...	dK1	61± 8	14	6·47± ·29	
3010	114606	8·74	0·52	0·61	0·05	G3V	52± 6	28	7·32± ·25	
3264	126053	6·26	0·52	0·63	0·08	dG3	61± 6	32	5·19± ·21	
3300	128167	4·46	0·24	0·36	−0·08	F2V	63± 6	27	3·48± ·21	σ Boo
3416	134083	4·93	0·31	0·42	−0·03	F5V	61± 7	22	3·87± ·25	45 Boo
3650	144579	6·66	0·63	0·73	0·21	dG8	80± 5	35	6·19± ·14	
3654	144872	8·58	0·82	0·96	0·71	K3V	56± 7	20	7·29± ·27	
3669	145417	7·54	0·70	...	...	KoV	63± 5	40	6·55± ·17	
3827	151877	8·42	0·72	0·82	0·44	K7V	50± 5	36	6·91± ·21	
3884	154577	7·43	0·78	...	...	KoV	79± 7	20	6·95± ·19	
...*	163810	9·62	0·52	0·62	−0·06	sdF8	group	...	6·0 ± ·10	Member 1830 Gr.
4782	191408	5·32	0·76	...	...	K3V	171± 8	16	6·49± ·13	SDS, HR 7703
4849	193664	5·94	0·48	0·58	0·06	G5V	66± 5	45	5·04± ·16	
5152	203608	4·24	0·36	...	...	F8V	111± 5	17	4·49± ·16	γ Pav
...†	219617	8·17	0·36	0·47	−0·20	sdF8	group	...	4·8 ± ·10	Member 1830 Gr.
5807‡		5·76	0·55	0·67	0·05	G2V	86± 4	69	5·43± ·10	85 Peg. ADS 17175A

* ADS 10938. $\Delta m = 1^m$.

† ADS 16644. The magnitude of one component is assumed to be $M_V = 5·55$ because $\Delta m = 0$ for the binary.

‡ 85 Peg. Not plotted in Figs. 1, 2, 3 or 4 because the photometric values refer to both components. $\Delta m = 2·93$.

$\pi \geqslant 0''{\cdot}05$ based on observations from more than one observatory have been used. The available data for these stars, and for the members of the Groombridge 1830 group discussed elsewhere (Eggen and Sandage 1959) are listed in Table I. The HD and the parallax catalogue (Jenkins 1952) numbers identify the stars. The values of V and $P-V$ are taken from a previous publication (Eggen 1955*a*); the values of $U-B$ and $B-V$ are taken from the photometric catalogues by Roman (1955), Johnson and Morgan (1953) and Johnson and Knuckles (1957). We have also determined $U-B$ and $B-V$ for three southern stars with the 18-inch reflector at the Cape Observatory.

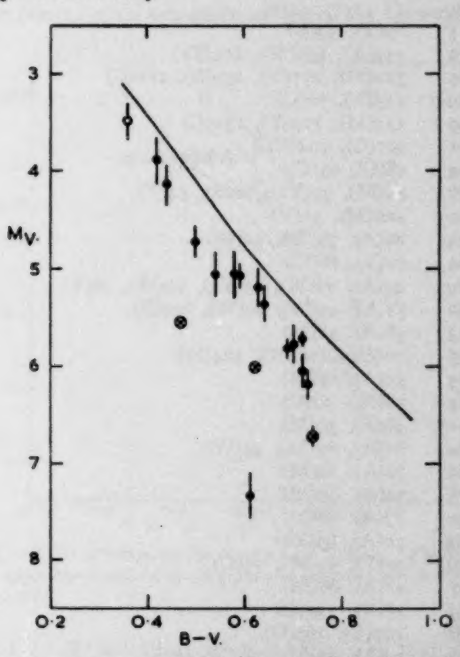

FIG. 1.—*The (M_V, $B-V$)-diagram for stars with $\pi > 0''{\cdot}05$ determined at more than one observatory which lie more than $0^m{\cdot}25$ fainter than the normal main sequence. The three crossed circles are members of the Groombridge 1830 group. The gap between the points and the main sequence is artificial and results from the requirement that $\Delta M_V > 0^m{\cdot}25$. The open circle indicates Yale No. 3300. The uncertainty in M_V due to the probable error of the parallaxes is indicated by vertical lines.*

It might be argued that the sample of subdwarfs in Table I is too small to be representative, especially since only five stars are common with a previous tabulation (Eggen and Sandage 1959, Table V) of subdwarfs discovered by their spectral characteristics. However, the previous tabulation includes the extreme subdwarf members of the Groombridge 1830 group, which are also included in Table I, and since the departure of the group members from the main sequence is nearly matched by other stars in Table I, it is thought that, except for one doubtful case discussed below, the data in Table I represent the total spread of subdwarfs in the (M_V, $B-V$)-diagram. As usual, the individual trigonometric parallaxes must be considered with some caution, as can be seen from the separate determinations listed in Table II; note particularly the disagreement for Yale

Nos. 1002, 2974, 3300. Yale No. 3300 is indicated in Figs. 2 and 6 as an open circle. The stars in Table I provide the only absolute magnitudes of sufficient precision to define the subdwarf region in the $(M_V, B-V)$-diagram.

TABLE II

Individual parallaxes for stars in Table I

(Unit 0″·001)

Yale No.	π_t
3	89(Y), 53(C)
219	143(A), 138(M), 105(Yk)
365	312(M), 277(Y), 257(S), 288(C)
479	115(Y), 76(C)
599	133(M), 113(Y), 131(C)
701	107(C), 104(C) } Adopted = 91
705	98(C), 63(C) }
887	45(M), 39(Yk), 72(S), 54(V)
1002	106(M), 30(V)
1314	86(A), 75(M), 54(W)
1864	71(Y), 68(C)
1889	42(A), 73(M), 55(Yk), 61(W), 66(V)
2082	51(A), 45(M), 49(W), 104(S)
2413	56(A), 56(M)
2745	108(A), 106(M), 164(St)
2935	58(A), 65(M)
2974	78(M), 37(C)
3010	46(A), 53(M)
3264	61(A), 65(M), 44(W)
3300	70(A), 28(M)
3416	54(A), 67(M)
3650	77(A), 78(M)
3654	50(A), 63(Yk)
3669	71(Y), 53(W), 75(C)
3827	42(A), 67(M)
3884	56(Y), 119(C)
4782	177(Y), 167(C)
4849	50(A), 85(M), 71(G), 66(S)
5152	124(Y), 98(C)
5807	84(A), 57(M), 77(Yk), 127(W), 114(S), 63(St)

Fig. 1 shows the $(M_V, B-V)$-diagrams defined by the stars in Table I that are bluer than $B-V=0^{m}\cdot80$ and for which values of $U-B$ are available. The main sequence of the Hyades (Heckmann and Johnson 1956) is shown for comparison, and members of the Groombridge 1830 group are shown as crossed circles. One star, Yale No. 3010, falls considerably outside the region of the $(M_V, B-V)$-diagram populated by the other stars in Table I. The spectroscopic observations of this star, discussed previously (Eggen 1955*b*), indicate that the spectrum is no more abnormal than the intermediate subdwarf μ Cassiopeiae and certainly not as abnormal as the extreme subdwarf Groombridge 1830. Although there are other stars, whose absolute magnitudes depend upon only one determination of the trigonometric parallax, that also fall in the same region of the $(M_V, B-V)$-diagram as Yale No. 3010, we will base our arguments on the remaining stars in Table I with well determined parallaxes. It is important, however, that the parallax of

Yale 3010 be checked and that a second determination be made for such stars as Yale Nos. 291, 595, 1282 and 4148.

Many of the stars in Table I show an ultra-violet excess with respect to a standard ($U-B$, $B-V$)-relation. The ($U-B$, $B-V$)-diagram is shown in Fig. 2 where the crossed circles are stars in the Groombridge 1830 group and the broken curve, parallel to the adopted, normal relation, is the position of the ($U-B$, $B-V$)-relation for giants and subgiants in M3 (Johnson and Sandage 1956). Note that the Groombridge 1830 stars follow the globular cluster relation fairly closely, a point discussed in a previous paper (Eggen and Sandage 1959) when fitting the globular cluster main sequence to that of the Groombridge 1830 group.

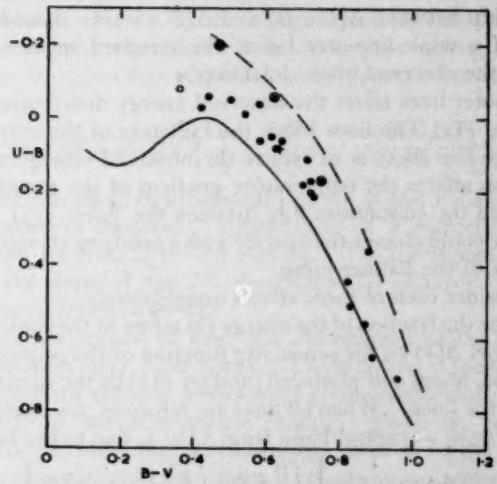

FIG. 2.—*The ($U-B$, $B-V$)-diagram for the stars in Table 1. The lower line is defined by Hyades stars. The upper line is defined by the giant and subgiant stars in M3. The same symbols as those in Fig. 1 are used.*

The standard ($U-B$, $B-V$)-relation in Fig. 2 is that defined by Hyades main sequence stars (Johnson and Knuckles 1955, Heckmann and Johnson 1956) which are probably unaffected by companions. Because the ($U-B$, $B-V$)-relation is known to vary from cluster to cluster, we will use both this relation and the (M_V, $B-V$)-relation for Hyades members alone in what follows. This is important because the theory in Section 2 gives ΔM_V from a main sequence defined by certain stars as a function of the ultra-violet excess with respect to the same stars.

We have not used the intrinsic ($U-B$, $B-V$)-relation given by Johnson and Morgan (1953, Table 14). Their mean values are nearly $0^m{\cdot}04$ brighter in $U-B$ than a sample of nearby stars from $B-V=0^m{\cdot}47$ to $0^m{\cdot}60$ (Johnson and Knuckles 1957). We suspect that some of the stars used by these authors in forming means in this range of $B-V$ are binary stars, evolved subgiants, or subdwarfs which should not have been used if a pure main sequence relation is desired. In any case, because the intrinsic relations for the Hyades, Praesepe, and Coma Berenices are known to differ from each other (Johnson and Knuckles 1955) the gross mean of all field stars is expected to have a scatter of at least $\pm 0^m{\cdot}04$ at a given $B-V$.

The differences can be interpreted on our present model if the metal abundance is lower in Coma Berenices stars than in Hyades members. This point is discussed in Section 3.

2. *The blanketing model.*—The essential point of the theory presented here is that the Fraunhofer lines affect the U, B and V regions of the spectrum in different ways so that a weakening of the lines produces changes in the observed colour indices, $U-B$ and $B-V$. If the relationship between the effect on $U-B$ and on $B-V$ is known, then the correction to the observed $B-V$ can be computed from the observed ultra-violet excess. Because the observed $B-V$ for weak line stars will be bluer than that for strong line stars of the same temperature, the weak line stars will fall below the standard main sequence. Therefore, because of the relationship between $\Delta(U-B)$ and $\Delta(B-V)$ we should expect that the displacement of a weak line star below the standard main sequence will be correlated with the observed ultra-violet excess.

The Fraunhofer lines affect the observed energy distribution of a star in at least three ways. (1) The lines block the radiation of the continuum and at a given wavelength the effect is to reduce the observed emergent flux. (2) The blocked radiation affects the temperature gradient of the atmosphere itself and therefore changes the continuum flux between the lines. (3) A change in the metal abundance could change the opacity with a resulting change in the emergent flux and the size of the Balmer jump.

We now consider each of these effects quantitatively.

(1) Let $\epsilon(\lambda)$ be the fraction of the energy (in terms of the continuum) absorbed by lines at λ. Let $S(\lambda)$ be the sensitivity function of the particular photometric system (telescope, filters and photocell) and let $F(\lambda)$ be the continuum flux of the source between the lines. When all lines are removed, the change in the magnitude of the source in a spectral band from λ_1 to λ_2 due to the first effect is

$$\Delta \text{ mag} = 2{\cdot}5 \log\left[\int_{\lambda_1}^{\lambda_2} FS d\lambda \Big/ \int_{\lambda_1}^{\lambda_2} FS(1-\epsilon) d\lambda\right]. \qquad (1)$$

Unfortunately, adequate values of $\epsilon(\lambda)$ do not exist for stars other than the Sun in the wavelength interval of the (U, B, V)-system. For a first approximation of this effect we are forced to use the Sun, for which values of $\epsilon(\lambda)$ from $\lambda = 3100$ to $\lambda = 8700$ are available (Michard 1950). Extensive blanketing measurements in stars of different spectral types are now in progress by the Burbidges, Sandage and Wildey, but the results are not yet available. A major difficulty in these measurements is in assigning a precise value of the continuum level in the shorter wavelengths of the spectra.

Michard's values for $\epsilon(\lambda)$, determined from a study of the continuum level in the Utrecht Atlas, were used. They refer to the centre of the disk. The $S(\lambda)$ values are taken from Johnson's definition of the (U, B, V)-system (1955). The values of $F(\lambda)$ were taken from Minnaert (1953, Table 2) and refer to the continuum between the lines at the centre of disk. The values of ϵ, S and F substituted in equation (1) show that if all lines are removed from the Sun the changes in U, B and V due to the first effect would be

$$\begin{aligned} \Delta U &= 0{\cdot}^{\text{m}}653 \\ \Delta B &= 0{\cdot}282 \\ \Delta V &= 0{\cdot}075 \\ \Delta(B-V) &= 0{\cdot}21 \\ \Delta(U-B) &= 0{\cdot}37 \end{aligned} \qquad (2)$$

(2) The most recent study of the change in the temperature gradient of the solar atmosphere due to the Fraunhofer lines is that by A. Przybylski (1957) where a historical summary with references should be consulted. The effect was first studied by Milne (1928) and was labelled "blanketing" because the lines act as a blanket on the solar atmosphere causing the continuum temperature to rise over what it would have been in the absence of lines. (In the present paper we use the term "blanketing" to denote the total effect of the lines on the emergent flux observed with wide filter bands, that is, the sum of our three effects.) Using Pecker's computations (1951) of the line absorptions for various optical depths, Przybylski shows that in the presence of lines, the temperature at the mean depth for continuum formation ($\tau \approx 0{\cdot}6$) is higher by about 200°K than it would be if the lines were removed. Hence, on removing all the lines, the continuum colours should be redder than those predicted in (2). Approximating the 200° change by a change in the emergent flux of a black body gives the correction due to this second effect as

$$\Delta(B-V) = 1{\cdot}086 C_2 \Delta(1/T)\left[\frac{1}{\lambda_1} - \frac{1}{\lambda_2}\right] = -\frac{1{\cdot}086 C_2 \Delta T}{T^2}\left[\frac{1}{\lambda_1} - \frac{1}{\lambda_2}\right] \qquad (3)$$

where λ_1 and λ_2 are the effective wavelengths of the B and V band-passes and C_2 is the second radiation constant. Substitution of $T = 5700$°K, $\Delta T = 200$°K, $\lambda_1 = 4430$ and $\lambda_2 = 5540$ gives $\Delta(B-V) = 0^m{\cdot}04$. The corresponding $\Delta(U-B)$ is estimated from the slope of the $U-B = f[(B-V)]$ relation (Table III) near $B-V = 0^m{\cdot}6$ to be $\Delta(U-B) = 0^m{\cdot}05$.

(3) Subdwarfs are known to have low abundances of the heavy elements (Chamberlain and Aller 1951, Aller 1958). The lowering of the metal abundance is expected to change the electron pressure at a given temperature in Go stars with a resulting change in the atmospheric opacity. However, computations by Kandell (unpublished) show that the change has no effect on the emergent continuum flux. A computation of the expected change in the colour temperature—effective temperature relation as a function of electron pressure gives the same result as is shown by comparison of Figs. 1 and 3 of Sandage (1956). Fig. 3 shows that a decrease in the metal abundance will decrease P_e at given θ_e and log g values if $\theta_e > 0{\cdot}8$. But Fig. 1 of the same reference shows that the (θ_e, θ_c) relation is insensitive to P_e for $\theta_e > 0{\cdot}8$, which proves the result. Consequently no effect on the colour is expected from the change in P_e by decreasing the metal abundance.

In summary then, the total change in the colour of the centre of the solar disk from these three effects is

$$\Delta(U-B) = 0^m{\cdot}37 - 0^m{\cdot}05 = 0^m{\cdot}32$$
$$\Delta(B-V) = 0^m{\cdot}21 - 0^m{\cdot}04 = 0^m{\cdot}17. \qquad (4)$$

The observed colours for the Sun are $B-V = 0^m{\cdot}63$ and $U-B = 0^m{\cdot}08$ (Stebbins and Kron 1957). These values refer to the integrated light of the entire solar disk. The $B-V$ value agrees well with that expected for a dwarf G2. Because the centre of the solar disk has a spectral type of dGo, we expect its colour to be $B-V = 0^m{\cdot}59$ and $U-B = 0^m{\cdot}04$; values obtained by interpolation in the standard spectral type-colour relation. These values indicate that the Sun has an ultraviolet excess of about $0^m{\cdot}08$ with respect to Hyades stars and, on the present model, this suggests that the Sun has weaker Fraunhofer lines than the Hyades. With the ratio $\Delta(U-B)/\Delta(B-V) = 0{\cdot}32/0{\cdot}17$ from equations (4) and with $\Delta(U-B) = +0^m{\cdot}08$ the predicted $\Delta(B-V)$ for the Sun is $0^m{\cdot}04$. Consequently, if all lines

were removed from the stronger-line Hyades stars, the predicted colour changes are $\Delta(B-V)=0^{m}\cdot17+0^{m}\cdot04=0^{m}\cdot21$ and $\Delta(U-B)=0^{m}\cdot32+0^{m}\cdot08=0^{m}\cdot40$. These changes define what might be called the "blanketing line" for Go Hyades stars in the $(U-B, B-V)$-diagram. The line is shown in Fig. 3 and is the path which a Go star in the Hyades would follow if we progressively weakened the Fraunhofer lines and if the weakening proceeds linearly for all wavelengths. When all lines are removed, the observed colours should be $B-V=0^{m}\cdot60-0^{m}\cdot21=0^{m}\cdot39$ and $U-B=0^{m}\cdot13-0^{m}\cdot40=-0^{m}\cdot27$.

For the present investigation we need the blanketing line for a range of spectral types from about Fo to Ko. These can be derived in the same manner once $\epsilon(\lambda)$ values are available for a variety of spectral types. However, until work now in progress is completed, we must use the Go line and assume that the error will not be too large for small differences in spectral type.

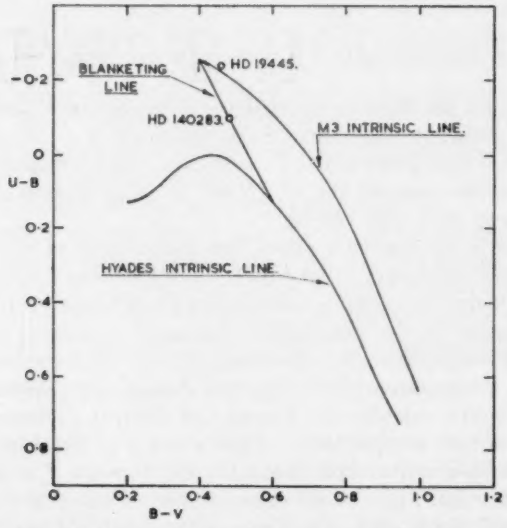

FIG. 3.—*The blanketing line for dGo stars is shown starting at* $B-V=+0^{m}\cdot60$, $U-B=+0^{m}\cdot13$ *and ending at* $B-V=+0^{m}\cdot39$, $U-B=-0^{m}\cdot27$. *The end point is the predicted position of a dGo Hyades star if all the Fraunhofer lines were removed. The two stars analysed by Chamberlain and Aller are shown as open circles.*

Let $\delta(U-B)$ be the observed ultra-violet excess [Fig. 4 illustrates the definition of $\Delta(U-B)$ and $\delta(U-B)$.] The values of $\Delta(B-V)$ corresponding to a given $\delta(U-B)$ can now be determined from Fig. 3. As an example, suppose a dGo star of normal colour, $B-V=0^{m}\cdot60$, is made bluer, $\Delta(B-V)=0^{m}\cdot10$, by slightly weakening the lines. The blanketing line in Fig. 3 predicts that the observed $U-B$ colour will be $-0^{m}\cdot06$ at $B-V=0^{m}\cdot50$. According to Table III, this observed colour corresponds to an excess of $\delta(U-B)=0^{m}\cdot09$. Consequently, on this model any star with an observed excess of $\delta(U-B)=0^{m}\cdot09$ should have the correction $\Delta(B-V)=0^{m}\cdot10$ applied to its observed $B-V$ to reduce it to the colour system of strong line stars (Hyades). The predicted values of $\Delta(B-V)=f[\delta(U-B)]$, derived in this manner, are listed in Table IV.

Table IV also lists the values of ΔM_V, the displacement below the Hyades main sequence, due to the effect of Fraunhofer lines on the colour alone. These values of ΔM_V are derived from the blanketing line which a dGo star will follow in the (M_V, $B-V$)-diagram as the lines are weakened. This line starts a $B-V=0^m.60$, $M_V=+4^m.78$ on the Hyades main sequence and ends at $B-V=0^m.39$, $M_V=+4^m.70$, when all the lines are removed. Combining the $\Delta(B-V)=f[\delta(U-B)]$ relation previously found with this $\Delta M_V=f[\Delta(B-V)]$ relation, gives the required theoretical relation between distance below the main sequence and the observed ultra-violet excess.

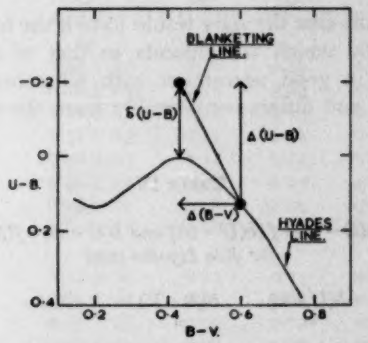

FIG. 4.—*The relation between observed ultra-violet excess, $\delta(U-B)$ and the blanketing corrections $\Delta(U-B)$ and $\Delta(B-V)$.*

TABLE III

Adopted main sequence and two colour relation

$B-V$	M_V	$U-B$	$B-V$	M_V	$U-B$
m	m	m	m	m	m
0·20	..	0·13	0·70	5·32	0·25
0·25	..	0·11	0·75	5·60	0·34
0·30	..	0·07	0·80	5·85	0·43
0·35	3·10	0·03	0·85	6·10	0·54
0·40	3·42	0·01	0·90	6·34	0·64
0·45	3·78	0·00	0·95	6·38	0·74
0·50	4·10	0·03	1·00	6·80	0·84
0·55	4·45	0·08			
0·60	4·78	0·13	1·05	7·02	0·94
0·65	5·02	0·19	1·10	7·25	0·99

A check on the procedure to this point is highly desirable. The first test concerns the extreme value which $\delta(U-B)$ can take when all the lines are removed from a dGo star. Table IV shows that this value is predicted to be $\delta(U-B)=0^m.28$ for the observed colours of $B-V=0^m.39$ and $U-B=-0^m.27$ (see Fig. 3). A plot of all stars of large ultra-violet excess in Roman's (1955) list of high velocity stars shows that stars at $B-V=0^m.39$ indeed are not bluer than $U-B=-0^m.27$ and this upper limit is well defined observationally.

The second test is concerned with the two subdwarfs HD 19445 and HD 140283 which Chamberlain and Aller (1951) have analysed. These stars, previously classed as A4p and A5p, are plotted in Fig. 3 with their observed colour

indices. If the blanketing model is correct, when these stars are moved back along the blanketing line they will fall on the $(U-B, B-V)$-diagram at a value of $B-V$ which corresponds to the effective temperature predicted by Chamberlain and Aller. The results are shown below where the tabulated $\delta(U-B)$ values were read from Fig. 2 and the corresponding $\Delta(B-V)$ values taken from Table IV.

HD	$(B-V)_{obs}$	$(U-B)_{obs}$	$\delta(U-B)$	$\Delta(B-V)$	$(B-V)_{Corr}$
19445	$+0^m.46$	$-0^m.24$	$0^m.21$	$0^m.18$	$+0^m.64$
140283	$+0^m.48$	$-0^m.10$	$0^m.08$	$0^m.08$	$+0^m.56$
					$+0^m.60$

The mean of the colours that the stars would have if the lines were not weakened is $(B-V)_{Corr}=+0^m.60$ which corresponds to that of a dGo star for which $T_e=6000^\circ$. This is in good agreement with Chamberlain and Aller's predicted value of 6300° and differs considerably from the temperature of A-type stars.

TABLE IV

Theoretical $\Delta(B-V)=f[\delta(U-B)]$ *and* $\delta(U-B)=f(\Delta M_V)$ *relations for dGo Hyades stars*

$\delta(U-B)$ m	$\Delta(B-V)$ m	ΔM_V m
0·00	0·00	0·00
0·02	0·02	0·14
0·035	0·04	0·26
0·05	0·06	0·37
0·075	0·08	0·51
0·09	0·10	0·63
0·11	0·12	0·75
0·13	0·14	0·91
0·17	0·16	1·02
0·21	0·18	1·14
0·26	0·20	1·26

A similar conclusion is available from Bahng's (1958) six-colour results and interpretation of Groombridge 1830 itself. Bahng shows that the red and infrared colours of Groombridge 1830 correspond to a temperature of a dK3 star but the observed $B-V$ of $0^m.75$ corresponds to an earlier spectral type; a difference which is attributed to the effect of the lines. The ultra-violet excess of Groombridge 1830 is $\delta(U-B)=0^m.15$. For this $\delta(U-B)$ Table IV shows that $\Delta(B-V)=0^m.15$, giving a corrected colour of $(B-V)_{Corr}=+0^m.90$. This value corresponds to a dK2 star, in good agreement with Bahng's estimated "temperature type" of dK2·8. Agreement between the observed and predicted values in both of these tests of the blanketing model gives some confidence in the $\Delta M_V=f[\delta(U-B)]$ relation tabulated in Table IV.

Using Table IV and the observed $\delta(U-B)$ values read from Fig. 2, we now correct the observed $(B-V)$ for the stars in Table I earlier than Ko. The results are given in Table V where successive columns contain (1) the Yale No., (2) the observed M_V copied from Table I, (3) the observed displacement below the Hyades main sequence, read from Fig. 1 at constant $(B-V)$, (4) the observed ultra-violet excess, (5) corrections to the observed $B-V$ taken from Table IV,

(6) the observed $B-V$ corrected for the line weakening and (7) added identifications for the stars. The correlation between ΔM_V and $\delta(U-B)$ in the third and fourth columns of Table V is shown in Fig. 5 together with the predicted correlation given in Table IV. The agreement between the observed and predicted correlation in Fig. 5 is fairly good, especially when the uncertainties in

TABLE V

Corrections to $B-V$ for stars in Table I earlier than Ko

(1) Yale No.	(2) M_V	(3) ΔM_V†	(4) $\delta(U-B)$	(5) $\Delta(B-V)$	(6) $(B-V)_{Corr}$	(7) Remarks
	m	m				
219	5·81 ± ·10	0·42 ± ·10	0·16	0·16	0·87	μ Cass
365	5·70 ± ·04	0·28 ± ·04	0·08	0·09	0·81	τ Cet
479	6·03 ± ·17	0·60 ± ·17	0·12	0·13	0·85	
701	5·31 ± ·25	0·31 ± ·25	0·11	0·12	0·76	ζ^1 Ret
705	5·02 ± ·27	0·40 ± ·27	0·14	0·14	0·72	ζ^2 Ret
1864‡	4·11 ± ·23	0·40 ± ·23	0·06	0·07	0·51	SDS, 3″ binary
1889	5·75 ± ·19	0·44 ± ·19	0·08	0·09	0·79	
2413*	4·70 ± ·18	0·60 ± ·18	0·08	0·09	0·59	39 Leo ADS 7712A
2745	6·72 ± ·09	1·17 ± ·09	0·15	0·15	0·89	Gmb 1830
2935	5·04 ± ·23	0·65 ± ·23	0·07	0·08	0·62	10 CVn
3010	7·32 ± ·25	2·51 ± ·25	0·09	0·10	0·71	
3264	5·19 ± ·21	0·27 ± ·21	0·09	0·10	0·73	
3300	3·48 ± ·21	0·30 ± ·21	0·11	0·12	0·48	σ Boo
3416	3·87 ± ·25	0·28 ± ·25	0·03	0·03	0·45	45 Boo
3650	6·19 ± ·14	0·69 ± ·14	0·09	0·10	0·83	
HD 163810	6·0 ± ·1	1·12 ± ·1	0·21	0·18	0·80	Member 1830 Gr
4849	5·04 ± ·16	0·40 ± ·16	0·05	0·06	0·64	
HD 219617	5·55 ± ·1	1·65 ± ·1	0·21	0·18	0·65	Member 1830 Gr

† Observed ΔM_V taken from Fig. 1.
‡ $\Delta m = 4$ mag. Secondary can be neglected.
* $\Delta m = 5{\cdot}5$ mag. Secondary can be neglected.

the absolute magnitudes of some of the stars is considered. This agreement is, perhaps, better seen in Fig. 6 where the (M_V, $B-V$)-diagram for all the stars is plotted after applying the theoretical corrections in Table IV. Omitting one star (Yale 3010), which we have already discussed, and the members of the Groombridge 1830 group which are indicated by crossed circles, no star deviates from the Hyades main sequence in Fig. 6 by more than three times the uncertainty in ΔM_V due to the probable error of the parallax. Furthermore, if we allow for the possibility of errors in the observed values of $U-B$ up to $0^m{\cdot}03$, all of the subdwarfs in Fig. 1, with the exceptions already noted, will fall within their probable errors on the Hyades main sequence in Fig. 6. We conclude, therefore, that these subdwarfs do not in fact form a separate region in the (M_{Bol}, log T_e)-diagram, even though it is probable that their heavy element content is lower than that of the Hyades. To interpret these results we now consider the equations from the theory of stellar interiors.

It is well-known (Strömgren 1952, Massewitch 1954, Swarzschild 1958) that subdwarfs can, theoretically, be produced in the (M_{Bol}, log T_e)-diagram by at least two processes. (1) If the internal opacity in normal main sequence

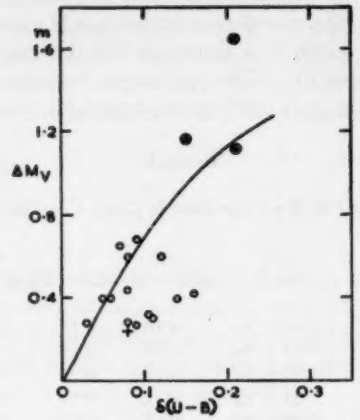

FIG. 5.—*The relations between observed ultra-violet excess, δ(U−B) and the distance below the Hyades main sequence due to the weakening of the Fraunhofer lines alone. The observational data are from Table V. The theoretical line is tabulated in Table IV. The Groombridge 1830 members are indicated by crossed circles.*

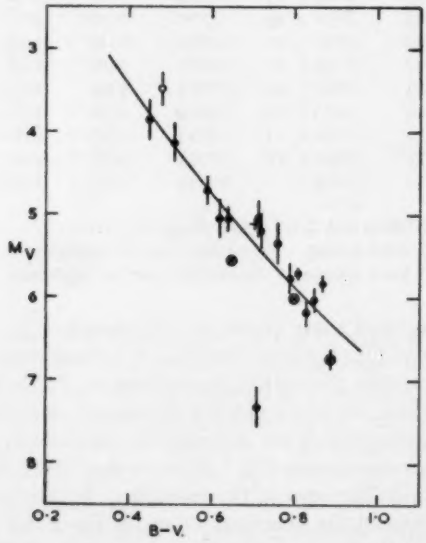

FIG. 6.—*Same as Fig. 1 but with the corrections to B−V applied to the individual stars according to the size of the observed ultra-violet excess.*

stars is primarily due to bound-free photoelectric transitions of the heavy elements, a decrease in the heavy element content will increase the luminosity, L, but will keep the radius, R, nearly constant, thereby placing the star below the main sequence (cf. Eqns. 9–12). If, on the other hand, the opacity of normal main sequence stars is due to free–free transitions of hydrogen and helium, no such effect is expected from changes in the heavy element abundance. (2) A decrease

of the hydrogen abundance with a corresponding increase in helium will also move a star below the main sequence. This is brought about by an increase in the mean molecular weight which causes L to increase and, because as above, R is nearly insensitive to the change, the star moves below the main sequence. Only properly computed models can show these effects precisely but the general outline can be demonstrated by the following simplified arguments.

Consider first the case where the opacity is primarily due to bound–free transitions of the heavy elements. Then

$$\kappa = \text{const}\ Z(1+X)\rho T_e^{-3.5}(g/t) \tag{5}$$

where g is the Gaunt and t the guillotine factor. For any star in hydrostatic equilibrium with energy transport by radiation, and with the opacity given by (5),

$$L = \frac{\text{const}\,\mu^{7.5} M^{5.5} R^{-0.5}}{Z(1+X)} \left(\frac{t}{g}\right). \tag{6}$$

A second equation for L comes from the requirement that the energy generated by nuclear processes be equal to the observed luminosity. If the $C-N$ cycle dominates, with the energy generation given by

$$\epsilon_{CN} = \text{const}\ ZX\rho T^n \quad \text{ergs/gm sec} \tag{7}$$

then

$$L = \frac{\text{const}\, ZX\mu^n M^{n+2}}{R^{n+3}}. \tag{8}$$

Equations (6) and (8) give two relations in 4 variables (L, M, R, composition). Equating (6) with (8), with $n = 20$, gives

$$L = \text{const}\ Z^{-1.04} X^{-4} M^{5.13} \tag{9}$$

$$R = \text{const}\ Z^{0.09} X^{-0.16} M^{0.73} \tag{10}$$

where the chemical parameters have been approximated by power series. The (g/t) factor is absorbed in the constant because we are interested only in differential effects at constant mass and nearly constant radius. From $T_e = \text{const}\ (LR^{-2}L)^{1/4}$ it follows that

$$T_e = \text{const}\ Z^{-0.30} X^{-0.92} M^{0.92} \tag{11}$$

Elimination of the mass from (9) and (11) gives

$$L = \text{const}\ Z^{0.63} X^{1.13} T_e^{5.6} \tag{12}$$

which is the equation for the main sequence in the (L_{Bol}, T_e)-diagram.

We must emphasize the approximate nature of these results. For one thing, convective energy transport and its effect on the surface conditions has been neglected (cf. Schwarzschild 1958). For another, if the structure of the star changes with changing X and Z (as it must to some degree) then the constants in equations (9), (10), (11) and (12) will themselves be functions of X and Z and the argument fails. However, our approximation is probably adequate because there is a check on the equations from the model computations by Blackler (1958) for main sequence stars with different hydrogen contents. Miss Blackler's models were computed for X values of 0·76, 0·85, 0·93, and 0·99. Equations 9 and 11 predict the change in L and T_e for constant mass, and constant Z, with X changing from 0·99 to 0·76, to be

$$\text{Log}\ (L_1/L_2) = 4 \log(X_2/X_1) = 0{\cdot}46 \tag{a}$$

$$\text{Log}\ (T_{e1}/T_{e2}) = 0{\cdot}92 \log\ (X_2/X_1) = 0{\cdot}105 \tag{b}$$

Miss Blackler's computed values are 0·64 and 0·47 for (*a*) with masses of $1\odot$ and $2\odot$, respectively and 0·203 and 0·126 for (*b*) with the same mass values. The agreement with our equations is satisfactory.

Equation (12) illustrates the two methods described above for producing subdwarfs. At constant T_e, either a decrease in Z or in X will decrease L, moving the star below the main sequence.

It should be pointed out that a decrease of Z will not produce subdwarfs if equation (5) does not correctly represent the opacity because of the predominance of free–free transitions of hydrogen and helium. If this is true, then equation (5) should be replaced by

$$\kappa = \text{const}\ (X+Y)(1+X)\rho T_e^{-3.5}(g/t) \tag{13}$$

and the resulting equations for L, R and T_e become

$$L = \text{const}\ Z^{-0.02}X^{-4}M^{5.13} \tag{14}$$

$$R = \text{const}\ Z^{0.05}X^{-0.16}M^{0.73} \tag{15}$$

$$T_e = \text{const}\ Z^{-0.13}X^{-0.02}M^{0.02} \tag{16}$$

$$L = \text{const}\ Z^{0.13}X^{1.16}T_e^{5.6}, \tag{17}$$

where L, R, and T_e are nearly independent of Z.

The above equations are derived on the assumption that the energy is generated by the *CN* cycle because we wished to compare our results with Blackler's model computations already mentioned. However, it is probable that the energy generation in most of the subdwarfs discussed here is by the proton–proton chain, for which $n=4$ in equation (7). Although the exponents in the equations are changed if $n=4$, the sign of the dependency of L on chemical composition in equations (12) and (17) is the same and therefore our general conclusions are independent of whether the energy is generated by the *CN* cycle or the *p-p* reaction.

The question is whether the opacity in real stars of solar mass is due primarily to bound–free or to free–free transitions. Nauer's models (1954) show that near the centre of the Sun most of the opacity comes from the free–free transitions while near the surface it is due to bound–free transitions. It is therefore not known, from these considerations, whether equation (12) or (17) will best relate T_e and L for main sequence stars of solar mass.

Because a change in the heavy element abundance must form subdwarfs if the opacity is due to bound–free photoelectric transitions (equations (5) and (12)), and because Fig. 6 shows that the difference in the heavy element content does not change the structure of the star as equation (12) predicts, it is suggested that equation (5) does not in fact represent the opacity correctly but rather equation (13) applies. This conclusion is not completely certain because equation (12) shows that some combination of increased Z with decreased X would cancel the effect on L of either difference working separately. If the combination was properly chosen ($Z^{0.63}X^{1.13} \approx$ const), no change in L at a given T_e would result and Fig. 6 could be explained even if equation (12) were valid. Such a combination might be justified from theories of element synthesis together with a changing chemical composition of the interstellar medium with time; ideas which are now in vogue. In particular, if heavy elements are made in stellar interiors and scattered into the interstellar medium by stellar explosions, an increased Z abundance might be expected to be accompanied by increased He abundance. Thus, an increase in Z might logically go in step with decreased X.

On the other hand, if it could be independently shown that equation (5) does not control the opacity, but that equation (17) correctly describes the situation, then the conclusion from Fig. 6 would be definite that no difference in the H/He abundance exists between Hyades stars and stars in Table I.

The case of the three Groombridge 1830 group stars is more interesting because the colour correction of the theory does not appear sufficient to move the stars to the main sequence. Before correction they average $1^m{\cdot}3$ below the Hyades main sequence. After correction they are still below the main sequence but only by $0^m{\cdot}35$ on the average. If this is significant, then equations (17) shows that the hydrogen content in Hyades stars is higher than that of stars in the Groombridge 1830 group. If, on the other hand, the opacity is controlled by equation (5), then the Z(Hyades)/(Z(Gr. 1830) ratio is approximately 2 by equation (12) if X is kept constant. However, Chamberlain and Aller (1951) and Kondo (1957) show that the heavy elements are down by at least a factor of 10 in stars like Groombridge 1830, a factor which is considerably greater than 2. Therefore, the present data suggest that a change in the heavy element content does not affect the stellar structure of the Groombridge 1830 Group members and that equations (13) and (17) probably represent the case better than (5) and (12). If this is true, then the data show that the H/He ratio must be different between the Hyades and the Groombridge 1830 group members.

Clearly these conclusions are quite tentative because the accuracy of the blanketing corrections is not high enough to decide if the deviation of the Groombridge 1830 stars from the main sequence of Fig. 6 is significant. Although the two tests of the theory previously mentioned seem definite, it should be remembered that the assumption that the blanketing corrections obtained from the Sun are also valid for early F and late G-type stars is an approximation which can be eliminated only when $\epsilon(\lambda)$ values are available for stars of different spectral types. The approximation is probably incorrect in detail and may account for the slight over-correction of a few stars in Fig. 6. It will be interesting to see if the blanketing line for Ko dwarfs in the ($U-B$, $B-V$)-diagram lies along the intrinsic ($U-B$, $B-V$)-line because such a possibility is suggested by the five subdwarfs later than Ko in Table I which have $\delta(U-B)\sim 0$. Clearly, the present method of correcting for line blanketing will fail in this case because the $\Delta(B-V)$ correction cannot be inferred from a non-existent $\delta(U-B)$.

As Schwarzschild has indicated (1958, Chapter IV), a check on some of these results is possible if the masses of subdwarfs were known. Equations (9) and (14) are the theoretical mass-luminosity relations on the two opacity assumptions. If the previous conclusion is correct that the colour correction is enough to make the mild subdwarfs disappear in the (M_{Bol}, log T_e)-diagram and therefore that the established low abundance of heavy elements does not affect the structure, then the subdwarfs should not deviate from the empirical mass-luminosity relation for strong line stars. The binary 85 Pegasi is the subdwarf with the best determined mass but uncertainties in the parallax, the semi-major axis, and the mass ratio (Eggen 1956, Wyller 1956) are great enough to make the decision of deviation from the mass-luminosity relation difficult. At present, all that can be said is that the observed mass neither confirms nor denies the theoretical expectation. As is pointed out in the previous paper (Eggen and Sandage 1959) the mass of ADS 16644 in the Groombridge 1830 group is also too uncertain for a decision on this critical point but if observations are continued, a check may be possible.

3. *Application to the nearby stars and galactic clusters.*—The (U, B, V)-data available for nearby stars and for the Hyades, Praesepe and Coma Berenices clusters show considerable differences in the $U-B=f[(B-V)]$ relation for F and G-type stars from $B-V=+0^{m}.40$ to $B-V=+0^{m}.70$. Within each of the three clusters, stars assumed to be free from companions show an almost negligible scatter in the $(U-B, B-V)$-diagram but the systematic differences between the clusters is appreciable. For a given $B-V$, the $U-B$ for the Hyades is larger than for Praesepe and Coma Berenices. The Praesepe stars show $\delta(U-B)\approx 0^{m}.020$ with respect to the Hyades in the range considered, while Coma Berenices stars show $\delta(U-B)\simeq 0^{m}.045$. Although the Hyades-Coma difference is large compared to the quoted probable errors in $U-B$ of $0^{m}.008$ for the photometric transfers to each cluster (Johnson 1952, Johnson and Knuckles 1955), the Praesepe-Hyades difference is only three times the probable errors of these transfers and may not be real. Table VI gives the mean values for the $(U-B, B-V)$-relation in each of the clusters and illustrates the effect.

TABLE VI

$U-B, B-V$ relations for Hyades, Praesepe, and Coma Berenices

	Hyades	Praesepe	Coma
$B-V$	$U-B$	$U-B$	$U-B$
0·44	−0·005	..	−0·035
0·46	+0·008	−0·005	−0·027
0·48	0·020	+0·005	−0·017
0·50	0·035	0·016	−0·006
0·52	0·050	0·030	+0·007
0·54	0·067	0·044	0·022
0·56	0·086	0·060	0·040
0·58	0·107	0·079	0·060
0·60	0·127	0·101	0·080
0·62	0·150	0·126	0·102
0·64	0·175	0·155	0·125
0·66	0·200	0·184	0·155
0·68	0·225	..	0·185
0·70	0·248	..	..

The $(U-B, B-V)$-diagram for the nearby stars shows a much larger scatter than is present for the individual clusters. The entire spread places some of these stars beyond the extremes of the Coma Berenices and Hyades lines respectively. The field stars are apparently much less homogeneous in chemical composition than the stars in a given cluster.

Very similar results were presented by Strömgren (1958) and Chalonge (1958) at the Rome Conference on Stellar Populations. Strömgren, using narrow-band, photoelectric photometry, found a difference between Coma Berenices and Hyades stars of the same order as that derived above but he found no difference between Praesepe and Hyades stars. (Since Strömgren's result is independent of inter-stellar absorption, the small difference in $(U-B)$ between the Hyades and Praesepe stars may indicate a reddening of $0^{m}.015$ in $B-V$ for Praesepe.)

There are two conclusions from these data. (1) Differences in heavy element abundance probably exist between stars in different clusters and in the general field, and these differences are not related by a simple time sequence. All evidence from composite $(M_V, B-V)$-diagrams (Eggen 1955*c*, Sandage 1957) put Coma Berenices younger than Hyades and Praesepe by the order of 2×10^{8} years, yet the heavy element abundance is smaller in Coma Berenices. The conclusion is that the heavy element abundance of prestellar matter does not increase

uniformly with the time from the formation of the galaxy because, if it did, Coma Berenices stars would have higher metal abundances than either Hyades or Praesepe. Although an average increase of heavy elements with time may indeed take place in the galaxy, evidently there are local irregularities of chemical composition in the galactic plane.

(2) The second conclusion from Table VI is that differences are expected in the position of the main sequences in the (M_V, $B-V$)-diagram for the Hyades and Coma Berenices due to differences in the $\Delta(B-V)$ values. The method of fitting main sequences to find photometric distances for these clusters is therefore more complicated than was once believed. Fortunately, the distance to the Hyades is fixed from geometrical arguments by the moving cluster method (van Bueren 1952, Eggen 1958). Therefore, if the Hyades is used as the standard main sequence to which other clusters are fitted, either the $B-V$ of these clusters must be corrected to the ($U-B$, $B-V$)-system of the Hyades by Table IV, or the ΔM_V corrections of Fig. 5 should be applied at constant $B-V$. Thus, the distance moduli derived by both Johnson and by Sandage for several clusters probably require small corrections. Eggen's procedure of using the slope of the Praesepe main sequence and the zero-point of field stars with $\Pi \geqslant 0''.200$ to define the standard main sequence also has the same objection because the $\delta(U-B)$ values of the field stars are not zero. The corrections to the separate values of Eggen, Johnson and Sandage are not negligible. For example, Table IV shows that the correction to the distance modulus of Coma Berenices is $\Delta M_V = 0^m.32$ if $\delta(U-B) = 0^m.045$.

The problem of fitting galactic cluster main sequences is a milder case of that encountered in globular clusters where the extreme excesses of $\delta(U-B) = 0^m.20$ are found. The preceding paper (Eggen and Sandage 1959) shows that if we neglect this excess for the globular clusters, an error of about $1^m.2$ results in the position of the main sequence. The entire problem of photometric distances to clusters where a fit to the main sequence is made in the Fo to Ko range should be re-examined from this point of view. Fortunately, the corrections are expected to be smaller than $0^m.4$ for most galactic clusters because the $\delta(U-B)$ values are known to be smaller than $0^m.05$ from data already in the literature. As an illustration, the tentative correction just mentioned changes the distance modulus of Coma Berenices from $m-M = 4^m.80$ (Eggen 1955 *c*) to $m-M = 4^m.48$. It should be mentioned that no effect is expected for clusters where the fit to the main sequence is made to the late B and A-type stars because a changing metal content should not affect the colours and no large change in the position of the observed main sequence is expected.

Finally, we enquire into the expected intrinsic width of the main sequence. On the present ideas this sequence can stretch from the Hyades stars, with no ultra-violet excess, through the Coma Berenices stars with $\delta(U-B) = 0^m.04$, to the Sun and mild subdwarfs like those in Table I with $\delta(U-B) \approx 0^m.10$ and finally to the Groombridge 1830 and globular cluster stars with $\delta(U-B) = 0^m.2$—a range of $1^m.5$ at a given $B-V$ in the (M_V, $B-V$)-diagram. Since Groombridge 1830 group members probably are at one edge of this continuum in the (M_V, $B-V$)-diagram and have very weak lines, they have usually been excluded from consideration as main sequence stars. The stars which are usually called "main sequence dwarfs" are not distinguished by their line weakening and lie in a band width of $\delta(U-B) = 0^m.10$ in the ($U-B$, $B-V$)-diagram. If these stars are taken to define the main sequence in the (M_V, $B-V$)-diagram, Table IV shows

that this sequence should have a total width of $\Delta M_V \sim 0^m{\cdot}60$ due to the effect of weak Fraunhofer lines on the $B-V$ colour alone. The (M_V, $B-V$)-diagram for stars with $\pi \geqslant 0''{\cdot}100$ (Eggen 1955*b*, Sandage 1958) does show some spread in the Fo G5 range but the ever present question of the accuracies in the trigonometric parallaxes makes the comparison uncertain.

Mount Wilson and Palomar Observatories,
Carnegie Institution of Washington,
California Institute of Technology,
Pasadena, California:
1959 *February* 27.

Royal Greenwich Observatory,
Herstmonceux Castle,
Sussex

References

Adams, W. S. and Joy, A. H., 1922, *Ap. J.*, **56**, 262.
Adams, W. S., Joy, A. H., Humason, M. L. and Brayton, A. M., 1935, *Ap. J.*, **81**, 187.
Aller, L. H., 1958, *Encycl. Physics*, **51**, 346.
Bahng, J. D. R., 1958, *Ap. J.*, **128**, 572.
Blackler, J. M., 1958, *M.N.*, **118**, 37.
Bueren, H. G. van, 1952, *B.A.N.*, **11**, 385.
Chalonge, D., 1958, *Stellar Populations* (Specola Vaticana, Vol. **5**, 345).
Chamberlain, J. W. and Aller, L. H., 1951, *Ap. J.*, **114**, 52.
Eggen, O. J., 1955*a*, *A.J.*, **60**, 65.
—— 1955*b*, *A.J.*, **60**, 401.
—— 1955*c*, *A.J.*, **60**, 407.
—— 1956, *A.J.*, **61**, 361.
—— 1958, *M.N.*, **118**, 65.
Eggen, O. J. and Sandage, A. R. 1959, *M.N.*, **119**, 255.
Greenstein, J. L., 1956, *Proc. Third Symposium Math. Statistics and Probability*, Univ. Cal. Press, p. 11.
Heckmann, O. and Johnson, H. L., 1956, *Ap. J.*, **124**, 477.
Jenkins, L., 1952, *General Catalogue of Trigonometric Stellar Parallaxes*, Yale Univ. Press.
Johnson, H. L., 1952, *Ap. J.*, **116**, 640.
—— 1955, *Ann. d'Ap.*, **18**, 292.
Johnson, H. L. and Knuckles, C. F., 1955, *Ap. J.*, **122**, 209.
—— 1957, *Ap. J.*, **126**, 113.
Johnson, H. L. and Morgan, W. W., 1953, *Ap. J.*, **117**, 313.
Johnson, H. L. and Sandage, A. R., 1956, *Ap. J.*, **124**, 379.
Kondo, M., 1957, *Pub. Astr. Soc. Japan*, **9**, 201.
Kuiper, G. P., 1939, *Ap. J.*, **89**, 549.
—— 1941, *Paris Colloquium on White Dwarfs.*
Massewitch, A. G., 1954, *Les Processus Nucleaires dan les Astres*, Liege, p. 170.
Michard, R., 1950, *B.A.N.*, **11**, 227.
Milne, E. A., 1928, *Observatory*, **51**, 88.
Minnaert, M., 1953, *The Sun*, Univ. Chicago Press.
Nauer, P., 1954, *Ap. J.*, **119**, 365.
Parenago, P. P., 1946, *Astr. Journal of Soviet Union*, **23**, 31.
Pecker, J. C., 1951, *Ann. d'Ap.*, **14**, 152.
Przybylski, A., 1957, *M.N.*, **117**, 483.
Roman, N. G., 1955, *Ap. J. Supplement*, **2**, 198.
Sandage, A. R., 1956, *Ap. J.*, **123**, 278.
—— 1957, *Ap. J.*, **125**, 435.
—— 1958, *Stellar Populations*, (Specola Vaticana, **5**, 287).
Schwarzschild, M., 1958, *Structure and Evolution of the Stars*, Princeton Univ. Press. Chapter IV, section 17.
Schwarzschild, M., Searle, L. and Howard, R., 1955, *Ap. J.*, **122**, 353.
Stebbins, J. and Kron, G. E., 1957, *Ap. J.*, **126**, 266.
Strömgren, B., 1952 *A. J.*, **57**, 65.
—— 1958 *Stellar Populations*, (Specola Vaticana, **5**, 245).
Wyller, A. A., 1956, *A. J.*, **61**, 76.

THE RADIO EMISSION FROM NORMAL GALAXIES

I. Observations of M31 and M33 at 158 Mc/s and 237 Mc/s

R. Hanbury Brown and C. Hazard

(Received 1959 March 9)

Summary

A survey of the radio emission from bright normal galaxies has been carried out at 158 Mc/s. This paper reports the results obtained on M31 and M33. The integrated radio magnitude (m_r) of these two galaxies has been measured and compared with their photographic magnitude (m_p); it is found that the difference ($m_r - m_p$) is almost the same for both.

The distribution of intensity across M31 shows two major components: a *disk* and a *corona*. The corona is responsible for 90 per cent of the total emission, has a true axial ratio of about 0·6, and has a major axis which is about three times greater than that of the visible nebula. The results show that M33 also has a corona; the ellipticity, emissivity and dimensions of the corona relative to the visible object are closely similar to the values found for M31.

A comparison between M31, M33 and the Galaxy suggests that the emissivity of the corona of the Galaxy is significantly higher than that of the other two galaxies.

---

1. *Introduction.*—In previous papers (**1, 2, 3**) we reported some observations of galaxies which were carried out at 158 Mc/s with the 218 ft fixed paraboloid at Jodrell Bank. The recent completion of the 250 ft steerable paraboloid (**4**), with its wider field of view and greater gain, has made it possible to observe a greater number of galaxies and also to improve the previous measurements. A survey has therefore been made at 158 Mc/s of the brightest normal* galaxies in the northern sky in an attempt to establish the relationship between their photographic and radio magnitudes. Subsequently a few galaxies have also been observed at 237 Mc/s; this was only done in those cases where the improved resolving power was considered to be useful in interpreting the results obtained at 158 Mc/s.

The account of this survey has been divided into two parts. The present paper (I) has been restricted to the two brightest spirals M31 and M33; these two objects have been studied in greater detail than the other galaxies and require individual discussion. A second paper (II) contains the results on the remaining galaxies together with a discussion of all the data.

2. *Description of apparatus.*—The observations were made at frequencies of 158 Mc/s and 237 Mc/s, using a receiver based on that described by Ryle and Vonberg (**6**). The parameters of this receiver are substantially the same as those of the equipment used in our earlier observations of M31 (**1**).

* In this context a *normal* galaxy, following Baade and Minkowski (**5**), is taken to be a galaxy which appears to be normal when examined photographically.

The aerial system used was the 250 ft steerable paraboloid (**4**). The primary feeds at the two frequencies were similar and consisted of a simple dipole and reflector connected to the receiver through 85 ft of low-loss coaxial cable. The shape of the aerial beam was measured in detail by observing the intense radio sources in Cygnus and Cassiopeia; as expected, it was found to be elliptical with the major axis parallel to the dipole. The values obtained for the total width of the beam between half-power points are given in Table I. The same observations were also used to determine the direction of the axis of the beam relative to the axis of the paraboloid. At both frequencies the misalignment between the two axes was about 10′ and the appropriate corrections have been applied to all the observations.

TABLE I

The beam-width of the aerial

Frequency (Mc/s)	Beam-width* in E plane	Beam-width* in H plane
158	2°·2	1°·6
237	1°·5	1°·1

* The beam-width is the total width between directions of half-power gain.

3. *Calibration of the intensity scale.*—In a previous paper (**2**) we defined a scale of radio magnitude, using NGC 5194/5 as a comparison source, which was intended to make the radio and photographic magnitudes of normal spiral galaxies numerically equal. On that scale a source with a flux density of S_{158} w. m.$^{-2}$ (c/s)$^{-1}$ at 158 Mc/s has a radio magnitude m_r defined by the equation

$$m_r = -53{\cdot}45 - 2{\cdot}5 \log S_{158}. \qquad (1)$$

For the purpose of the present work it is more convenient to use the discrete source 14N5A as a standard of comparison instead of NGC 5194/5. This source has a small angular diameter (**7**) and is circumpolar at Jodrell Bank; the equipment was calibrated by observing it at least once during each observing period. Preliminary measurements show that it has a flux density of 75×10^{-26} w. m.$^{-2}$ (c/s)$^{-1}$ at 158 Mc/s which, from equation (1), corresponds to a radio magnitude of +6·86. Whitfield (**8**) finds that it has a spectral index of −0·6.

It is desirable, when observations of sources at different frequencies are to be compared, that their radio magnitudes should be defined in such a way that they do not vary greatly with frequency; in particular it is convenient that the magnitude of the comparison source should be independent of frequency. For this reason we have assumed arbitrarily that the radio magnitude of 14N5A is independent of frequency and has the value $m_r = +6{\cdot}86$ derived at 158 Mc/s.

To facilitate comparison of our results with those of southern observers we have compared the intensity of 14N5A with that of 12N1A in Virgo. The 12N1A source is the more intense by 2·77 mag. at 158 Mc/s and hence at this frequency its radio magnitude is +4·09.

4. *Observations of M31 (NGC 224)*

4.1. *Method of observation.*—The observations were made during the late summer and autumn of 1958. The region surveyed was bounded by declinations

N 34° and N 47° and right ascensions $00^h\,10^m$ and $01^h\,10^m$. The beam of the 250 ft paraboloid was scanned over the region at one degree per minute along lines of constant declination, the scans being separated by 0·5° in the central parts of the survey and 0·75° in the outer parts. These scans were then linked together by scanning along lines of constant right ascension at $00^h\,10^m$, $00^h\,40^m$ and $01^h\,10^m$. Finally, to make certain of the extent of the nebula, the beam was scanned along the major and minor axes. Each scan was repeated several times to minimize the effects of interference and receiver drift; all the measurements were made at both 158 Mc/s and 237 Mc/s. Some sample scans are shown in Fig. 1.

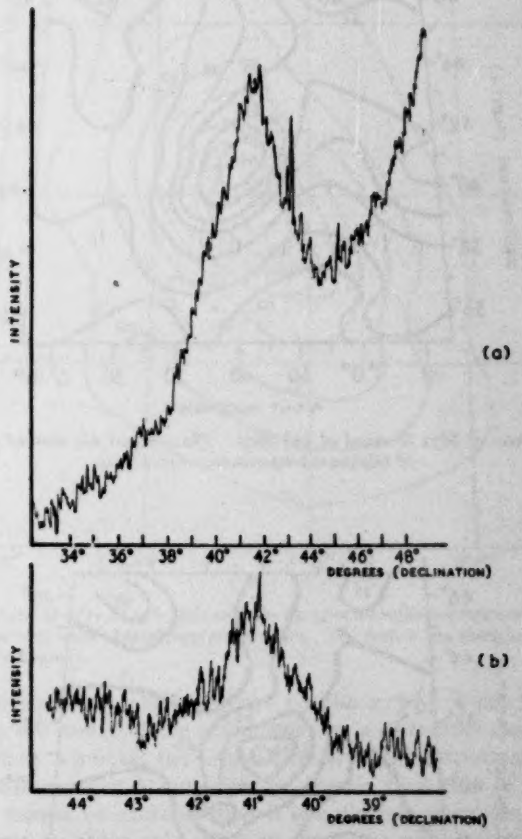

FIG. 1.—*Sample scans across M31. (a) A scan along the major axis at 158 Mc/s. (b) A scan along the minor axis at 237 Mc/s. Ordinates: intensity in arbitrary units. Abscissae: declination in degrees.*

4.2. *The radio isophotes of M31.*—The records have been converted into contours which show the distribution of brightness over the region; the results are shown in Figs. 2, 3 and 4. The contours represent lines of equal observed brightness and they have been plotted above an arbitrary zero.

The outline of the visible nebula is indicated in Fig. 4 by the broken line which, following de Vaucouleurs (**9**), encloses 95 per cent of the total luminosity. It can be seen clearly that the radio emission is much more widely distributed than the light, although the shape of the contours is obviously distorted by localized sources and irregularities in the general background radiation.

The localized sources are more prominent on the 237 Mc/s contours, as would be expected with the narrower beam. The source at 00^h33^m, N 39° is particularly prominent, and is probably the source originally identified with

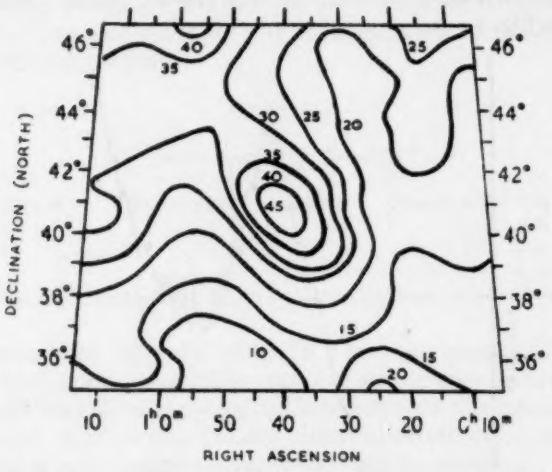

FIG. 2.—*Isophotes of M31 observed at 158 Mc/s. The contours are marked in arbitrary units of brightness temperature. Epoch 1950.*

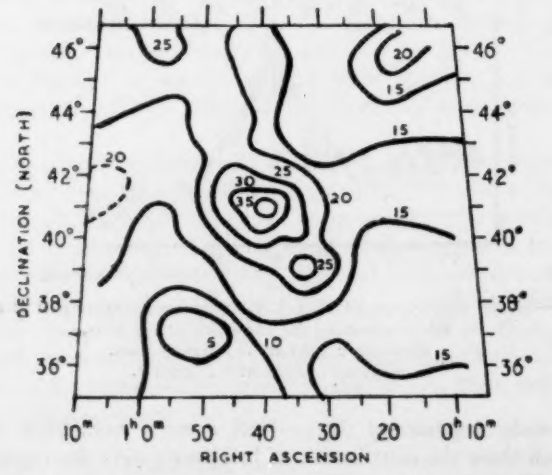

FIG. 3.—*Isophotes of M31 observed at 237 Mc/s. The contours are marked in arbitrary units of brightness temperature. Epoch 1950.*

M31 by Ryle, Smith and Elsmore (**10**). It is now known to have an angular diameter which is considerably less than that of the visible nebulae and this fact, together with the discrepancy between the positions of the two objects, makes it unlikely that they are physically associated.

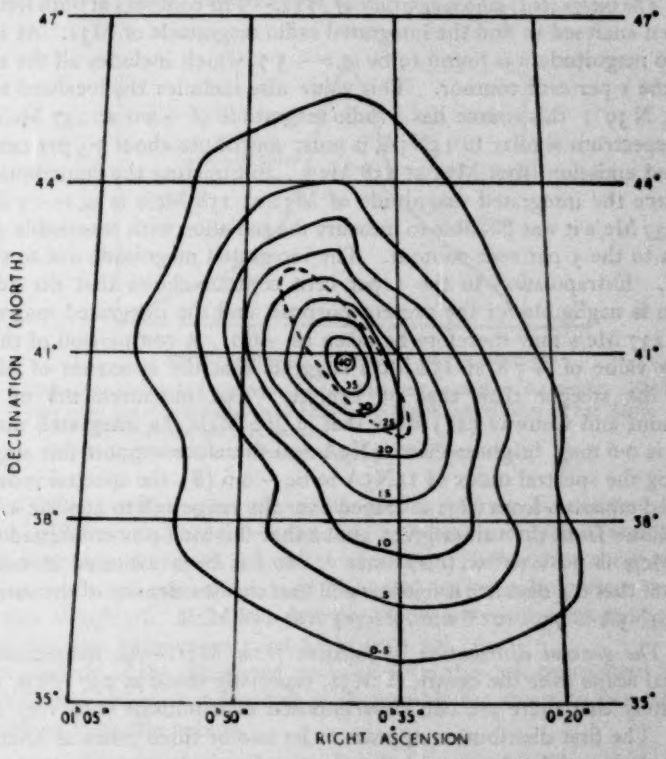

FIG. 4.—*Isophotes of M31 at 158 Mc/s with the background radiation removed. The contours are marked in arbitrary units of brightness temperature. The broken line shows the outline of the visible nebula. Epoch 1950.*

The small irregularity which appears on the 237 Mc/s contours at about one degree from the centre of the nebula may be a discrete source with a radio magnitude of about +9·6; at the distance of M31 this corresponds to a source with a total radio emission about 2·5 mag. greater than that of Cassiopeia A. The possibility cannot be excluded that it is a discrete source in M31.

In an attempt to show the radiation from the nebula more clearly the background brightness has been removed from the contours observed at 158 Mc/s. The background was extrapolated smoothly over the region of the nebula and contours of brightness measured above this somewhat arbitrary baseline are shown in Fig. 4. At 158 Mc/s the outlines of the nebula are clearly defined on the original records and the distorting effects of discrete sources appear to be comparatively small; it is therefore likely that the derived contours in Fig. 4 give a reasonably accurate picture of the radio emission associated with the nebula when smoothed with a 2° beam

An attempt was also made to remove the background radiation from the contours observed at 237 Mc/s. The derived contours proved to be similar to those obtained at 158 Mc/s but are not so reliable on account of their lower signal-to-noise ratio.

4.3. *The integrated radio magnitude of M31.*—The contours at both frequencies have been analysed to find the integrated radio magnitude of M31. At 158 Mc/s the radio magnitude was found to be $m_r = +5{\cdot}7$, which includes all the radiation within the 1 per cent contour. This value also includes the localized source at $00^h\,33^m$, N 39°; this source has a radio magnitude of +9·0 at 237 Mc/s and, if it has a spectrum similar to 14N5A, it must contribute about 5·5 per cent of the integrated emission from M31 at 158 Mc/s. Subtracting the contribution from this source the integrated magnitude of M31 at 158 Mc/s is $m_r = +5{\cdot}8$.

At 237 Mc/s it was possible to measure the radiation with reasonable certainty only out to the 5 per cent contour. The integrated magnitude out to this level is +6·1. Extrapolation to the 1 per cent contour shows that the additional radiation is negligible for the present purpose, and the integrated magnitude of M31 at 237 Mc/s may therefore be taken as +6·1. A comparison of this result with the value of +5·8 at 158 Mc/s suggests that the spectrum of M31 may perhaps be steeper than that of 14N5A. The measurements of Seeger, Westerhout and Conway (**11**) show that at 400 Mc/s the integrated magnitude of M31 is 0·6 mag. brighter than 14N5A and therefore support this suggestion. Assuming the spectral index of 14N5A to be −0·6 (**8**), the spectral index of the integrated emission from M31 averaged over the range 158 to 400 Mc/s is −1·1.

It follows from the values given above that the total power emitted by M31 at 158 Mc/s is $7{\cdot}8 \times 10^{20}$ w. $(c/s)^{-1}$ ster^{-1}. It has been assumed in calculating this power that the distance is 630 kpc and that the flux density of the comparison source 14N5A is 75×10^{-26} w.m.$^{-2}$ $(c/s)^{-1}$ at 158 Mc/s.

4.4. *The general distribution of emission from M31.*—An inspection of the individual scans over the centre of M31, especially those at 237 Mc/s, suggests immediately that there are two superimposed distributions with very different widths. The first distribution appears to be two or three times as broad as the visible nebula, while the second distribution is much narrower than the first and by comparison is highly concentrated towards the centre of the nebula. A sample scan along the minor axis at 237 Mc/s is shown in Fig. 1.

We propose to treat these two distributions as distinct, and to discuss them separately. On the basis of the present results alone such a division is necessarily rather arbitrary; however, it is supported by a study of the Galaxy. Surveys of the non-thermal radiation from the Galaxy have shown that there are at least two principal components of the emission: (i) an extended *corona* which is almost spherical and is responsible for the majority of the emission (**12**); and (ii) a second component which is concentrated towards the galactic plane and which appears to be roughly coextensive with the visible parts of the Galaxy. The second component has been called the *disk* by Mills (**13**). We shall therefore tentatively identify the two distributions which appear to exist in M31 with those found in the Galaxy, and we shall refer to the broad component as the *corona* and to the narrow component as the *disk*.

4.5. *The disk component of M31.*—The disk component has been separated from the corona by extrapolating the broad distribution over the centre of the

nebula as illustrated by the broken line in Fig. 5. The width of the disk component obtained in this way is clearly subject to considerable uncertainty; nevertheless we have concluded that the 237 Mc/s records do not show any significant broadening of the beam, and it follows that the total width between half-power points cannot exceed about 1°.

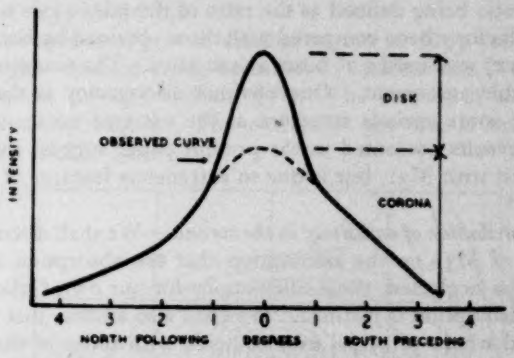

FIG. 5.—*Illustrating the method of separating the disk component from the corona. The solid line represents the observed distribution along the major axis of M31 at 237 Mc/s.*
Ordinates : intensity.
Abscissae : degrees measured along major axis.

Some further evidence on the width of this narrow distribution has been provided by Palmer and his colleagues (14) who have surveyed M31 at 160 Mc/s using an interferometer with a baseline of 220λ. The records show that there is no source near the optical centre of M31 with an intensity greater than about 0·05 of that of 14N5A. It follows that the maximum width between half-power points of the disk component must be at least 20′.

A comparison of the integrated emission from the disk component with that from the corona shows that the disk is responsible for about 10 per cent of the total emission from the nebula.

4.6. *The corona of M31*

(i) *The apparent distribution of intensity over the corona.*—Since the contribution of the disk component is only 10 per cent of the total radiation, the 158 Mc/s measurements in Fig. 4 are effectively contours of the corona smoothed with a 2° beam. The irregularities in the outline of the corona, which are particularly marked on the outside contour, are probably not significant and may represent minor errors in the separation of the corona from the background.

The general shape of the contours is elliptical and the observed widths of the 1 per cent contour are about 10° (major axis) × 7° (minor axis). The position angle of the major axis is about 44° and, taking into account the uncertainty in the radio isophotes, this is in reasonable agreement with the value of 37°·7 given by de Vaucouleurs (9) for the visible nebula.

The observed results were analysed in an attempt to arrive at a closer approximation to the true distribution of the coronal component. The radiation due to the disk was subtracted from the observed distribution, and corrections were made for the smoothing effects of the aerial beam. The analysis

showed that the observations can be reproduced closely if the true isophotes of the corona are elliptical with gaussian brightness distributions along both axes. The total apparent widths of these distributions are $4^\circ{\cdot}1$ (major axis) $\times$ $2^\circ{\cdot}6$ (minor axis) between half-brightness points, and $10^\circ{\cdot}6$ (major axis) $\times$ $6^\circ{\cdot}7$ (minor axis) between 1 per cent contours. The apparent axial ratio of the corona is therefore 0·6, the axial ratio being defined as the ratio of the minor axis to the major axis.

These results have been compared with those obtained by Seeger, Westerhout and Conway (**11**) who used a 2° beam at 400 Mc/s. The two sets of observations are in reasonable agreement. One obvious discrepancy is that the 400 Mc/s contours show some curious structure at the extreme north and south of the corona. The results presented in the present paper suggest that this structure is not associated with M31, but is due to extraneous features of the background radiation.

(ii) *The distribution of emissivity in the corona.*—We shall discuss the emissivity of the corona of M31 on the assumption that the absorption in the nebula at 158 Mc/s can be neglected, since calculations for our own Galaxy (**15**) indicate that such an assumption is justified. We shall also assume that the corona is an oblate spheroid whose principal axes coincide with those of the visible nebula. On these assumptions it can be shown (**16**) that p, the true axial ratio of the ellipsoid, is given by

$$p^2 = \frac{(b/a)^2 - \sin^2 i}{1 - \sin^2 i} \qquad (2)$$

where i is the inclination of the nebula to the line of sight and b/a is the apparent axial ratio of the corona. Taking $i = 14^\circ{\cdot}5$ and $b/a = 0{\cdot}6$ the true axial ratio of the corona is 0·57.

It was stated in the previous section that the apparent variation of brightness along the principal axes of the corona may be represented by gaussian distributions. It is simple to show that these distributions are exhibited by a model of the corona in which the surfaces of equal emissivity are concentric ellipsoids of fixed axial ratio and in which the emissivity follows a gaussian decrease with distance from the centre. In this model the emissivity $\epsilon(a, z)$ at a point with coordinates a, z with respect to the centre of the corona is given by

$$\epsilon(a, z) = \epsilon_0 \exp\left(-\frac{a^2}{2\sigma_1^2} - \frac{z^2}{2\sigma_2^2}\right) \qquad (3)$$

where ϵ_0 is the emissivity at the centre, a is measured in the plane of the nebula and z is measured perpendicular to the plane.

Assuming the distance of M31 to be 630 kpc and taking the widths of the apparent distributions given in the previous section, it can be shown that $\sigma_1 = 19{\cdot}3$ and $\sigma_2 = 11{\cdot}0$, where a and z are measured in kiloparsecs. It follows that the total widths of the corona between half-emissivity points are 45 kpc (major axis) $\times$ 26 kpc (minor axis), and that the total widths between the 1 per cent contours are 117 kpc (major axis) $\times$ 67 kpc (minor axis).

The emissivity of the corona was found by integrating the radiation from the model and equating the result to the observed total power from the nebula. The emissivity at the centre of the corona was found to be $0{\cdot}12 \times 10^{8}$ w. $(c/s)^{-1}$ ster^{-1} pc^{-3} at 158 Mc/s. This result is in reasonable agreement with the value given by Baldwin (**17**) of $0{\cdot}24$–$0{\cdot}35 \times 10^{8}$ w. $(c/s)^{-1}$ ster^{-1} pc^{-3} at

81·5 Mc/s for the mean emissivity of the corona of M31. He assumed in deriving this value that the corona is spherical with a diameter of 36 kpc.

It is interesting to note that, taking the dimensions of the *disk* component suggested in Section 4.5, the emissivity in the disk must be significantly greater than that in the corona.

5. *Observations of M33 (NGC 598)*

5.1. *The region around M33.*—A detailed survey of M33 was carried out at 158 Mc/s, the region covered being bounded by declinations N 26° and N 36° and right ascensions $01^h 15^m$ and $01^h 55^m$. The results of the surveys are plotted as isophotes in Fig. 6. The outline of the visible nebula has been superimposed as a broken line.

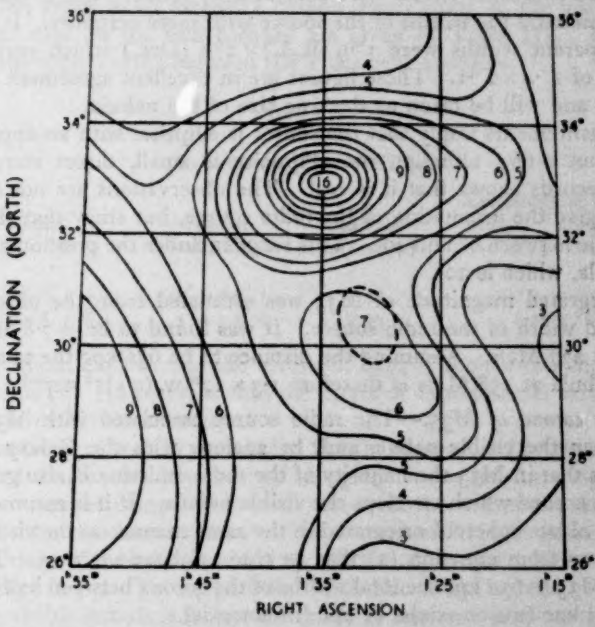

FIG. 6.—*Isophotes of M33 observed at 158 Mc/s. The contours are marked in arbitrary units of brightness temperature. Epoch 1950.*

The most prominent feature of the map is the source at approximately N 33°, $01^h 35^m$, which has an intensity of about 60×10^{-26} w.m.$^{-2}$(c/s)$^{-1}$ at 158 Mc/s. Some observations made on this source at 237 Mc/s show that it has an angular diameter which is considerably less than 1°. Its position is so close to M33 that it complicates the observations of the radiation from the nebula, and in an early interferometer survey made by Ryle, Smith and Elsmore (10) it was itself identified with the nebula.

The isophotes also show an extended region of low intensity whose centre appears to lie somewhat to the south of the nebula. However, the contour system is distorted by severe gradients in the background radiation and an inspection of the individual records shows that in fact this extended region consists of two sources. One of these sources, which has a small angular diameter

and an intensity of 13×10^{-26} w.m.$^{-2}$ (c/s)$^{-1}$, lies at about $01^h 25^m$, N 29°. The other source, which has a large angular diameter, is centred at $01^h 32^m$, N 30° 15′. These latter coordinates agree closely with the optical centre of M33 and we therefore propose to identify this extended source with the nebula.

After correcting for the effects of the confusing sources, it was found that at 158 Mc/s the apparent widths of the extended source associated with the nebula were 2°·45 in right ascension and 2°·8 in declination between points of half-intensity. When allowance is made for the smoothing produced by the aerial beam these figures give the corresponding widths of the radio nebula as 1°·5 (R.A.) × 2°·1 (Dec.). These figures have been checked by making some scans through the centre of the visible nebula at 237 Mc/s. At this higher frequency the confusion effects were considerably reduced and it was therefore possible to measure the widths of the source with more certainty. It was found that the apparent widths were 1°·9 (R.A.) × 2°·5 (Dec.) which correspond to true widths of 1°·4 × 2°·1. These figures are in excellent agreement with those at 158 Mc/s and will be taken as the true size of the nebula.

The measurements imply that the source is elliptical with an apparent axial ratio of about 0·66; although the ellipticity is small, direct comparison of individual records shows that it is real. The observations are not sufficiently accurate to give the orientation of the radio source, but show that the position angle must lie between 0° and 40°. This range includes the position angle of the visible nebula, which is 20°.

The integrated magnitude of M33 was estimated from the observed peak intensity and width of the radio source. It was found to be +7·8 at 158 Mc/s and +7·7 at 237 Mc/s. Assuming the distance to be 630 kpc the total emission from the nebula at 158 Mc/s is therefore $1{\cdot}3 \times 10^{20}$ w. (c/s)$^{-1}$ ster^{-1}.

5.2. *The corona of M33.*—The radio source associated with M33 is more extensive than the visible nebula and, by analogy with the Galaxy and M31, this suggests that in M33 the majority of the radio emission is also generated in an extensive corona which envelops the visible nebula. If it is assumed that the corona is an oblate spheroid orientated in the same manner as the visible nebula, then it follows from equation (2) that its true axial ratio is 0·45. Taking the distance of M33 as 630 kpc the total widths of the corona between half-emissivity points are 23 kpc (major axis) × 11 kpc (minor axis).

The emissivity of the corona was estimated by assuming that, as in the case of M31, the emissivity follows a gaussian decrease with distance from the centre. The value of the emissivity at the centre of the corona was found to be $0{\cdot}15 \times 10^8$ w. (c/s)$^{-1}$ ster^{-1} pc^{-3} at 158 Mc/s.

6. *Comparison of M31 and M33*

6.1. *Comparison of the radio and photographic magnitudes.*—The photographic and radio magnitudes (at 158 Mc/s) for the two nebulae are given in Table II.

TABLE II

Comparison of the radio and photographic magnitudes of M31 and M33

Object	Type	Photographic magnitude (18)	Radio magnitude	$m_r - m_p$
M31 (NGC 224)	Sb	+4·3	+5·8	+1·5
M33 (NGC 598)	Sc	+6·2	+7·8	+1·6

It can be seen from Table II that, if it is assumed that the distances of the two nebulae are the same, then the total radio emission from M31 is greater by two magnitudes than the total radio emission from M33. However, the ratio of the total radio emission to the total light emission ($m_r - m_p$) shows no significant difference although the two nebulae differ in type. This subject will be discussed more fully in Part II of this paper.

The measurements of M33 are not sufficiently accurate and cover too small a frequency range to decide if there is a significant difference between the spectral indices of the two nebulae.

6.2. *Comparison of the corona of M31 with the corona of M33.*—The results presented here show that in the case of both M31 and M33 the majority of the radio emission arises in an extensive corona which envelops the visible nebula. The relevant data on the two coronae are given in Table III. The widths quoted are the total widths between the 1 per cent contours.

TABLE III

The coronae of M31 and M33

Nebula	Size of corona	Axial ratio of corona	Emissivity at centre, w. $(c/s)^{-1}$ $ster^{-1}$ pc^{-3} at 158 Mc/s
M31 (NGC 224)	$10°{\cdot}6 \times 6°{\cdot}1$	0·57	$0{\cdot}12 \times 10^{8}$
M33 (NGC 598)	$5°{\cdot}4 \times 2°{\cdot}4$	0·45	$0{\cdot}15 \times 10^{8}$

The maximum extension of the corona of M31 is about twice the maximum extension of M33. However, within the limits of experimental error, the axial ratios and the emissivities are equal.

The visual sizes of both M31 and M33 have been measured by Holmberg (18), who obtained a value for M31 of 197′ along the major axis, and 83′ for M33. These values may be compared in each case with the size of the major axis of the corona; the maximum extent of the corona of M31 is greater than the maximum extent of the visible nebula by a factor of 3·2 while the corresponding factor for M33 is 3·9. To compare the axial ratio of the corona with the axial ratio of the visible nebula it is first necessary to take into account the effects of inclination. Examination of several edge-on spirals (19) indicates that, neglecting the central bulge, the minor and major axes of Sb and Sc type spirals are in the ratio of about 1 : 12 and therefore they have an axial ratio of about 0·08 : 1. This is much smaller than the axial ratio of the corona of M31 and M33 given in Table III. However, although the distributions of the radio emission perpendicular to the planes of M31 and M33 are much broader than the distributions of light the ratio of the widths appears to be much the same for each nebula. It may, therefore, be concluded that the sizes of the coronae of M31 and M33 are approximately proportional to the sizes of the visible nebulae, the maximum extent of the coronae being about three times greater than the maximum extent of the visible nebulae.

7. *Comparison with the Galaxy.*—It has been shown by Mills (13) that about 90 per cent of the total radiation from the Galaxy arises in the corona and about 10 per cent in the disk component; this result is in agreement with the relative

proportions of the two components in M31. He also concluded that the corona of the Galaxy is spheroidal with a ratio of minor to major axis of 0·69 and that the central emissivity is $4{\cdot}3 \times 10^{8}$ w. $(c/s)^{-1}$ ster^{-1} pc^{-3} at a frequency of 85 Mc/s. In an earlier study of the corona of the Galaxy at 81·5 Mc/s, Baldwin (**12**) showed that the axial ratio was greater than 0·5, and he estimated the mean emissivity as $1{\cdot}8 \times 10^{8}$ w. $(c/s)^{-1}$ ster^{-1} pc^{-3} in good agreement with the results of Mills.

The axial ratio of the corona of the Galaxy therefore appears to be similar to the axial ratio of the corona of M31. The central emissivity of $4{\cdot}3 \times 10^{8}$ w. $(c/s)^{-1}$ ster^{-1} pc^{-3} at 85 Mc/s, which corresponds to an emissivity of about $2{\cdot}3 \times 10^{8}$ w. $(c/s)^{-1}$ ster^{-1} pc^{-3} at 158 Mc/s, is greater by a factor of about 16 than the corresponding emissivities of M31 and M33. As the total radio emission from the Galaxy appears to be comparable to the total emission from M31, it follows that the corona of the Galaxy is probably smaller than that of M31 by a factor of about 2·5 and that it is more nearly equal in size to the corona of M33. These conclusions are in reasonable agreement with the results of Baldwin (**17**); he found the emissivity of the corona of the Galaxy to be greater by a factor of 6 than that of M31, and his figures also show that the corona of the Galaxy is significantly smaller than that of M31.

8. *Acknowledgments.*—We thank Professor A. C. B. Lovell for making available the facilities for this investigation, and Dr H. P. Palmer for the use of his unpublished results on the Andromeda Nebula.

Jodrell Bank Experimental Station,
Macclesfield,
Cheshire :
1959 *February.*

References

(1) R. Hanbury Brown and C. Hazard, *M.N.*, **111**, 357, 1951.
(2) R. Hanbury Brown and C. Hazard, *Phil. Mag.*, **43**, 137, 1952.
(3) R. Hanbury Brown and C. Hazard, *Nature*, **172**, 853, 1953.
(4) A. C. B. Lovell, *Nature*, **180**, 60, 1957.
(5) W. Baade and R. Minkowski, *Ap. J.*, **119**, 215, 1954.
(6) M. Ryle and D. D. Vonberg, *Proc. Roy. Soc.* A, **193**, 98, 1948.
(7) D. Morris, H. P. Palmer and A. R. Thompson, *Observatory*, **77**, 103, 1957.
(8) G. R. Whitfield, *M.N.*, **117**, 680, 1957.
(9) G. de Vaucouleurs, *Ap. J.*, **128**, 465, 1958.
(10) M. Ryle, F. G. Smith and B. Elsmore, *M.N.*, **110**, 508, 1950.
(11) C. L. Seeger, G. Westerhout and R. G. Conway, *Ap. J.*, **126**, 585, 1957.
(12) J. E. Baldwin, *M.N.*, **115**, 690, 1955.
(13) B. Y. Mills, at the Paris Symposium on Radio Astronomy, 1958.
(14) H. P. Palmer, private communication.
(15) R. Hanbury Brown and C. Hazard, *Phil. Mag.*, **44**, 939, 1953.
(16) E. Hubble, *Ap. J.*, **64**, 321, 1926.
(17) J. E. Baldwin, Symposium No. 5 of the I.A.U., ed. N. Roman, p. 44, Cambridge, 1958.
(18) E. Holmberg, *Medd. Lund. Obs. Ser.* 2, No. 136, 1957.
(19) A. B. Wyse and N. U. Mayall, *Ap. J.*, **95**, 24, 1942.

STEADY-STATE COSMOLOGY TREATED ACCORDING TO GENERAL RELATIVITY

W. Davidson

(Received 1958 November 17)

Summary

The interpretation of steady-state cosmology according to general relativity, initiated by McCrea (1), is extended in this paper by the investigation of external and internal metrics for the static superposition of a spherically symmetric mass concentration, or rarefaction, in a "steady-state" medium.

It is found that a constant total density ρ_0 and negative pressure p_0 $(=-\rho_0)$ appear to constitute a natural state of relative stability for the steady-state medium, and the analysis suggests that this state may be realized between the galaxies of a steady-state universe. From a discussion of the world-lines of the medium in the neighbourhood of a static disturbance it is deduced that such a disturbance has the effect of countering cosmic repulsion, or intensifying it, according as it represents a concentration of mass, or a rarefaction, relative to the natural state. A mechanism for the creation of matter is presented by which the rate of creation is seen to be strongly dependent on local gravitational influence, being positive where the medium is expanding, and negative (annihilation) where it is contracting.

Physical limits of size and density are found for a static disturbance of the natural state. It is shown that in a disturbed medium the sign of the gravitational field depends on the local state of the medium, and in a rarefaction the density of inertia, in the Newtonian sense, is found to be negative. A theoretical basis for the relative stability of the natural state is indicated.

---

1. *Introduction.*—It has been shown by McCrea (1) that the continuous creation of matter required by steady-state cosmology, first proposed by Bondi and Gold (2), and by Hoyle (3), can be based on the existing field equations of general relativity, without introducing, *ad hoc*, extra terms into these equations. In the theory of continuous creation advanced by Hoyle an extra term is added to the equations of general relativity, distinct from the energy tensor, so that energy is no longer conserved but created out of nothing at a rate determined by the extra term.

McCrea showed that by absorbing the extra term proposed by Hoyle into the energy tensor it could be interpreted as a cosmological stress, which in Hoyle's model was taken to be zero. The metric of space-time in the "smoothed out" steady-state model is established on the basis of Bondi and Gold's "perfect cosmological principle" to be that of the de Sitter universe. Accordingly, the application by McCrea of the field equations of general relativity to this metric showed that the stress must be uniform, constant, and negative, being the negative of the constant energy density in the model. The matter created in the model, at the constant rate necessary to maintain the steady state, was then interpreted by McCrea as the mass equivalent of the work done by the negative stress in the expansion of the model.

In this paper we extend the interpretation of steady-state cosmology according to general relativity by investigating external and internal metrics for the static superposition of a spherically symmetric mass concentration, or rarefaction, on a smoothed out steady-state medium. In this way it is found possible to throw more light on zero-point stress and energy, to indicate possible factors in the mechanism of steady-state cosmology, and to reveal new phenomena which are consistent with general relativity, and perhaps with present quantum theory, but which have no analogues in classical mechanics.

2. *The smoothed out steady-state medium according to general relativity.*—The space-time metrics of those expanding or contracting cosmological models which are spatially isotropic at every point, and therefore spatially homogeneous, are now well known to have the form (**4**, **5**)

$$dS^2 = dt^2 - R^2(t)\left\{\frac{dr^2 + r^2\,d\theta^2 + r^2\sin^2\theta\,d\phi^2}{(1+kr^2/4)^2}\right\}, \tag{2.1}$$

where $R(t)$ is a disposable function of cosmic time t and k may take the values 1, 0, or -1. Such a model serves to represent a universe in which a spatial isotropy which it possesses in the large becomes extended to the small, by means of an ideal smoothing out of its local irregularities arising from mass concentrations.

The steady-state metric is a special case of (2.1), with $R(t) = e^{t/a_0}$ (a_0 constant) and $k = 0$, thus (**2**)

$$dS^2 = dt^2 - e^{2t/a_0}(dr^2 + r^2\,d\theta^2 + r^2\sin^2\theta\,d\phi^2). \tag{2.2}$$

(It will be convenient in this paper to let suffix 0 refer to quantities associated with the smoothed out steady-state model of this metric.) It is well known that (2.2) is also the metric of the de Sitter universe in the form obtained by Lemaitre (**6**), and by Robertson (**7**). This was related to the useful earlier form (**8**)

$$dS^2 = (1 - l^2/a_0^2)\,d\tau^2 - dl^2/(1 - l^2/a_0^2) - l^2\,d\theta^2 - l^2\sin^2\theta\,d\phi^2 \tag{2.3}$$

according to the transformation

$$r = \frac{le^{-\tau/a_0}}{\sqrt{1 - l^2/a_0^2}}, \qquad t = \tau + \tfrac{1}{2}a_0\log(1 - l^2/a_0^2). \tag{2.4}$$

The field equations of general relativity applied to the general metric (2.1) yield for the uniform, and in general time-dependent, proper energy density ρ and proper pressure p the equations (**9**)

$$\left.\begin{aligned} \kappa\rho &= 3\dot{R}^2/R^2 + 3k/R^2 \\ -\kappa p &= 2\ddot{R}/R + \dot{R}^2/R^2 + k/R^2 \end{aligned}\right\}, \tag{2.5}$$

where a dot indicates differentiation with respect to t and κ is the Einstein gravitational constant.

In these equations the cosmological constant has been omitted since it is superfluous in the steady-state cosmology with which we are concerned in this paper. This is because, for the metric (2.2), ρ and $-p$ are themselves equal constants. Thus, following McCrea (**1**), we put $R(t) = e^{t/a_0}$, $k = 0$, and find that according to general relativity the density and pressure in a smoothed out steady-state medium must be taken to be

$$\rho_0 = -p_0 = \frac{3}{\kappa a_0^2}. \tag{2.6}$$

3. *The exterior metric for a static mass concentration or rarefaction in a steady-state medium.*—It is clear that a static exterior metric for a spherically symmetric mass concentration in a cosmological medium, which at great distance is in the physical state of the smoothed out steady-state universe considered in Section 2, will go over to a form equivalent to (2.3) at sufficient distance, and go over to this form at all points when the mass of the concentration tends to zero. On the other hand, in the neighbourhood of the disturbance it will approximate to the well-known Schwarzschild solution. We shall therefore adopt the procedure of writing down a well-known metric which satisfies these conditions and then interpreting the associated physical state according to general relativity.

It is clear that a metric satisfying the conditions described is

$$dS^2 = \left(1 - \frac{2m}{l} - \frac{l^2}{a_0^2}\right) d\tau^2 - dl^2 \Big/ \left(1 - \frac{2m}{l} - \frac{l^2}{a_0^2}\right) - l^2\, d\theta^2 - l^2 \sin^2\theta\, d\phi^2, \quad (3.1)$$

where m is a constant. It will be noted that the metric (3.1) is familiar as that for a Schwarzschild particle embedded in the empty but curved world which results from admitting the cosmological constant Λ into the field equations, (10). The metrics become formally the same if we put $1/a_0^2 = \Lambda/3$.

However, as stated earlier, we abandon the cosmological constant in this paper and interpret the curvature of space-time for large l as arising from the smoothed out steady-state medium whose density and pressure are given by (2.6). A new problem therefore arises of discussing according to general relativity how the physical state of the medium is modified by the permanent presence of the body embedded in it. The author is aware that the possibility of this interpretation of the metric (3.1) has been recognized before (e.g. Pirani (11)), but puts forward as new the present investigation of its implications.

From the equations relating the components of the energy tensor T_μ^ν to the coefficients of a static metric of spherical symmetry (12) it is a straightforward calculation to show that, for the case (3.1),

$$T_\mu^\nu = \frac{3}{\kappa a_0^2}\, \delta_\mu^\nu, \quad (3.2)$$

where δ_μ^ν represents the Kronecker symbol. The Greek indices may take the values 1, 2, 3, 4 associated with the coordinates l, θ, ϕ, τ respectively.

We shall make the reasonable assumption that the stress in the exterior fluid can be attributed to the random motion of primary particles, material and otherwise, and is therefore everywhere isotropic relative to observers in locally inertial frames which are instantaneously moving with the fluid. That is, the medium constitutes a perfect fluid characterized by a proper energy density ρ and pressure p. The T_μ^ν are therefore related to the 4-vector of velocity of the fluid, in its mean motion, by the relation

$$T_\mu^\nu = g_{\mu\alpha}(\rho + p)\frac{dx^\nu}{dS}\frac{dx^\alpha}{dS} - \delta_\mu^\nu p. \quad (3.3)$$

By spherical symmetry we can put $d\theta/dS = d\phi/dS = 0$, so that $T_2^2 = T_3^3 = -p$. Hence, by (3.2),

$$\left.\begin{aligned} p &= -\frac{3}{\kappa a_0^2} \\ &= p_0, \text{ by (2.6)} \end{aligned}\right\}. \quad (3.4)$$

Furthermore, by (3.2) we can substitute $T_4^4 = -p_0$ into (3.3), so that we find $g_{44}(\rho+p)(d\tau/dS)^2 = 0$, and since $g_{44} \neq 0$, $d\tau/dS \neq 0$, we must have $\rho+p=0$. Whence

$$\left.\begin{aligned} \rho &= \frac{3}{\kappa a_0^2} \\ &= \rho_0, \text{ by (2.6)} \end{aligned}\right\}. \tag{3.5}$$

It transpires, therefore, that at all points for which the metric (3.1) is valid, that is, outside the postulated mass concentration, the density and pressure take the constant values associated with the smoothed out steady-state universe of metric (2.3). The presence of a stable mass concentration in the medium does not evidently affect the maintenance of this density and pressure. *Thus, according to general relativity the total density ρ_0 and negative pressure p_0 appear as a natural state of relative stability for the steady-state medium.* A possible mechanism for this stability which is suggested by general relativity will be indicated in Section 11.

Since we have postulated the existence of a stable mass concentration in the medium it is necessary to suppose that the relative stability of the medium can be upset by sufficiently powerful disturbing factors leading to local gravitational condensations. It will be shown in Section 11 that according to general relativity there is a critical state of disturbance of the medium at which stable mass concentrations may in fact occur.

If $m < 0$ in the metric (3.1) the disturbance of the medium has to be interpreted as a rarefaction, and not a concentration, as will be shown in Section 8. Reasons will be given in Section 11, however, for believing that such rarefactions cannot be permanent. Nevertheless, its inclusion here as a case of stability will lead to conclusions which may reasonably be assumed to have some relevance to slowly varying disturbances involving rarefactions of the medium.

If one now considers the actual expanding universe, that is of galaxies immersed in an intergalactic medium of an unknown nature, the notion of a steady state in the sense just described might be realized by supposing that the intergalactic medium should, despite its general expansion, maintain a natural state characterized by a constant density ρ_0 and constant stress p_0. If exceptionally disturbed, due perhaps to the random motions of galaxies relative to the medium as envisaged by Sciama (13), the medium would contract locally to form new galaxies.

The density ρ_0 given by (2.6) may be evaluated approximately by identifying a_0 as the reciprocal of the Hubble constant for the model. In this way Hoyle (3), and more recently McCrea (14), have arrived at the conclusion that in view of the estimated amount of matter in galaxies, the great bulk of the matter in a steady-state universe must reside in the intergalactic medium. This fact lends support to the above interpretation of our results. That is, *the constant density ρ_0* and *negative pressure p_0* are not necessarily to be regarded as, in a somewhat obscure sense, "average" characteristics derived for a steady-state universe by smoothing it out, since it is possible that they *may actually be realized in the intergalactic medium of such a universe.*

The physical origin of the negative pressure in such a universe can at the present time be only a matter of conjecture. McCrea (1) did not propose any physical basis for zero-point stress. He pointed out, however, that a zero-point

stress, and perhaps an associated zero-point energy, other than what were usually assumed arbitrarily on the basis of classical mechanics, were consistent with the field equations of general relativity and also with the virtual zero-point properties accorded to space by the current quantum theory of fields.

In this paper (Section 10) we shall find that under certain conditions our steady-state medium possesses inertial characteristics which are similar to those that have been described by Massey (15) in relation to negative energy states in present quantum theory. In addition, as shown in Section 9, the negative pressure in our steady-state medium must be associated with the generally repulsive gravitational field that exists in it. Indeed, if the expansion observed in the actual universe is in fact accelerating, then general relativity would tell us, ruling out the unsatisfactory cosmological constant, that there must exist both anti-gravity and negative stress-energy.

4. *The world-lines of the exterior medium.*—It is inherent in the representation of the undisturbed steady-state medium by the metric (2.2) that the fluid elements are treated as at rest in the coordinate system r, θ, ϕ. It follows that the medium is in motion in the coordinate system l, θ, ϕ of (2.3). In fact the 4-velocity of the medium in this system will be, by (2.3) and (2.4),

$$\left(\frac{dl}{dS}, \frac{d\theta}{dS}, \frac{d\phi}{dS}, \frac{d\tau}{dS}\right) = \left(\frac{l}{a_0}, 0, 0, \frac{1}{1-l^2/a_0^2}\right). \tag{4.1}$$

We proceed to find the corresponding 4-velocity for the motion of the medium concerned in (3.1), noting that we have not now got a reference system corresponding to (2.2) in which the medium is at rest.

The motion is naturally required to be purely radial, i.e. $d\theta/dS = d\phi/dS = 0$. Also, since we are explicitly concerned with a local disturbance of the steady state, the motion must agree with (4.1) for large l, i.e.

$$\frac{dl}{dS} \sim \frac{l}{a_0} \qquad (l \text{ large}), \tag{4.2}$$

and agree exactly when $m \to 0$.

It should now be observed that, so far as the energy tensor is concerned (equation (3.3)), the motion may be quite arbitrary, for this tensor does not depend on the motion when $\rho + p = 0$. It should be noted, too, that the usual proof in general relativity that the world-lines of the elements of an isotropic fluid are geodesics if the pressure is constant fails when $\rho + p = 0$. (Thus, in general, the equating to zero of the covariant divergence of (3.3) yields, for the case when p is a constant, the relation $(\rho + p)\lambda^r \lambda^\mu{}_{;r} = 0$, in which $\lambda^\mu \equiv dx^\mu/dS$. Unless $\rho + p = 0$ one may therefore conclude that the geodesic equation $\lambda^r \lambda^\mu{}_{;r} = 0$ is satisfied.) Nevertheless, even in the present exceptional case it is reasonable to expect that in any local inertial frame the medium will in fact maintain the law of inertia for a fluid of constant pressure, and therefore follow a geodesic in a general reference frame. *A geodesic 4-velocity for the medium* will therefore be *postulated*. This postulate is of course satisfied in the undisturbed medium ($m = 0$).

It may easily be shown that the relevant geodesic equations are

$$\frac{d^2 l}{dS^2} = -\frac{m}{l^2} + \frac{l}{a_0^2}, \tag{4.3}$$

and

$$\frac{d}{dS}\left\{\left(1 - \frac{2m}{l} - \frac{l^2}{a_0^2}\right)\frac{d\tau}{dS}\right\} = 0. \tag{4.4}$$

From (4.3) we see that the presence of a *mass concentration* ($m>0$) *has the effect of countering cosmic repulsion* in the neighbouring medium, *while a rarefaction* ($m<0$) *intensifies the repulsion.*

The integrals of these equations are

$$\left(\frac{dl}{dS}\right)^2 = \alpha^2 - 1 + \frac{2m}{l} + \frac{l^2}{a_0^2}, \tag{4.5}$$

$$\frac{d\tau}{dS} = \frac{\alpha}{1 - \frac{2m}{l} - \frac{l^2}{a_0^2}}, \tag{4.6}$$

where α is a constant of the motion. The graphs of dl/dS as given by (4.5), in the range $l \geqslant 0$ for the cases $m>0$, $m=0$, $m<0$ with varying α, are shown in Figs. 1, 2, and 3 respectively. We comment on these curves as follows:

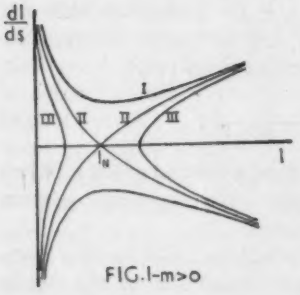

FIG.1-m>0

(i) $m>0$. Three curves are shown which indicate the three different types possible. Curves of type I correspond to

$$\alpha > \left\{1 - 3\left(\frac{m}{a_0}\right)^{2/3}\right\}^{1/2}$$

for which $(dl/dS)^2$ has a minimum non-zero value. This will occur where d^2l/dS^2 vanishes which, by (4.3), is at $l=l_N$ where

$$l_N^3 = ma_0^2. \tag{4.7}$$

The surface $l=l_N$ forms a neutral surface in the medium where we can regard the attraction of the mass m as just balancing cosmic repulsion. Curve II is unique, corresponding to

$$\alpha = \left\{1 - 3\left(\frac{m}{a_0}\right)^{2/3}\right\}^{1/2}$$

for which dl/dS vanishes at the neutral surface $l=l_N$. Type III curves correspond to

$$\alpha < \left\{1 - 3\left(\frac{m}{a_0}\right)^{2/3}\right\}^{1/2}.$$

These curves have two branches in between which, for a range of l containing $l=l_N$, dl/dS is imaginary.

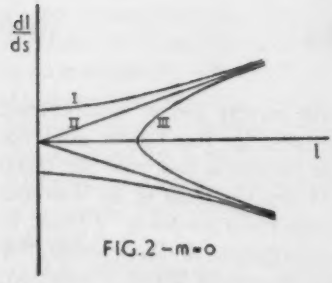

FIG.2-m=0

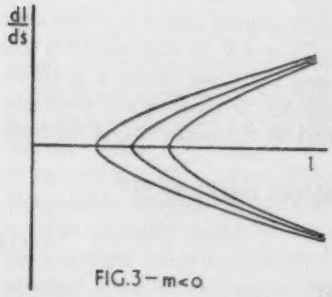

FIG.3-m<0

(ii) $m=0$. This is the case of the undisturbed medium. From the present point of view of possible geodesic motions the curves divide themselves into three types similar to (i), according as $\alpha \gtrless 1$. The case $\alpha=1$ gives $dl/dS = \pm l/a_0$.

(iii) $m<0$. In this case the acceleration d^2l/dS^2 is always directed away from the disturbance. Three typical curves are shown.

As $\alpha \to \infty$ the curves tend to coincide with $dl/dS = \pm l/a_0$. In general dl/dS is imaginary for sufficiently small l.

We now consider which of these curves may represent the motion of the medium in the various cases. Equation (4.5) indicates that $|dl/dS| \to l/a_0$ when l becomes large, for any finite α, so that condition (4.2) is satisfied if we take for dl/dS the positive root of (4.5) when l is large. The fact that $dl/dS \to l/a_0$ independently of α and m shows that the natural large scale motion of galaxies and medium in a steady-state universe can be described by $dl/dS = l/a_0$. The interest of the present discussion is in the small scale effects of disturbances in the intergalactic medium.

It is naturally required that the motion of the medium should be continuous with l. Hence, when $m > 0$ we must take the upper branch of curves I and the right hand branch (upper half) of curves III (or those portions of them which correspond to the exterior of the mass concentration). Both these curves would require the medium to be moving outwards everywhere, even near the disturbance. This might be possible if m is very small.

If m is sufficiently large, as in the case of a galaxy, the unique curve II would seem to be the most reasonable possibility. In this case *the medium would be at rest in unstable equilibrium on the neutral surface $l = l_N$, accelerating towards the mass concentration for $l < l_N$, and accelerating outwards for $l > l_N$.*

In case (iii), when $m < 0$, the medium must everywhere move away from the rarefaction. There seems nothing to choose between the various curves for this case and indeed they may all be possible since, as we show in Section 11, a rarefaction is likely to be unstable.

5. *The rate of creation of matter outside a static disturbance in the medium.*—In this section we consider the important question of how the rate of creation of matter associated with steady-state cosmology is affected by the proximity of a mass concentration or rarefaction in the medium.

For this purpose we divide the proper energy density ρ of general relativity into two parts. One, denoted by ρ_+, will incorporate the contribution from all known kinds of ordinary energy, including the energy equivalent of the mass of fundamental particles and also their associated kinetic energy due to random velocities, and the energy of radiation. The other part, ρ_-, will represent "zero-point" energy incorporating any other energy which may possibly contribute to ρ in general relativity. Thus

$$\rho = \rho_+ + \rho_- . \tag{5.1}$$

Similarly the pressure p may be written

$$p = p_+ + p_- . \tag{5.2}$$

The proper density ρ and pressure p of a perfect fluid are invariants in general relativity. We shall assume that the properly measured quantities ρ_+, ρ_-, p_+, and p_- are also invariants. This means, for instance, that all observers would infer, if it were possible, the same ratio of plus to minus energy in the *rest* mass of a given fluid element.

According to general relativity total energy is conserved. Creation of ordinary energy must decrease the absolute value of zero-point energy, and vice versa for annihilation of ordinary energy. The work done by stress must of course be taken into account in the conservation process. For a perfect fluid this is

expressed by the generally covariant equation of conservation of energy, viz.

$$(\rho\lambda^\nu)_{;\nu}+p\lambda^\nu_{;\nu}=0, \tag{5.3}$$

where λ^μ is the unit tangent to the world-lines of the fluid elements.

In virtue of (5.1) and (5.2) we may write (5.3) in the form

$$(\rho_+\lambda^\nu)_{;\nu}+p_+\lambda^\nu_{;\nu}=-\{(\rho_-\lambda^\nu)_{;\nu}+p_-\lambda^\nu_{;\nu}\}. \tag{5.4}$$

The left-hand side is the invariant representing the rate of creation, E_+, of ordinary energy in unit *proper* volume. Similarly, the right-hand side is $-E_-$, where E_- is the rate of "creation" of zero-point energy or the rate of annihilation of ordinary energy.

For the steady-state medium ρ and p are constant, equal to ρ_0 and p_0 respectively. We have found in Section 3 that according to general relativity this density and pressure are maintained in the medium, despite the influence of local static disturbances on its motion.

We now make the reasonable *assumption* that in this steady state the balance between what may be termed "positive" and "negative" states of energy will depend only on the total density ρ_0 and pressure p_0, and consequently ρ_+ and p_+, ρ_- and p_-, will also remain constant independent of local influences on the motion.

Accordingly, for E_+ in the steady state we can write

$$E_+=(\rho_++p_+)\lambda^\nu_{;\nu}, \tag{5.5}$$

$$=(\rho_++p_+)\frac{1}{\sqrt{-g}}\frac{\partial}{\partial x^\nu}(\sqrt{-g}\lambda^\nu), \tag{5.6}$$

where g is the determinant of the metric coefficients. Substituting from (3.1), (4.5), and (4.6), we derive

$$E_+=(\rho_++p_+)\frac{1}{l^2}\frac{d}{dl}\left(l^2\frac{dl}{dS}\right),$$

$$=\frac{3}{a_0}(\rho_++p_+)\left\{\frac{1+\frac{2}{3}(\alpha^2-1)a_0^2/l^2+ma_0^2/l^3}{\sqrt{1+(\alpha^2-1)a_0^2/l^2+2ma_0^2/l^3}}\right\}. \tag{5.7}$$

It is evident that this rate of creation of material and radiation energy is influenced by the gravitational effect of the disturbance on the motion of the medium. From (5.5) we see that the local sign of E_+ will be the sign of $\lambda^\nu_{;\nu}$, since ρ_++p_+ will be positive. Now the invariant $\lambda^\nu_{;\nu}$ measures the *proper* rate of expansion of the medium. Accordingly, we conclude that *where the medium is expanding locally matter is being created, and where it is contracting matter is being annihilated.*

By letting $l\to\infty$, or equivalently $\alpha\to1$, $m\to0$, we get the value of E_+ for the undisturbed steady-state medium, namely $(3/a_0)(\rho_++p_+)$. If p_+ is negligible compared with ρ_+, as is likely to be the case, then this is approximately $3/a_0$ times the density of material energy. This agrees with the results of Hoyle (3) and McCrea (1), as interpreted by them.

As an example of the effect of a static disturbance in the medium we suppose that m is large and positive as in the case of a galaxy. We have indicated in Section 4 that in such a case the critical value for α, namely $\alpha=\{1-3(m/a_0)^{2/3}\}^{1/2}$, is the most likely. Substitution of this value into (5.7) yields, on simplification,

$$E_+=\frac{3}{a_0}(\rho_++p_+)\left\{\frac{1+l_N/l-l_N^2/l^2}{\sqrt{1+2l_N/l}}\right\} \tag{5.8}$$

where l_N is the l coordinate of the neutral surface introduced in Section 4.

The behaviour of the disturbance factor is easily investigated. We omit the details and conclude as follows. Due to the effect of the mass concentration the *rate of creation in the medium decreases steadily as l decreases*, from the undisturbed steady-state value at great distance to $1/\sqrt{3}$ of this value at the neutral surface, decreases further for $l<l_N$ until, at $l=\{2/(1+\sqrt{5})\}l_N \doteq 0{\cdot}62l_N$, *annihilation* sets in for smaller l.

We conclude, therefore, that, according to our present analysis based on general relativity, the creation of matter in a steady-state universe is by no means a statistically uniform and random process in space, but on the contrary is *highly sensitive to local gravitational influence.*

6. *The interior solution for a static disturbance of uniform density.*—Our main concern in obtaining an interior solution of the field equations for a spherically symmetric disturbance in the steady-state medium will be with a sphere of fluid in which the density is not greatly different from ρ_0, the constant density of the exterior medium. It is only in this case that taking explicit account of the cosmological background can be expected to lead to significant information about the behaviour of the fluid *inside* such a sphere; and it is with regions of this order of density that any theory of the mechanism of steady-state cosmology must be concerned.

For densities ρ of this order it might be most natural for ρ to vary continuously in the interior, acquiring the value ρ_0 at the boundary, and also for the 4-velocity of the fluid to be continuous through the interior into the steady-state medium. Because it is mathematically more tractable, however, yet valuable to illustrate physical principles that will be involved in quasi-static regions also, we postulate that the proper density in the sphere is uniform and constant. This ensures a static interior metric and a fixed boundary for the disturbance.

Let ρ be the constant proper density and p the pressure (which will be a variable determined from the derived metric) of a perfect fluid occupying the region $0 \leqslant l \leqslant l_1$, where l is the radial coordinate. Outside this region the conditions of the steady-state medium obtain. The energy tensor components T_μ^ν will be given by (3.3), and their relation to a static metric of spherical symmetry of the form

$$dS^2 = e^{\nu(l)}d\tau^2 - e^{\lambda(l)}dl^2 - l^2 d\theta^2 - l^2\sin^2\theta\, d\phi^2 \tag{6.1}$$

is expressed by the equations referred to in Section 3 (12). From these equations, in a manner completely analogous to the derivation of the well-known Schwarzschild interior solution (16), we find that the interior metric can be written

$$dS^2 = (A - B\sqrt{1-l^2/a^2})^2 d\tau^2 - dl^2/(1-l^2/a^2) - l^2 d\theta^2 - l^2\sin^2\theta\, d\phi^2, \tag{6.2}$$

where A and B are constants, and a is related to ρ by

$$\rho = \frac{3}{\kappa a^2}, \tag{6.3}$$

while the pressure p is the variable

$$p = \frac{1}{\kappa a^2}\left(\frac{3B\sqrt{1-l^2/a^2}-A}{A-B\sqrt{1-l^2/a^2}}\right). \tag{6.4}$$

The constants A and B have to be found from the boundary conditions at $l=l_1$. These we shall base simply on continuity of pressure, and continuity of the metric components $g_{\alpha\beta}$, at $l=l_1$.

Putting $p=p_0$ when $l=l_1$, where by (2.6) $p_0=-3/(\kappa a_0^2)$, we find

$$\frac{1}{A-B\sqrt{1-l_1^2/a^2}}=\frac{3a^2}{2A}\left(\frac{1}{a^2}-\frac{1}{a_0^2}\right). \tag{6.5}$$

Continuity of the metric at $l=l_1$, demands that, by (3.1),

$$\left.\begin{aligned}(A-B\sqrt{1-l_1^2/a^2})^2&=1-\frac{2m}{l_1}-\frac{l_1^2}{a_0^2}\\&=1-\frac{l_1^2}{a^2}\end{aligned}\right\}. \tag{6.6}$$

Whence, by (6.5) and (6.6)

$$\left.\begin{aligned}A&=\pm\tfrac{3}{2}(1-a^2/a_0^2)\sqrt{1-l_1^2/a^2}\\B&=\pm\tfrac{1}{2}(1-3a^2/a_0^2)\end{aligned}\right\}. \tag{6.7}$$

The signs correspond in the order given, so that there is no loss of generality in taking them both positive, in view of (6.2).

It is to be noted that our interior solution, which has been joined to the exterior metric (3.1) by the boundary conditions stated, satisfies the boundary conditions established by O'Brien and Synge (**17**) for discontinuous mass distributions in general relativity. For our case of spherical symmetry these conditions require that

$$g_{\alpha\beta},\qquad \frac{\partial g_{\alpha\beta}}{\partial x^1},\qquad T_\alpha{}^1,\qquad g_{\alpha r}T_\beta{}^r-g_{\beta r}T_\alpha{}^r$$

should be continuous at $l=l_1$. Here Greek letters represent indices 1, 2, 3, 4 while Latin letters may represent indices 2, 3, 4 only, corresponding to coordinates θ, ϕ, τ respectively. It is easily verified that our solution satisfies these requirements.

We point out, also, that the fluid in the sphere is at rest in the reference frame. This follows from the fact that for the metric (6.1) the energy tensor components $T_4{}^1$, $T_4{}^2$, $T_4{}^3$ vanish identically. Hence, by (3.3) we have, for example,

$$e^{\nu}(\rho+p)\frac{dl}{dS}\frac{d\tau}{dS}=0,$$

and since $\rho+p\neq 0$ in general, it follows that $dl/dS=0$. Thus the fluid is unambiguously at rest in this case. There is, consequently, a discontinuity of velocity at $l=l_1$, in general, but this is evidently not inconsistent with the O'Brien–Synge boundary conditions. It is to be observed that *no energy is gained or lost by the sphere* since $T_4{}^1$ also vanishes in the exterior medium due to the relation $\rho_0+p_0=0$.

7. *Limits of density and size for a static disturbance in the steady-state medium.*— To avoid singularities of the interior metric (6.2), which would correspond to unacceptable physical singularities, the two expressions $1-l^2/a^2$ and $A-B\sqrt{1-l^2/a^2}$ must be of constant sign in the range $0\leqslant l\leqslant l_1$. For instance we see from (6.4) that if $A-B\sqrt{1-l^2/a^2}$ vanishes for some l then the pressure becomes infinite there. We can assume that the physical situation would adjust itself to prevent this. We shall restrict our considerations here to the case $a^2>0$, which by (6.3) means $\rho>0$.

For $1-l^2/a^2$ to be of constant sign in the range $0\leqslant l\leqslant l_1$, we require simply

$$l_1/a<1. \tag{7.1}$$

In the case of $A-B\sqrt{1-l^2/a^2}$ we note that at $l=l_1$ this expression is

$$A-B\sqrt{1-l_1^2/a^2}=\sqrt{1-l_1^2/a^2}>0,$$

using (6.7). Hence we require $A-B\sqrt{1-l^2/a^2}$ to be always >0 in the specified range. That is, if $0\leqslant l\leqslant l_1$,

$$\tfrac{3}{2}(1-a^2/a_0^2)\sqrt{1-l_1^2/a^2}-\tfrac{1}{2}(1-3a^2/a_0^2)\sqrt{1-l^2/a^2}>0. \tag{7.2}$$

It is easily established that as a^2 varies between 0 and ∞ (ρ varying between ∞ and 0) the most stringent condition which ensures the satisfaction of (7.2) is

$$l_1/a<\sqrt{8/9}, \tag{7.3}$$

this lowest upper limit for l_1/a occurring when $\rho\to\infty$.

Thus, the condition for the absence of singularities varies between the inequalities (7.1) and (7.3) according to the value of ρ. These inequalities may be expressed in terms of measurable quantities if we note that the proper radius δ of the sphere is given by

$$\delta=\int_0^{l_1}\frac{dl}{\sqrt{1-l^2/a^2}}=a\sin^{-1}(l_1/a). \tag{7.4}$$

The physical limits vary, therefore, between

$$\left.\begin{aligned}&\delta<\sqrt{\frac{3}{\kappa\rho}}\sin^{-1}\sqrt{\frac{8}{9}},\\ \text{and}\qquad&\\ &\delta<\sqrt{\frac{3}{\kappa\rho}}\frac{\pi}{2},\end{aligned}\right\} \tag{7.5}$$

according to the value of ρ.

This result indicates a physical *upper limit to the size of a static body of given density*, or an *upper limit to the density of a body of given size, in the steady-state universe.*

It is interesting to calculate on this basis the upper limit of size for an object of the mean density of an average galaxy. Taking this density to be 10^{-23} gm cm^{-3} we find $\delta<10^7$ light years approximately. This would seem to be very generous according to observational data, but it may place an upper bound to growth with age by capture of smaller condensations.

8. *Sign of m as a criterion for a concentration or rarefaction.*—The constant m in the case of the Schwarzschild solution for a body of spherical symmetry in empty space can be identified as the gravitational mass of the body (in relativistic units). But here, when the steady-state background is taken into account, this matter needs review.

By (6.6) we find

$$m=\frac{l_1^3}{2}\left(\frac{1}{a^2}-\frac{1}{a_0^2}\right), \tag{8.1}$$

so that

$$m\gtrless 0 \text{ according as } \rho\gtrless\rho_0. \tag{8.2}$$

Thus, the parameter m of a static disturbance is positive for a mass concentration relative to the undisturbed steady-state medium, and negative for a mass rarefaction.

Since m vanishes when $\rho=\rho_0$, the form of the equation (4.3) for the geodesic motion of the exterior medium indicates that m may be regarded as the *excess* of gravitational mass, taken algebraically, over that which would occupy the same coordinate volume in the undisturbed steady-state medium.

9. *Dependence of the sign of the gravitational field on the local state of the medium.*—The fact that the pressure, given by (6.4), in the interior of the disturbance is in general non-uniform indicates that a gradient of pressure is in general necessary to keep the fluid in the equilibrium that we have postulated. Stated otherwise, there is a gravitational "force" in the sense of Whittaker (**18**), acting at each point of the medium. The measure of this force, relative to the static fluid, is the initial acceleration d^2l/dS^2 of a test particle released from rest at coordinate l and "allowed" to follow a geodesic. For this one easily finds

$$\frac{d^2l}{dS^2} = \frac{-Bl\sqrt{1-l^2/a^2}}{a^2(A-B\sqrt{1-l^2/a^2})}. \tag{9.1}$$

We observe that, since $A-B\sqrt{1-l^2/a^2}$ is always positive in the interior (Section 7), the sign of d^2l/dS^2 depends only on the sign of B, and not on l. Thus, by (6.7),

$$\frac{d^2l}{dS^2} \gtrless 0 \text{ according as } \rho \lesseqgtr 3\rho_0. \tag{9.2}$$

It follows that the *gravitational field in a static disturbance is repulsive if* $\rho < 3\rho_0$ *and attractive if* $\rho > 3\rho_0$. *The sign of the field depends, therefore, on the state of the medium.*

It may be mentioned that the sign of the gravitational field as defined rather differently by Synge (**19**) depends on exactly the same criterion as found above. Based on his definition of gravitational "force" Synge obtains a local form of Gauss' theorem in general relativity. This states that relative to the world lines of matter the local gravitational mass in an isotropic medium is $\rho+3p$. For our case, referring to (6.3) and (6.4), we find that

$$\rho+3p = \frac{6B\sqrt{1-l^2/a^2}}{\kappa a^2(A-B\sqrt{1-l^2/a^2})}, \tag{9.3}$$

which takes the sign of B, with the same conclusion as before.

10. *Positive and negative inertia.*—The gradient of pressure in the static interior, referred to in Section 9, is found from (6.4) to be

$$\frac{dp}{dl} = \frac{-2ABl}{\kappa a^4\sqrt{1-l^2/a^2}(A-B\sqrt{1-l^2/a^2})^2}. \tag{10.1}$$

The sign of this expression throughout the medium depends only on the sign of AB. The following cases arise:

(i) $\rho > 3\rho_0$ $(a^2 < \frac{1}{3}a_0^2)$

In this case $dp/dl < 0$, which is a phenomenon familiar to our experience of mass concentrations.

(ii) $\rho = 3\rho_0$ $(a^2 = \frac{1}{3}a_0^2)$

The pressure is now constant at the value $p = p_0 = -3/(\kappa a_0^2)$.

(iii) $\rho_0 < \rho < 3\rho_0$ $(\frac{1}{3}a_0^2 < a^2 < a_0^2)$

For this case $dp/dl > 0$ so that, since $p = p_0 < 0$ at $l = l_1$, the pressure is always negative its least value being at $l = 0$.

(iv) $\rho = \rho_0$ $(a^2 = a_0^2)$

The sphere is now identical with a portion of the undisturbed steady-state medium as regards its uniform pressure p_0 and density ρ_0. The argument given at the end of Section 6 establishing that the interior fluid is at rest in the

coordinate frame now breaks down since $\rho_0+p_0=0$; the fluid must in fact be expanding in its natural geodesic motion under the repulsive gravitational field that exists when $\rho<3\rho_0$ (equation (9.2)), there being no pressure gradient to counteract it.

(v) $\rho<\rho_0$ $(a^2>a_0^2)$

Here $dp/dl<0$. The pressure is always negative in the interior but decreases with l in absolute value.

It may be surprising that when ρ decreases through the value ρ_0 the pressure gradient necessary to maintain equilibrium changes sign from positive to negative, despite the fact that the gravitational "force" at each value of coordinate l varies continuously with ρ, without changing sign. In fact, by referring to (9.1), we find that the initial acceleration d^2l/dS^2 of a geodesic test particle, released from rest at coordinate l, varies continuously with ρ when ρ decreases through the value ρ_0, taking the value

$$\left(\frac{d^2l}{dS^2}\right)_{\rho=\rho_0}=\frac{l}{a_0^2} \tag{10.2}$$

when $\rho=\rho_0$.

The explanation of this phenomenon can be expressed by saying that the *density of inertia, in the Newtonian sense, changes sign from positive to negative when ρ decreases through the value ρ_0, so that to produce the same effect the motivating force of pressure must be reversed.* This is seen as follows.

According to the mechanics of general relativity the acceleration of the fluid relative to the rest frame of the test particle mentioned above must be attributed to the pressure gradient in that frame. The equations of mechanics for a perfect fluid are expressed by equating to zero the covariant divergence of $T_\mu{}^\nu$ given by (3.3). In a local system of coordinates which is instantaneously co-moving with the fluid, but geodesic—that is "freely falling" unaffected by any stress gradient existing in the fluid, three of the resulting equations yield the momentum equation

$$\nabla p+(\rho+p)\,d\mathbf{q}/dt=0, \tag{10.3}$$

where $\mathbf{q}$ is the velocity of the fluid, $d\mathbf{q}/dt$ its acceleration, and ∇p the gradient of pressure. The fourth equation is the energy equation

$$dp/dt+(\rho+p)\,\mathrm{div}\,\mathbf{q}=0, \tag{10.4}$$

$\mathrm{div}\,\mathbf{q}$ being the spatial divergence of $\mathbf{q}$. Equation (10.4) is the local expression of (5.3).

The momentum equation shows that the proper density of inertia, in the Newtonian sense, for a stressed isotropic medium is $\rho+p$; this takes account of the contribution to momentum of the stress in a moving medium. The energy equation takes account of the work done by this stress.

These results are well known in various forms, but their application to a medium of negative p of the same order as ρ has not generally been envisaged. For our interior solution we find, by (6.3) and (6.4), that

$$\rho+p=\frac{2A}{\kappa a^3(A-B\sqrt{1-l^2/a^2})} \tag{10.5}$$

which, since $A-B\sqrt{1-l^2/a^2}>0$, takes the sign of A. Thus

$$\rho+p\gtrless 0 \text{ according as } \rho\gtrless\rho_0. \tag{10.6}$$

From (10.3) we see how the sign of $\rho+p$ determines the sign of the stress gradient necessary to induce in the medium a given acceleration $d\mathbf{q}/dt$ relative to a geodesic reference frame. We understand from (10.6), therefore, the change in sign of stress gradient when ρ passes through the value ρ_0, despite only infinitesimal change of the repulsive gravitational field indicated by (10.2).

Thus, like the sign of the gravitational field, the *sense of inertial effects in the steady-state universe depends on the local state of the medium, according to general relativity.*

11. *The stability of the steady-state medium.*—The analysis in Section 3 suggested that the state $\rho=\rho_0$, $p=p_0$ may be a natural one of relative stability realized in the intergalactic medium of a steady-state universe. In this section we put forward, tentatively, a mechanism for this stability based on the mechanics of general relativity.

For this purpose we make use of the results that have been established in this paper for static disturbances in the steady-state medium. We make the basic inference from the interior solution that, because of its static character, there must be a dynamic equilibrium set up between "positive" and "negative" states of energy of the primary particles of the fluid. (We recall that we are considering only *small* disturbances of the steady-state medium.) Consequently, the derived pressure distribution must be associated with this dynamic equilibrium for the different values of ρ considered.

On the basis of the consideration that the expansion of any limited region of the intergalactic medium will be extremely slow we make the *fundamental hypothesis* that even when the medium is non-static the pressure distribution will be adjusted to the prevailing density to secure dynamic equilibrium between positive and negative states. In particular, in a spherically symmetric disturbance of the medium in which the average density is ρ at a given local time t the same relation between ρ and p will hold at this moment as was found in the case of a static disturbance of the same size and density. It follows according to this hypothesis that when a disturbance develops the relative acceleration of the fluid elements will be reduced to zero, and the disturbance will simply expand uniformly. Also, from this point of view it is the local expansion or contraction of the medium that upsets the dynamic equilibrium between positive and negative states, causing a net creation or annihilation of matter to restore this equilibrium.

Suppose then that in a limited region of the intergalactic medium a slight disturbance of the steady-state conditions arises so that the average value of ρ changes from the value ρ_0. We now notice from (10.4) that, on account of (10.6), *the effect of the expansion tends to restore the steady-state conditions*, i.e. $\rho\to\rho_0$, $p\to p_0$. For since $\operatorname{div}\mathbf{q}>0$ then we shall have

$$\left.\begin{aligned}\frac{d\rho}{dt}\gtrless 0 \text{ according as } \rho+p\lesseqgtr 0,\\ \text{i.e. according as } \rho\lesseqgtr\rho_0 \text{ by (10.6)}\end{aligned}\right\}. \qquad (11.1)$$

A basis for the relative stability of the steady state is thus apparent.

Consider now a disturbance of the natural state in a region where the medium is contracting. We have seen in Section 5 that inside the neutral surface $l=l_N$ associated with a large mass such as a galaxy there will be, when the natural state $\rho=\rho_0$, $p=p_0$ prevails, annihilation of matter for $l<0{\cdot}62l_N$ due to the local

contraction of the medium ($\lambda_{,r}=\operatorname{div}\mathbf{q}<0$) in that region. Suppose now that natural state conditions do not obtain in this region, which might happen if the galaxy was moving relative to the medium leading to a concentration of mass in its wake (Sciama (**13**)). By (10.6) $\rho+p>0$ for a mass concentration so that, if $\operatorname{div}\mathbf{q}<0$, (10.4) indicates that ρ would tend to increase further. If the point is reached when $\rho>3\rho_0$ we notice from (9.2), or (9.3), that the interior gravitational field becomes attractive, so that even without the influence of the passing galaxy the mass concentration is stable and a new galaxy would form.

On the other hand the gravitational field in a *rarefaction* is always repulsive, and the rarefaction is *unstable* by the analysis associated with (11.1).

The question of the stability of smoothed out expanding universes has been investigated on a Newtonian basis by Bonnor (**20**). Employing the methods of Newtonian cosmology Bonnor shows that, for *small* perturbations from the smoothed out density, the classical formula of Jeans giving the critical condition for gravitational condensations is applicable to the expanding universes in which matter is conserved, but not to the steady-state model. Bonnor finds in fact that condensations could not form in the steady-state model from *small* perturbations.

This conclusion by Bonnor is of course in agreement with what we have found here to be the basis of the relative stability of the steady-state medium. It does not preclude the possibility, however, of condensations forming from large disturbances of the medium under the influence of existing condensations in the manner we have described.

Bonnor's analysis based on Jeans' formula involves the notion of condensations built up by waves of compression arising by statistical variations of density and his discussion therefore involves a second-order equation of motion. Our own approach is appropriate to the change of a given portion of the fluid as a whole, ignoring wave motion on a smaller scale and requiring only the continuity equation and the relation between p and ρ determined by our hypothesis of dynamic equilibrium during slow motions.

12. *Acknowledgments.*—A considerable portion of the material of this paper formed part of the author's Ph.D. thesis submitted in March 1958 to the University of London, to whom thanks are due for permission to publish.

The author also wishes to thank Professor W. H. McCrea, for his continued interest, encouragement, and helpful criticisms.

Royal Holloway College (University of London),
Englefield Green,
Surrey:
1958 *November* 15.

References

(1) W. H. McCrea, *Proc. Roy. Soc.* A, **206**, 562, 1951.
(2) H. Bondi and T. Gold, *M.N.*, **108**, 252, 1948.
(3) F. Hoyle, *M.N.*, **108**, 372, 1948.
(4) H. P. Robertson, *Ap. J.*, **82**, 284, 1935.
(5) A. G. Walker, *Proc. Lond. Math. Soc.* (2), **42**, 90, 1936.
(6) G. Lemaitre, *J. Math. and Phys.* (*M.I.T.*), **4**, 188, 1925.
(7) H. P. Robertson, *Phil. Mag.*, **5**, 835, 1928.
(8) W. de Sitter, *Proc. Akad. Wet. Amsterdam*, **19**, 1217, 1917: **20**, 229, 1917.
(9) H. Bondi, *Cosmology*, Cambridge: U.P., p. 103, 1952.

(10) A. S. Eddington, *The Mathematical Theory of Relativity*, Cambridge: U.P., p. 100, 1922.
(11) F. Pirani, *Proc. Camb. Phil. Soc.*, **50**, 637, 1954.
(12) R. C. Tolman, *Relativity, Thermodynamics, and Cosmology*, Oxford: Clarendon Press, p. 242, 1934.
(13) D. W. Sciama, *M.N.*, **115**, 1, 1955.
(14) W. H. McCrea, *Endeavour*, **17**, 5, 1958.
(15) H. S. W. Massey, *Endeavour*, **15**, 117, 1957.
(16) K. Schwarzschild, *Berlin S.B.*, p. 424, 1916.
(17) S. O'Brien and J. L. Synge, *Comm. Dublin Inst. Adv. Studies* A, **9**, 1952.
(18) E. T. Whittaker, *Proc. Roy. Soc.* A, **149**, 384, 1935.
(19) J. L. Synge, *Proc. Edin. Math. Soc.* (2), **5**, 93, 1937.
(20) W. B. Bonnor, *M.N.*, **117**, 104, 1957.

Russian summaries of preceding papers

(Russian summaries of the foregoing papers are unavoidably held over until the next issue.)

(ПЕРЕВОДЫ РЕЗЮМЕ ПРЕДЫДУЩИХ ДОКЛАДОВ НА РУССКИЙ ЯЗЫК НЕИЗБЕЖНО ЗАДЕРЖИВАЮТСЯ ДО СДЕДУЮЩЕГО ВЫПУСКА.)

NOTICE TO AUTHORS

1. *Communications.*—Papers must be communicated to the Society by a Fellow. They should be accompanied by a summary at the *beginning* of the paper conveying briefly the content of the paper, and drawing attention to important new information and to the main conclusions. The summary should be intelligible in itself, without reference to the paper, to a reader with some knowledge of the subject; it should not normally exceed 200 words in length. **Authors are requested to submit MSS. in duplicate. These should be typed using double spacing and leaving a margin of not less than one inch on the left-hand side. Corrections to the MSS. should be made in the text and not in the margin.** Unless a paper reaches the Secretaries more than seven days before a Council meeting it will not normally be considered at that meeting. By Council decision, MSS. of accepted papers are retained by the Society for one year after publication; unless their return is requested by the author, they are destroyed.

2. *Presentation.*—Authors are allowed considerable latitude, but they are requested to follow the general style and arrangement of *Monthly Notices*. References to literature should be given either in the traditional form of serial numbers in the text related to a numbered list at the end of the paper, or in the form recommended in *Notes on the preparation of scientific papers to be communicated to the Royal Society*.

3. *Notation.*—For technical astronomical terms, authors should conform closely to the recommendations of Commission 3 of the International Astronomical Union (*Trans. I.A.U.*, Vol. VI, p. 345, 1938). Council has decided to adopt the I.A.U. 3-letter abbreviations for constellations where contraction is desirable (Vol. IV, p. 221, 1932). In general matters, authors should follow the recommendations in *Symbols, Signs and Abbreviations* (London: Royal Society, 1951) except where these conflict with I.A.U. practice.

4. *Diagrams.*—**These should be designed to appear upright on the page, drawn about twice the size required in print and prepared for direct photographic reproduction except in the lettering, which should be inserted in pencil. Legends should be given in the manuscript indicating where in the text the figure should appear.** Blocks are retained by the Society for 10 years; unless the author requires them before the end of this period they are then destroyed.

5. *Tables.*—**These should be arranged so that they can be printed upright on the page.**

6. *Proofs.*—Costs of alteration exceeding 5 per cent of composition must be borne by the author. Fellows are warned that such costs have risen sharply in recent years, and it is in their own and the Society's interests to seek the maximum conciseness and simplification of symbols and equations consistent with clarity.

7. *Revised Manuscripts.*—When papers are submitted in revised form it is especially requested that they be accompanied by the original MSS.

Reading of Papers at Meetings

8. When submitting papers authors are requested to indicate whether they will be willing and able to read the paper at the next or some subsequent meeting, and approximately how long they would like to be allotted for speaking.

9. Postcards giving the programme of each meeting are issued some days before the meeting concerned. Fellows wishing to receive such cards whether for Ordinary Meetings or for the Geophysical Discussions or both should notify the Assistant Secretary.

CONTENTS

PAGE

H. H. Plaskett, Motions in the Sun at the photospheric level, VIII. Solar rotation and photospheric circulation 197

F. Saiedy and R. M. Goody, The solar emission intensity at 11 μ 213

L. Mestel, The magnetic and dynamical fields outside a proto-star 223

L. Mestel, A note on the magnetic braking of a rotating star 249

Olin J. Eggen and Allan R. Sandage, Stellar groups, IV. The Groombridge 1830 group of high velocity stars and its relation to the globular clusters 255

Allan R. Sandage and Olin J. Eggen, On the existence of subdwarfs in the (M_{Bol}, log T_e)-diagram 278

R. Hanbury Brown and C. Hazard, The radio emission from normal galaxies, I. Observations of M31 and M33 at 158 Mc/s and 237 Mc/s 297

W. Davidson, Steady-state cosmology treated according to general relativity ... 309

Russian translations of summaries of original papers 324

РЕЗЮМЕ ДОКЛАДОВ, В ПЕРЕВОДЕ НА РУССКИЙ ЯЗЫК 324

Printed in London by Taylor & Francis, Ltd., 1959 *September*